ABSTRACT

Title of Dissertation:	ILLUMINATING DINOFLAGELLATES: INTEGRATING TECHNOLOGY FOR MOVEMENT AND LIGHT SENSING
	Jens Wira Doctor of Philosophy, 2025
Dissertation directed by:	Allen R Place Professor MEES

Movement is a fundamental feature of life that shapes ecological dynamics. This dissertation advances the study of movement behavior in dinoflagellates, a diverse group of algal protists best known for forming harmful algal blooms. Understanding their movement capacities, drivers, and mechanisms is essential for improving ecological modeling, developing accurate sampling methodologies, monitoring proliferation and colonization, and uncovering the traits that have sustained the dinoflagellate lineage for millennia.

To expand behavioral research in this group, open-source imaging hardware and software were developed to enable accessible, reproducible studies across different experimental contexts. Using various types of microscopic imaging techniques, including multiple solutions developed as part of this dissertation, the

movement of 13 strains from six *Gambierdiscus* species was characterized, revealing species-specific activity rhythms, and distinct diel movement patterns. Experiments with modified lighting conditions and schedules revealed endogenous circadian rhythms that regulate this movement, as well as what appears to be three different oscillator systems and entrainment systems in as many species. These point to the movement of *Gambierdiscus* being a key part of its ecology and life strategy, although the underlying mechanisms and reasons remain enigmatic. In exploring links between gene and function in dinoflagellates, the rhodopsin repertoires of *Amphidinium carterae* and *Karlodinium veneficum*, two species with well developed genomic or transcriptomic resources, were characterized. Only two canonical rhodopsins were identified from the transcriptomes out of 28 total putative rhodopsins, including the first discovery of a heliorhodopsin in dinoflagellates, found in *K. veneficum*. No canonical ion-pumping or phototactic capacity was found in *A. carterae,* whereas these were retained in *K. veneficum*. Both species also exhibited a preponderance of chimeric gene fusions of the rhodopsin backbone with novel accessory domains, indicating functional diversification of originally ion-pumping rhodopsins into yet undescribed light-gated functions.

Taken together, this dissertation work enables faster, more efficient behavioral and bioinformatic studies into the dinoflagellates, as well as illuminates new aspects of dinoflagellate biology while revealing just how much of their complexity remains hidden, underscoring the remarkable evolutionary divergence that makes these tiny algal cells fascinating.

ILLUMINATING DINOFLAGELLATES: INTEGRATING TECHNOLOGY FOR MOVEMENT AND LIGHT SENSING

by

Jens Wira

Dissertation submitted to the Faculty of the Graduate School of the
University of Maryland, College Park, in partial fulfillment
of the requirements for the degree of
Doctor Of Philosophy
2025

Advisory Committee:
Allen R. Place, Chair
Greg Silsbe
Joseph Katz
Kathleen Cusick
Li Yantao

Acknowledgements

I would like to express my gratitude to many people and persons without which this work would not have been possible, but more so without which my time as a PhD student and candidate would have been far less fruitful, fun, and rewarding.

My PI advisor, Dr Allen R. Place, and the dissertation committee for guidance throughout the process of this research. Al, thanks for giving me the freedom to explore new avenues and learn new skills, without which I would not have been able to accomplish the many parts of this work. Members of the Place and Bachvaroff Labs, for their assistance and support, both intellectual and emotional. Tsetso, for invaluable help with Chapter 4, allowing me free rein to learn about computational resources and management, and supporting Miranda and I in getting the UNIX class started.

Drs Tester, Litaker, for help and inspiration for work on *Gambierdiscus* movement, for starting the work. To Chris Holland and the NOAA Beaufort Lab, for providing the cultures used.
Drs Po, Leaw, Hii, as well as Ms. Wani, from UM, and Jack and National Aquarium staff for help with testing, deployment, and use of the SuMOS.

To my multitude of funding sources for allowing me to work on a multitude of projects while still focusing on this work. These include the Maryland Industrial Partnerships, Maryland Department of Agriculture, Maryland Department of the Environment, MOTE Marine Labs, and UMCES. Also thank you to the UMCES Board Of Visitors for awarding me the Endeavor Fund for Innovative Science, with which I was able to not just push development of the SuMOS further, but in that process learn the skills necessary for so many other parts of my research.
To my friends and family, my church families, QOC, and those who provided me the fuel and motivation to make it through the tough times, and also celebrated the good times and wins with me. I would not be able to have gone through this all without you guys!

Table of Contents

List of Tables

List of Figures

Chapter 1: Introduction

The Importance of Studying Movement Ecology

Movement is a fundamental feature of life that shapes ecological dynamics across scales – from microscopic microbes to large marine animals, organisms move to fulfill basic needs and cope with their environment (Miyata et al., 2020; Nathan et al., 2008; Wisnoski & Lennon, 2023). Some of the greatest movements of biomass on the planet, from the great wildebeest migrations in the Serengeti-Mara ecosystems, the salmon runs spanning oceans to forested streams, to the daily vertical migrations of plankton in the oceans, are driven by survival, sustenance, and succession (Hays, 2003; Holdo et al., 2009; Schindler et al., 2003). Building on this foundation, movement shapes not only the daily survival of organisms but also our interactions with them — miss the timing of fish migrations, and the result is an empty net and a weak harvest (Block et al., 2001; Dedman et al., 2023). Consequently, understanding organismal behavior is crucial both for accurately studying and monitoring species of interest and understanding their ecology.

This understanding is even more important in microbes, whose small individual sizes contrast with their foundational importance to ecosystems and the planet (P. G. Falkowski et al., 2008; Whitman et al., 1998). Unicellular algae produce ~50% of the earth's oxygen, and the largest migration of biomass on the planet is of the diel vertical movement of plankton (Field et al., 1998; Hays, 2003). Amongst the myriad microorganisms, movement behaviors strongly influence proliferation, dispersal, and colonization (Alexandre et al., 2004; Echenique-Subiabre et al., 2025). Movement also influences life history strategies, moving from favorable conditions and away from disfavored ones (Menon et al., 2020, 2021). Illustrating this point at the

microscale, motile bacteria and protists are better able to colonize particulate matter in marine systems than non-motile counterparts that rely solely on random encounters, and only the motile life-stages of marine turtle parasitic copepods *Balaenophilus manatorum* can exploit host social interactions to colonize new hosts (Artolozaga et al., 2000; Domènech et al., 2017; Lambert et al., 2019). Phototactic, chemotactic, and other forms of energy-tactic behaviors are also widespread, enhancing strategies such as nutrient and prey uptake, depth station-keeping, and accumulation of cells in favorable regions, to name a few (Aihara et al., 2019; Alexandre, 2010; Alexandre et al., 2004; Hartz, 2010; Hasle, 1950; Menon et al., 2021).

Dinoflagellates – Why Study Their Movement

Dinoflagellate behavioral traits are likely a contributing factor to their long tenure on planet Earth, as evidenced by their presence in the fossil record dating back up to 600 million years (Riding et al., 2023). Dinoflagellates are an ancient branch of the alveolate lineage, named for their helical swimming behavior (dinos, Greek for whirling), and their two dissimilar flagella (flagellum, Latin for whip) (Gómez, 2012). They are a massively diverse group, with tremendous diversity in their morphological and trophic roles – from photosynthetic symbiotic zooxanthellae at the order of 10s of microns in size, to free-living heterotrophs in the millimeter range, and are some of the most diverse and abundant eukaryotes known (de Vargas et al., 2015; Fitt, 1984; Janouškovec et al., 2017; Marcinko et al., 2013). Their divergent nature is of great scientific curiosity but also makes them notoriously difficult to study – massively inflated genomic sizes, strikingly different chromosome structures from other eukaryotes, the loss of true histones, tandem gene arrangements, large swaths of genes with unknown functions, and a lack of transcriptional regulation, are all hallmarks of the dinoflagellate lineage (Bachvaroff & Place, 2008; Gornik et al., 2019; Hackett et al., 2004; Lin, 2011, 2024; Nand et al., 2021; Riaz et al.,

2018; Stephens et al., 2018). More importantly, these features hamper understanding their ecological and economic importance. More than 70% of eukaryotic phytoplankton species that produce toxins are dinoflagellates, and a similar proportion of harmful algal bloom forming species are dinoflagellates too (Anderson et al., 2021; Oh et al., 2023; Zingone & Oksfeldt Enevoldsen, 2000). These blooms have far-reaching impacts, including human health risks such as paralytic, diarrhetic, and ciguatera shellfish poisoning, massive mortalities of fish and other marine life, disruption of aquaculture and fisheries, and significant economic losses to coastal communities (Anderson et al., 2021; Berdalet et al., 2015; Chinain et al., 2021; Larkin & Adams, 2013; Oh et al., 2023; Yuan et al., 2024). Beyond their harmful impacts, dinoflagellates drive tourism and local economies in bioluminescent bays, support coral reefs through symbiosis, and provide significant biotechnological and pharmacological value and potential from the suite of bioactive molecules, especially polyunsaturated fatty acids (Assun ão et al., 2017; Davy et al., 2012; Gallardo-Rodríguez et al., 2012; Govender et al., 2024; Y. Jiang et al., 1999; Suggett et al., 2017).

Ultimately, like all other life, it is through movement that dinoflagellates interact with their environment—seeking light and nutrients, escaping stressors, colonizing new substrates, and even structuring harmful blooms (Nathan et al., 2008; Wisnoski & Lennon, 2023). Their movement ecology thus provides a critical entry point for unraveling both their biology and their broader ecological impacts, and some research has progressed into cell movements.

Dinoflagellate Movement as Described In The Literature

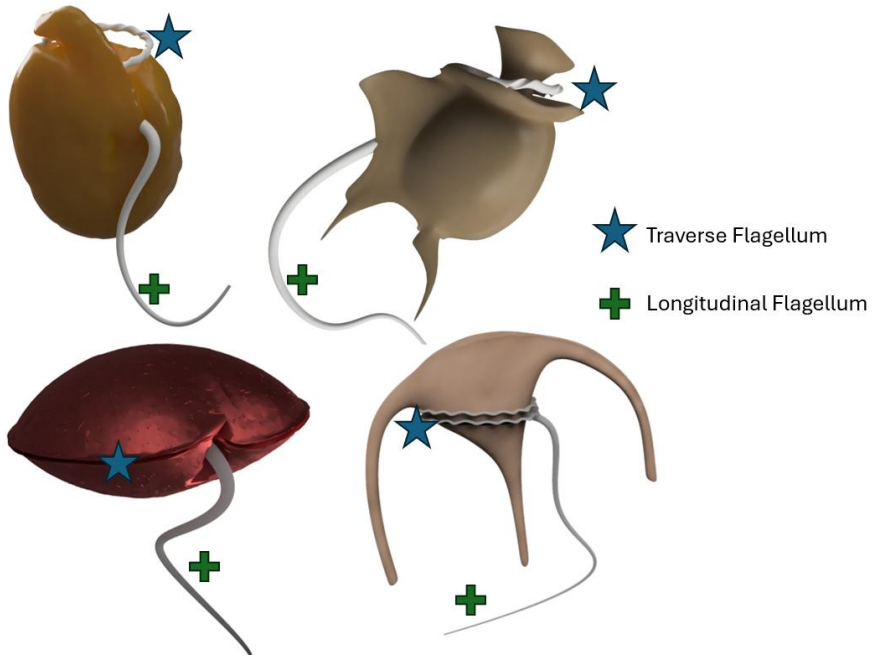

Figure 1:Examples of different dinoflagellates with flagella added in. From top left: *Amphidinium carterae*, *Dinophysis*, *Gambierdiscus*, *Ceratium*. The traverse flagellum is annotated with the blue stars, and longitudinal or trailing flagellum marked by the green cross. The cingulum, or traverse groove is shown and marked in *Gambierdiscus* instead of the flagellum, in order to show the groove where the flagellum encircles the cell. The original models (without flagella) for *Dinophysis*, *Gambierdiscus*, and *Ceratium* were taken from the US National Office for Harmful Algal Blooms.

To situate this work within the broader context, this introduction provides the existing knowledge base for dinoflagellate movement behaviors and how they relate to the ecology of the cells, focusing on movement capabilities, and their use of movement for migration and phototaxis.

Dinoflagellates swim in the water column by means of two dissimilar flagella, a transverse flagellum that circles the cingulum, and a longitudinal flagellum that originates from the sulcus (Fenchel, 2001). Figure 1 shows several examples of dinoflagellates, the diversity of their morphologies and flagella. They take large helical trajectories, a strategy common in aquatic protists termed “helical klinotaxis” that allows for greater sensory capabilities and responses to stimuli (Fenchel, 2001; Long et al., 2003; Sheng et al., 2007). There is no consensus

on the roles of each flagellum in propulsion, rotation, and steering, or rather different species or genera might use different strategies. High-resolution observations in *Dinophysis* and *Cryptothecodinium* show that movement ceases with the beating of the longitudinal flagellum, while flow visualization and computational models and fluid dynamics in *Protoceratium* and *Prorocentrum* show that the transverse flagella provides propulsion while the longitudinal flagella steers (Fenchel, 2001; H. Jiang et al., 2018; Miyasaka et al., 2004; Schuech et al., 2025).

The swimming rates and migration rates of many dinoflagellates have also been studied, using different methods. Microscopic methods tracking instantaneous swimming speeds show swimming speeds under 100μm/s for some species to above 1mm/s, a range an order of magnitude apart, with most measurements falling in the range of 2-500 μm/s (Kamykowski, 1986; Kamykowski et al., 1992; Lewis et al., 2006; Sheng et al., 2007; Smayda, 2010).

In-situ measurements tracking the movement of the thin layer of cells across depth profiles show populations can migrate vertically at similar speeds, with rates of 1-2 m/h (250-500 μm/s), showing that the movement is highly directional (Clayton et al., 2024; Olli, 1999; Smayda, 2010). The migration rates indicate an ability to migrate several tens of meters across a diel day, and sustained migrations that approach this magnitude of movement have been observed (Eppley et al., 1968; Zheng et al., 2023).

This migration and display of movement and swimming ability are most visible in diel vertical migration (DVM); the accumulation of cells at different depths over time has been observed since before the early 20th century, with improved cell division rates when cells were able to maintain a depth that matched their optimal lighting levels (Hasle, 1950; Lohmann, 1908). The DVM phenomenon is distributed across many aquatic and marine lineages, which enables cells to acquire nutrients, prey, light, or conspecifics with greater efficiency (Baek et al.,

2009; Bollens et al., 2012; Eggersdorfer & Häder, 1991; Hasle, 1950; Hays, 2003). Early conceptual models pointed to locomotion as a key driver in this movement, not just mechanical forcings of water movement, as summarized by Langhans in 1907 (Langhans, 1907). Many pelagic dinoflagellate species utilize their swimming ability to migrate vertically, forming vertically patchy distributions, or thin layers where cell densities are significantly higher within the layer than above or below (Blasco, 1978; Clayton et al., 2024; de Souza et al., 2014; Jephson & Carlsson, 2009; Zheng et al., 2023). In photosynthetic dinoflagellates, this DVM is largely thought to provide cells with light during the day for photosynthesis, and nutrient uptake and possibly predator avoidance at night (Clayton et al., 2024; Jephson & Carlsson, 2009). In heterotrophic species DVM allows cells to follow their prey across different depth profiles, increasing encounter rates and feeding efficiency (Hansen, 1991, p. 1; Lessard, 1991; Olli, 1999).

This DVM can be regulated under an endogenous circadian clock regulation, as described in *Lingulodinium polyedra* (previously *Gonyaulux*) by Roenneberg *et. al.* (Roenneberg et al., 1989). Dinoflagellates have been a key group in the study of circadian rhythms, with many of the associated behaviors and phenotypes observed to be entrained by endogenous circadian rhythms having discrete benefits to the cells to justify the investment into the molecular mechanisms involved (Hastings, 2007, 2013; Vicker et al., 1988). This is best seen in the rhythmic synthesis and destruction of proteins involved in bioluminescence, as found and summarized by Hastings' body of work (Hastings, 2007, 2013; Johnson et al., 1984). Protein synthesis for luminescence begins before the onset of night, enabling the anti-predation effect of bioluminescence without delay (Hastings, 2013; Lindström et al., 2017). The motivations for movement on a circadian

clock can be similarly determined – if migrations can provide benefits to cells, pre-empting those benefits could provide greater advantages (Roenneberg et al., 1989).

This migratory behavior is also coupled with phototaxis for station keeping, where cells move to and stay at preferred light levels, a behavior similarly ubiquitous throughout the microbial world (Eggersdorfer & Häder, 1991; Menon et al., 2021; Roenneberg et al., 1989; Strasburger, 1878). Eduard Strasburger first coined the term "phototaktisch" in 1878 with his experiments showing several different unicellular motile organisms moving swarming towards or away from light (Strasburger, 1878). Phototaxis differs from phototropism, the behavior where plants grow towards a light source, in that phototaxis involves motile organisms like plankton, while phototropism is the growth of sessile organisms towards the light source (Jékely, 2009; Liscum et al., 2014; Yang et al., 2025). Most known dinoflagellates are phototactic with few exceptions, one notable example being *Amphidinium carterae* (Eggersdorfer & Häder, 1991; Forward, 1974; Halldal, 1958; Kamykowski et al., 1998). Phototactic behavior in dinoflagellates is also not limited to vertical migration and station keeping, but has also been hypothesized to be used for prey location, where red light from chlorophyll fluorescence attracts cells of *Oxyrrhis marina*, and green light from cnidarian fluorescence and attracts *Symbiodiniceae* symbionts (Aihara et al., 2019; Hartz et al., 2011).

For the effector of phototaxis, the eyespots, or stigma, are pigmented regions thought to provide directional shading of a region of photoreceptor proteins that allow cells to discern direction of a light stimulus. There is a great diversity with eight different types of stigma known throughout the dinoflagellate taxon (Dodge & Crawford, 1969; Hoppenrath, 2017; Takeo et al., 1999). Many phototactic dinoflagellate species do not possess eyespots, and it is hypothesized that shading is provided by the entire cellular body as opposed to specialized organelles (Dodge

& Crawford, 1969; Foster & Smyth, 1980; Slamovits et al., 2011; Takeo et al., 1999). The current consensus for the molecular light receptors responsible for phototaxis implicate a retinal binding rhodopsin as the protein involved in photoreception (Aihara et al., 2019; Hartz et al., 2011). Additional evidence includes a concentration of retinoid compounds, rhodopsin gene fragments, and rhodopsins in the eyespots of species that possess them, however identification of the specific proteins or molecular mechanisms of phototaxis is lacking (Colley & Nilsson, 2016; Francis, 1967; Hayakawa et al., 2015).

Introduction

This diversity and divergence leads us to a reality of dinoflagellate research that was alluded to earlier – that dinoflagellates are extremely difficult organisms to study with current and canonical methods (Hackett et al., 2004; Lin, 2011; Stephens et al., 2018). Their behavior is similarly enigmatic, but important to understand in order to better mitigate their human impacts, as well as potentially unearth novel discoveries from their unique biology (Chinain et al., 2021; Crump et al., 1999; Oh et al., 2023). Understanding their movement capacities, drivers, and mechanisms is important for modeling efforts, establishing accurate sampling methodologies, monitoring proliferation and colonization of new areas, and understanding what has given the dinoflagellate lineage success over millennia (Hackett et al., 2004; Lewis et al., 2006; Riding et al., 2023; Sheng et al., 2007; Tester et al., 2014). A recent example that highlights this is a spate of spinning fish disease, potentially caused by elevated levels of normally benthic *Gambierdiscus* in the water column; we do not know what triggered the cells to leave the benthos in large numbers, but understanding the triggers of these movements is important for future mitigation efforts (Chateau-Degat et al., 2005; *Fish along the Florida Keys Are Spinning in Circles until They Die—and No One Knows Why*, 2025).

This dissertation is a collection of chapters aiming to advance the study of dinoflagellate behavior from multiple avenues – expanding the use of open-source hardware and software methods for behavioral studies, establishing the baseline movement schedules and capability of benthic dinoflagellate ciguatera causing *Gambierdiscus*, and a bioinformatic survey of the microbial rhodopsin complement of two free-living dinoflagellates *Amphidinium carterae* and *Karlodinium veneficum*.

Chapter 2: Expanding Access to Benthic Organism Studies using Open-Source Materials and Methods

Introduction

The rise in open source microscopy and imaging systems has greatly assisted in our study of the microscopic world, especially with the ability to design and customize hardware setups to probe and answer specific questions (Feng et al., 2025; Gervasi et al., 2022; Morelle et al., 2024; Salido et al., 2020). This has been fueled in part by advancements in computational algorithms, the increased commercial availability of consumer grade hobbyist hardware such as Raspberry Pis, as well as an increased reliance for all facets of science to learn software development and coding (Juavinett, 2022; Mathe et al., 2024). Increased accessibility enables smaller research groups to not only develop and utilize previously inaccessible methods, but also to replicate those methods based on open-sourced tools and software (R. Bowman et al., 2024; R. W. Bowman, 2023; Oellermann et al., 2022). This enables not just better reproducibility, but also shared platforms reducing variability between labs, improving comparability of results and accelerating the development of best practices (R. Bowman et al., 2024; R. W. Bowman, 2023; Oellermann et al., 2022; Salido et al., 2020). A considerable benefit of this is a democratization and expansion of the tools to study the marine microbial world.

Microscopic life in the marine environment has significant impacts on our human environment and the global climate – from driving a planet-wide carbon cycle to harmful algal blooms (HABs) that affect local communities and fisheries (P. Falkowski, 2012). Individual processes at this scale may seem inconsequential, but aggregation at the scale of the oceans gives them a massive impact (Levin, 1992). Of these, organisms and processes occurring in the benthos are more diverse and myriad than those in the water column, and just as, if not more,

important. Examples of such processes include transparent exopolymer (TEP) deposition and biofilm initiation, benthic harmful algal blooms, and benthic invertebrate diel ecology (Hotos & Bekiari, 2023; Institute of Marine Sciences (CSIC), Barcelona et al., 2017; Kennelly & Underwood, 1984; Neushul, 1972; Passow, 2002). However, studying these processes is often difficult due to logistical constraints arising from high heterogeneity and an inability to integrate large areas or volumes as is possible with an unstructured water column (Delgado et al., 2023; Erickson et al., 2012; Kennelly & Underwood, 1984; Lalli & Parsons, 1997; Lobel et al., 1988).

Studying benthic processes in-situ has been of interest for many years, where the earliest methods involved partially or fully submersible light microscopes, operated by divers or scientists to take observations (Kennelly & Underwood, 1984; Neushul, 1972; Staley, 1971). However, as automated monitoring of phytoplankton in the pelagic region has taken off, advances in the study of aquatic benthic processes has lagged significantly (Erickson et al., 2012). For example, the study of biofouling on various materials is an area of active research, but in-situ rate measurements often offer limited temporal resolution based on human operator sampling schedules, which restricts the potential understanding of how different treatments or materials might affect the colonization process (Delgado et al., 2023).

This chapter details the development and implementation of two microscopy devices, built on low-cost, readily available hobbyist or commercial hardware. The first is an in-situ substrate monitoring timelapse microscope for monitoring colonization and attachment to substrates. The second is a long-term culture monitoring microscope for measuring benthic cell movement across multiple diel periods, alongside a software analysis stack for cell tracking to produce trajectories from videos, for analysis. Both are open-source to further advance the study of the benthos and benthic organisms.

Submerged Microscope for Observing Substrates (SuMOS)

Instrument in Context

Several groups have incorporated video or image recording capabilities into underwater microscopes for observing benthic processes in-situ (Mullen et al., 2016; Shahani et al., 2021). These devices are designed for high temporal resolution studies of microscopic processes, and as such are also designed to be handled directly by an operator for data collection. These underwater microscopes are meant to be used to study a large variety of natural substrates, which makes the manual setup and target acquisition critical to their use. These devices provide flexible experimental platforms, providing variable focusing, magnification, and study subject choices, since the operator is able to make decisions throughout the data acquisition process. However, the requirement for a diver operator greatly limits the time over which data can be continuously collected, which makes such designs insufficient for studying attachment and colonization kinetics for substrates, especially when diel patterns may be at play (Moriera & Tester, 2016). In addition, the inhomogeneity and stochastic nature of the marine/aquatic environment demands large numbers of replicates for making statistically sound claims, which requires a more purpose-built design to facilitate experimental replication (Taylor & Gustavson, 1986; Tester et al., 2022).

The novel Submerged Microscope for Observing Substrates (SuMOS) is a standalone submerged camera device designed to fit this niche, to study small-scale processes on underwater surfaces. The device provides an easily adaptable framework that can be used to study a variety of artificial substrates in a variety of aquatic environments. Substrates are mounted in front of an auto-focusing macro camera, and a timelapse video is taken of processes occurring on the substrate.

The SuMOS opts for a “place-and-forget”, operator-free data acquisition process. Allowing the device to be fixed in place and subsequently collected for data retrieval greatly extends the possible study time, especially important for collecting data throughout the different parts of the diel period. The study substrate being mounted to the device housing within the autofocusing distance of the optics allows for a set-and-forget data collection process, where diver involvement is limited to placing and retrieving the device. The low cost and ease of deployment of the design also makes it possible for multiple devices to be built and deployed in parallel, to collect statistically significant sample sizes on realistic budgets. The device was designed as a framework with adaptability in mind, enabling a wide range of experiments to be conducted with different optical configurations or imaging schedules.

Hardware Description

The SuMOS is a fully standalone camera system that allows macro imaging of mounted substrates under various lighting conditions, and even in complete darkness. The device is designed to be assembled and deployed by operators in field conditions like dive boats with minimal tooling required, allowing ease of data collection from multiple locations or over multiple consecutive days. The device is assembled and activated outside of the water, and unlike previous underwater microscopes, human involvement is only during positioning and deployment of the device.

The main design objective of the SuMOS is to allow data collection with minimal operator interaction, which allows for data collection periods for longer than a diver can be deployed and study processes that occur at different rates across the day-night cycle. As such, it focuses on recording the activity on fresh substrates mounted to the device and is designed to be

placed in natural environments without fine user adjustments. This deviates from other currently available hardware that requires operator control, but is able to observe natural substrates for short periods of time (Mullen et al., 2016; Shahani et al., 2021).

The external waterproof housing was inspired by PipeCam, an open-source autonomous camera, in which the main body is a length of capped PVC piping and a threaded PVC union with a clear plastic window for sealing and access (*PipeCam*, n.d.). The main change to the housing design is the use of a 3D-printed washer in the female end of the union that allows for the mounting of the study substrates, and for better distribution of the clamping force on the acrylic window required for maintaining waterproofing. The study substrate is attached to the camera via a removable holder, and gross positioning to the focal plane is achieved by the use of spacers on the holder. This design was deployed at depths of 15m with no signs of water ingress. Additionally, the housing was internally pressurized to 5,000 kPa of water and air and held the pressure for at least 24 hours, equivalent to pressure at approximately 50m of depth.

Inside the housing, electronics are housed in a 3D-printed assembly that is designed to slip into the waterproof 3D-printed housing. A compliant spacer is used in the assembly to apply compression of the assembly against the acrylic panel, as well as provide allowance for the use of PVC parts from different manufacturers, which tend to have some variability in design. The outer diameter of the assembly is designed to fit the interior diameter of a PVC Schedule 80 pipe, while the length of the assembly is adjusted by spacers. All housing bodies are designed for ease of production with a hobbyist grade fused-deposition modelling 3D-printer, with geometry optimized to reduce post-processing requirements.

Imaging is driven by a Raspberry Pi Camera Module v3 NoIR and illuminated by two 940nm IR LEDs in low light conditions. Ambient light levels are measured via a TSL2591 light

sensor, and illumination is triggered when light levels fall below a user defined lux threshold. The device makes use of the Camera Module v3's autofocusing capabilities coupled to macro lenses held before the lens, to provide the desired magnification and working distance while removing the need for manual fine focusing of the camera on to the imaged substrate. The Pi Camera allows for manual control of focus, which opens the possibility of data acquisition with focus stacking for future iterations, however the design choice was made to rely on a single autofocus due to battery and compute constraints.

Device control is achieved by a Python script running on a Raspberry Pi Zero 2W single board computer. Data is saved locally on the Raspberry Pi's local storage and subsequently shuttled in chunks onto an attached USB device for data offload in order to reduce power draw over USB. Many of the software parameters, such as the imaging interval, the schedule for data offload from the Pi to the USB drive, and minimum lux threshold for IR illumination, can be controlled by modifying a configuration file loaded on the USB drive. This allows the device to carry out different experimental designs and conditions simply by editing a text file with a standard text editor. Without the configuration file, the device defaults to a set of sensible parameters that can be modified by the user but requires access to the Pi either via SSH or wired connection.

Using the SuMOS is simple: mount a study substrate, install a USB drive and power bank, seal the waterproof housing, deploy and retrieve the device, and the data is ready to be analyzed. The SuMOS captures a time-lapse video of the substrate at fixed intervals, as well as records the ambient light levels in lux, until the battery is depleted or removed. Both battery and USB drives are commercially available, and can be replaced while in the field, allowing for rapid redeployment of the device.

To summarize the advantages of the device:

- Operator-free method for studying colonization behavior of underwater substrates, enabling full day-night cycles to be captured.
- Ability to image underwater under different lighting conditions, including pitch darkness by means of IR illumination.
- Low cost and commercially available off-the-shelf parts, as well as ease of deployment and setup, allow for concurrent collection of multiple replicates on smaller budgets, enabling greater statistical power in experiments.
- Customizable framework for changing optical and data acquisition parameters provides flexibility in experimental design.

Build Instructions

External Waterproof Enclosure

The construction of the enclosure is heavily inspired by the PipeCam project (*PipeCam*, n.d.), with the key deviation being the use of the substrate mounting flange. A more detailed build instruction can be found at the source, but briefly:

1. Cut the Schedule 80 4” PVC pipe to 6.5”.
2. Using the appropriate primers and PVC cement, attach the PVC cap to one end, and the side of the union with the O-ring groove to the other. An example of the assembled housing can be seen in Figure 2B.
3. Cut an 1/4” acrylic panel to fit over the O-rings, and in the union. This can be done with a bandsaw or router as available.
4. 3D-print the appropriate mounting flange for the union type.

Figure 2: (A, left) Parts for the waterproof enclosure and internal electronic housing, note the O-ring mounting groove on the union fitting. (B, right) Two completed housings using the two configurations of commercially available PVC Unions, as well as substrate mounting flanges. The mounting flange is fitted in the collar of the right one.

Note: Different union manufacturers have different designs. Specifically, the O-ring may be housed on different sides of the union in relation to the threading, which dictates the design of the substrate mounting flange. Depending on availability and cost, users may run into one of two design options. The first (left of Figure 1B) has the threaded fitting on the opposite piece of the O-ring, and the 3D printed mounting flange is threaded and secured against the threaded union collar to provide compression between the acrylic panel and O-ring for sealing. In testing, the mounting flange could be printed with 4-5 walls and 30% infill, since the force was spread across the threads. The second (right of Figure 1B) has the threaded fitting on the same piece as the O-ring groove, and the threaded collar alone is sufficient to provide compression for sealing. In this configuration, the mounting flange is inserted into the collar and will be the mating interface with the acrylic panel. The mounting flange had to be printed fully solid since the compressive force was concentrated on the top and bottom surfaces. The .f3d design files for both options are provided but may require modifications for the specific thread specifications of different manufacturers and are provided as editable parameters.

The external waterproof housing seal can be tested by pressurizing it internally. A valve drilled into a spare acrylic panel can be used to provide means to pressurize the housing upon sealing and can be swapped between multiple housings to be tested. An important safety note is to minimize the amount of compressible air inside the system to reduce explosion risk at high pressures, so if hydrostatic testing facilities are not available, filling the housing with water before pressurizing with air reduces the risk significantly.

A full bill of materials for the waterproof housing is found in Appendix 1.

Internal Electronics Housing

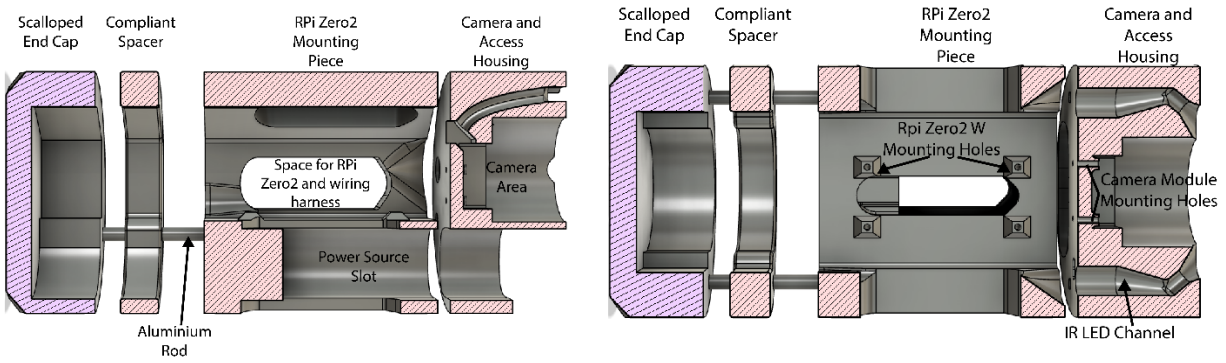

Figure 3: Section view schematics for 3D printed internal electronic housing.

1. 3D-print the Camera and Access Housing, RPi Zero2 Mounting Piece, and Scalloped End Cap in a rigid filament, and the compliant spacer in a flexible elastomer.
2. Insert two heatset inserts into the top face of the RPi Zero2 Mounting Piece for securing the Camera and Access housing.
3. Cut the 5mm Aluminium rods to length and slide the assembly into place as indicated in Figure 3.
4. Using hot glue or epoxy, attach the Scalloped End Cap to the inside of the waterproof housing cap, and mark on the external housing where “up” is for the camera. This ensures

the internal housings do not rotate freely, and the device can be mounted in the proper orientation.

5. If necessary, measure any excess space in the external housing after insertion of the electronic housings, and 3D-print an additional spacer in a rigid filament to fill the space. In practice, this is a simple method to account for variation in the external housing lengths.

Electronics Assembly

1. Connect the ribbon cable to Raspberry Pi Camera Module, the Stemma QT connector to the TSL2591, and solder wires to the leads of the LEDs.
2. Solder a 56Ω resistor to each IR LED, and a 68Ω to the 2.2V red indicator LED
3. Remove jumper housing from female jumpers and pass wires through appropriate channels. Figure 4 provides a visual guide for where each cable goes.
4. Crimp female jumper heads to the end of the LED leads.
5. Attach the camera and TSL2591 to the Camera Housing with M2 hex screws. Insert the macro-lenses into the channel above the camera, and hot glue them in place.
6. Connect the power, ground, data and clock lines to the DS3231 RTC, and splice the data and clock lines to the same lines as the TSL2591 so they share the same I2C bus.
7. Insert jumper leads into the plastic housings, and connect these to the RPi Zero 2W, following the wiring diagram in Figure 4B. For added security, breadboard jumper housings can be used as to provide more surface area for mounting. The assembly in Figure 4C uses a 6x2 and 5x2 set for connection.
8. Connect the camera ribbon cable to the CSI port, the male-male microUSB – USB cable to the power port, and the male-female microUSB – USB cable to the USB port.

9. Insert the USB end of the power cable through the channel in the rear of the RPi Zero 2W Mounting Piece, taking care that the orientation matches that of the power bank. Secure with hot glue.
10. Pass the female end of the data cable through the data cable channel in the Camera Housing.
11. Attach the RPi Zero 2W to the Mounting Piece with M2.5 screws, through the holes in the housing.
12. After loading the OS onto the microSD card, insert the microSD card into the RPi Zero 2W, then using the appropriately sized machine screws, attach the two housings together.

The housing was designed in two pieces to facilitate assembly as well as production, with the use of the heat-set inserts and machine screws to join them into a single unit for security. In our prototyping, both lever nut and solder joins were suitable, with the lever nuts being easier to use but slightly bulkier in the final assembly. Use of hot-glue on the GPIO jumpers also provided additional security in case of vibrations/movement when deployed. Figure 4C serves as a useful reference for connections to the Raspberry Pi board, and Figure 4D for the final assembly.

A full bill of materials for the components is found in Appendix 2, and parametric design files are accessible from links in Appendix 3.

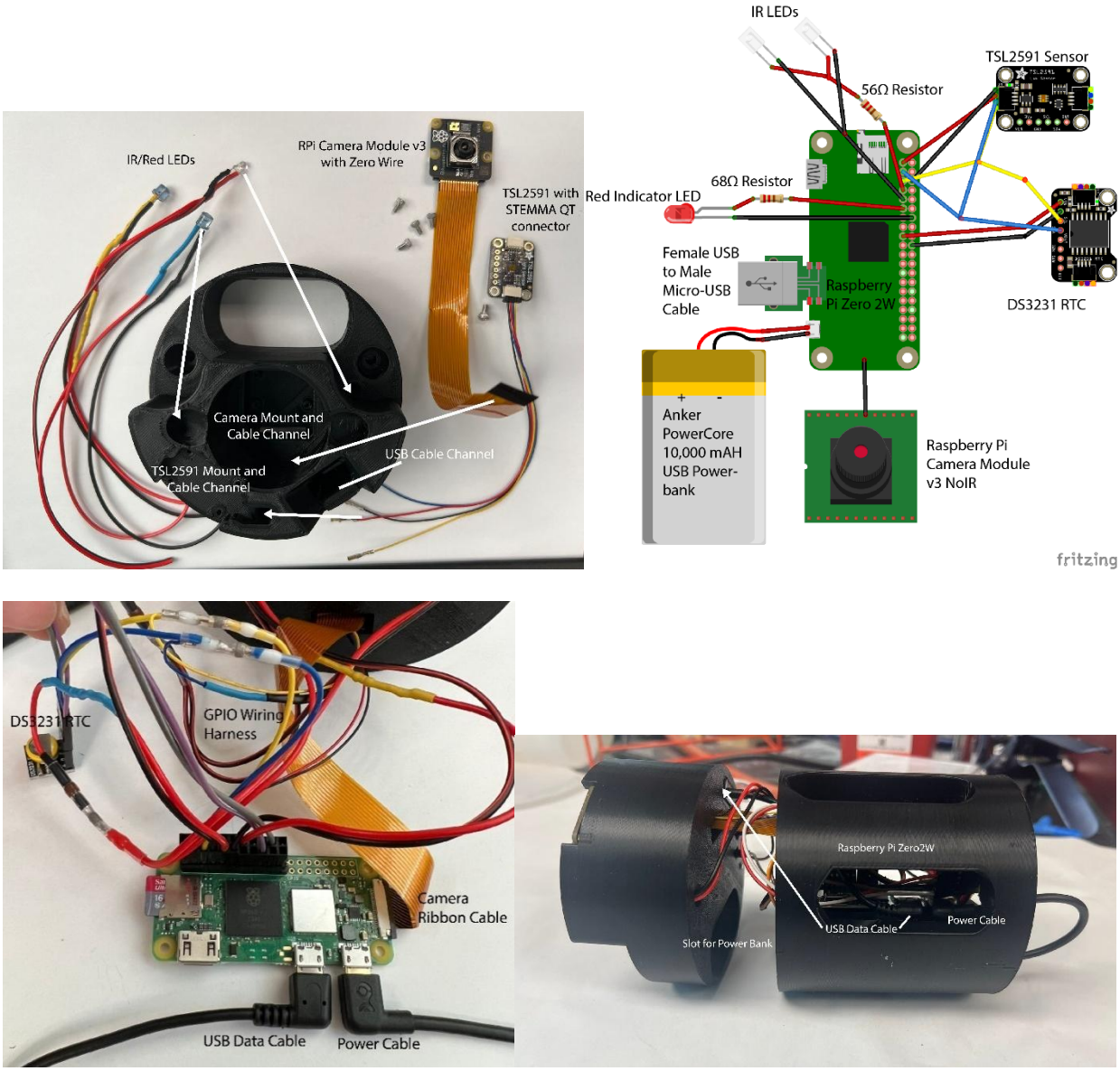

Figure 4: (A) Unassembled view of parts for front facing camera mount, showing appropriate mounting areas and channels for different wires. (B) Wiring diagram sketch. (C) Electronics connected and labeled, showing appropriate connections to the Raspberry Pi board. (D) Electronics assembled in housing, showing location of cabling and battery bank.

Software Installation

1. Using the provided Raspberry Pi OS imager (https://www.raspberrypi.com/software/) install the legacy lite 64-bit OS (Bullseye) onto an SD card of at least 8GB, with the

username “sumos”. It is also convenient at this step to provide details of an available WiFi network in the configuration.

2. From the associated SuMOS repository, download the python and shell scripts located in the “Install Scripts” folder. Transfer them onto the SD card into the home directory, or via SCP after initialization.
3. Insert the SD card, into the RPi Zero 2W, and power it on. Wait for the device to initialize.
4. Find the IP address of the device over the local network and connect to it over SSH.
5. With the install.sh script in the home directory, run “sudo bash install.sh”. The device will carry out the installation and require a restart to determine that everything has successfully been set up.

After the restart, the SuMOS can be fully assembled and is ready to be used. The install.sh script installs the prerequisite packages, sets up the GPIO pins and activates the I2C channel, and creates a system service that calls the data acquisition script at startup. An included script “streamControlLED.py” is included to test the device hardware attachments and also provides a livestream of the camera over a LAN webserver. Scripts used can be accessed from the links available in Appendix 3.

Operation Instructions

The SuMOS was designed for ease of deployment and replacement in the field, and as such operational steps are few once the device is fully assembled. The device simply needs to be initialized, sealed, and deployed.

1. Device initialization

Initializing the SuMOS is as simple as inserting a USB storage device and USB power bank into the appropriate ports. The red indicator LED will turn on when the system boots successfully. The device then runs through an initial startup check, during which if any step of the regular imaging and data transfer workflow fails, the device enters an error state, and the red LED will persistently flash in a pattern that depends on which subsystem triggered an error. Should the startup sequence finish successfully, the red LED will turn off, and the device will continue to record data until the battery is removed or runs dry.

A set of default data acquisition settings is stored on the device and can be changed in the main capture script (captureScript.sh) over a ssh connection, or when first loaded. A configuration file can also be placed in the main directory of the USB device that is used to set the recording parameters on a per run basis without the need for access to the OS of the SuMOS. The configuration file is provided in the source repository (divePiSettings.conf).

2. Sealing waterproof housing

Upon successful powering up of the device, the outer housing needs to be sealed. The acrylic panel is placed over the top of the union, and the 3D-printed mounting flange is then screwed in to seal the device. Care should be taken to keep the O-rings clean and free from debris, as well as to lubricate the O-rings with silicone grease. Additional torque for sealing the PVC union is provided by use of pipe wrenches. A set of 3D model files for wrenches that fit the exact unions used are provided, and the parameterized .f3d files are provided for modifying the wrench to fit other unions.

Multiple waterproof housings were constructed and tested for their sealing. All were able to hold 50PSI of pressure for at least 24 hours, which would indicate a static waterproof rating of at least 50m. Although not a direct test of watertightness due to the different direction of the

pressure delta from field conditions, both this testing and the pressure ratings of the different joins exceed the depths which divers would usually reach. The waterproof housing was also tested at a depth of 15m in calm protected seawater, without any evidence of water ingress.

3. SuMOS deployment

The SuMOS can be deployed in a variety of ways dependent on the environmental conditions and requirements. Two mounts are provided for mounting the device vertically or horizontally via the use of hose clamps onto available hardware, depending on field conditions and requirements (Figure 5).

Figure 5: Examples of how the SuMOS can be deployed. Left to right, in calm protected waters with a dive weight, attached to a mushroom anchor off a pier, or on a weighted transect sampler.

Measuring Benthic Amphipod Settling

The SuMOS in the described configuration provides a field of view of 18x10 mm, with a resolution of 4608x2592 pixels (12 MP), resulting in a pixel pitch of 3.9µm/pixel, at a working distance of approximately 10mm from camera to substrate. At this short working distance, the LEDs did not uniformly illuminate the imaging area, but sufficient light would reach the field of view to enable imaging. Operating at an imaging schedule of 1 photo/min, the camera was capable of up to 30 hours of non-stop imaging, exceeding the 24 hours required for a full day-night cycle.

To observe in-field performance, the SuMOS was tested over a period of 24 hours at the PhytoChop Observatory, at Horn Point Laboratory, Cambridge MD. Deployment was carried out by mounting the SuMOS onto a mushroom anchor, and lowering the device off a pier to rest on the riverbed of the Choptank River at a depth of about 2 m (Figure 5B). This provided challenging optical conditions for imaging, due to moderate current and constant sediment resuspension, as well as overcast conditions on the first day. The light levels as measured by the SuMOS can be seen in Figure 6. The study substrate was a mounted 1 mm fiberglass mesh, and the device was able to keep focus on the mesh for the entire deployment across the differing conditions, as seen in Figure 7.

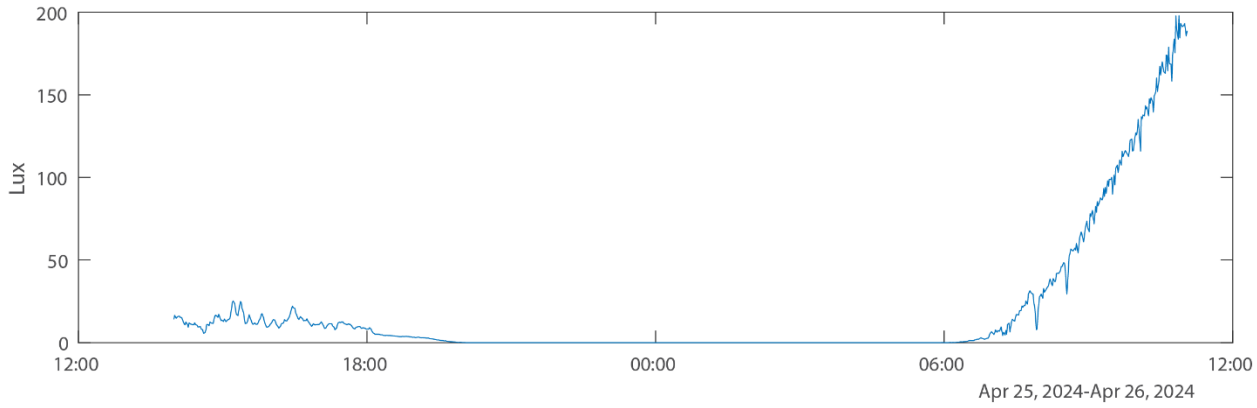

Figure 6: Graph of measured light levels across the 24-hour deployment, showing strong variability in lighting during the day periods.

The resulting data is a timelapse video of what occurred on the substrates, and as such, processing is highly dependent on the type of experiment that is being carried out. Here we describe an exemplar method of data analysis that takes advantage of regular image processing techniques to filter out amphipods and other large objects of interest in the field of view for manual annotation.

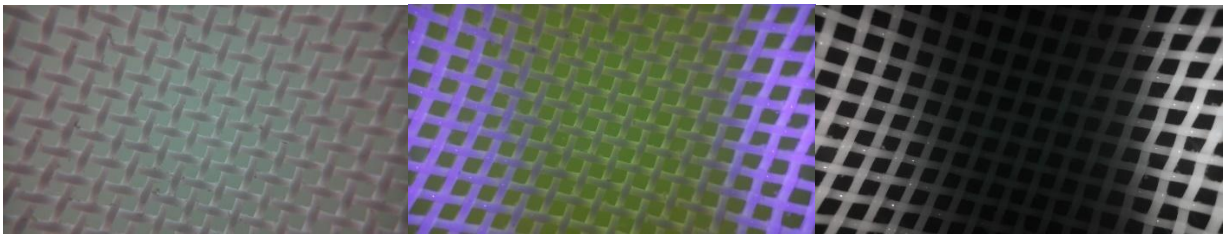

Figure 7: Example images from SuMOS deployment showing images over decreasing light levels, with the final image in complete darkness.

The RGB image is first converted to the L*A*B space, and a flatfield correction is applied to the L channel. The L channel is then subtracted from a moving median window. The magnitude of the difference is thresholded to determine regions with significant departures from the average image and also subjected to a Canny edge filter to connect adjacent regions together, important for slightly transparent samples. The two binary masks are combined, and the resulting blobs are morphologically opened to remove small blobs. Many amphipods, as well as regions with large organic matter attachment were successfully extracted. For our purposes, this resulted in a substantially smaller data set in which amphipods could be manually annotated. With more data, the annotations can also be used to train convolutional neural network (CNN) recognition models for a more objective method of analysis, if desired. Examples of the amphipods detected are shown across different light levels (Figure 8).

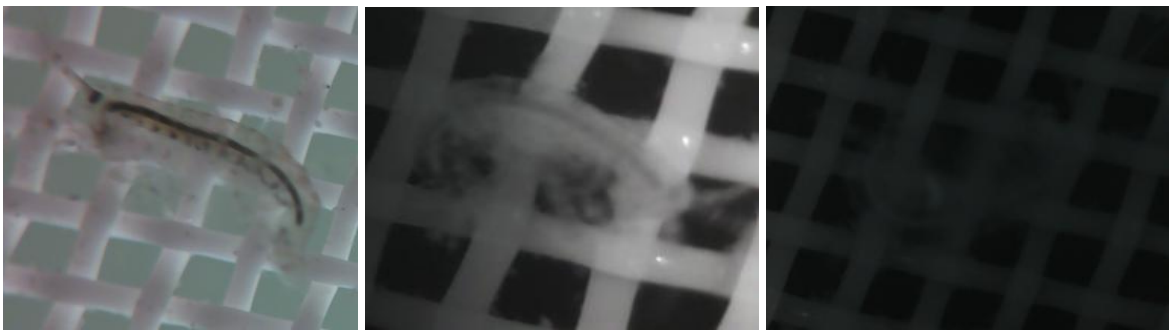

Figure 8: Example of filtered amphipod images across multiple light levels, showing the utility of the segmentation method for picking out images of interest.

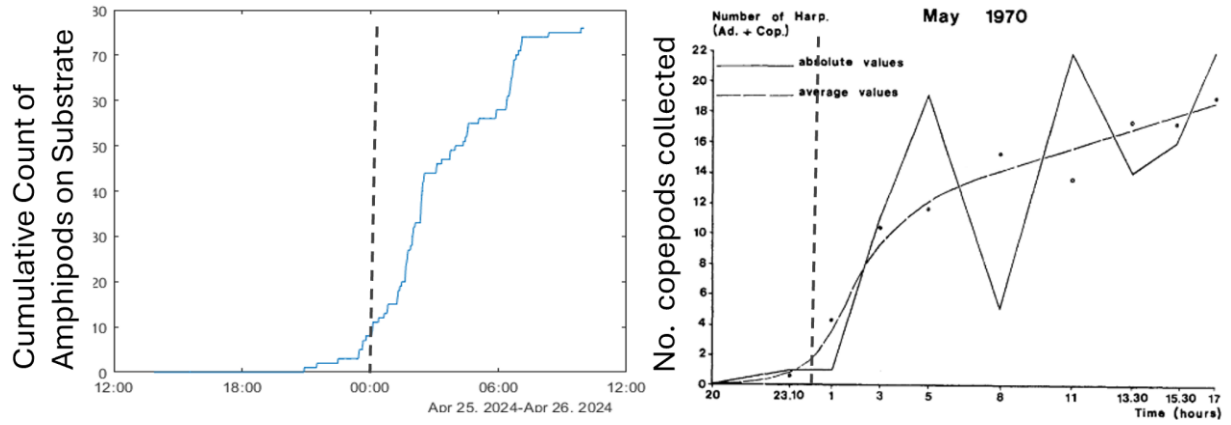

Figure 9: (A, left) Cumulative count of amphipods measured using the SuMOS as deployed in the Choptank River over 24h starting from noon, detected using the described segmentation method. (BF, right) count of benthic copepods on collected substrates over time, taken from (Hauspie & Polk, 1973). The dotted vertical line has been added to both plots to indicate midnight (0000h).

The image annotation results were analyzed to demonstrate the utility of the SuMOS, and show the presence of amphipods after midnight, only approx. 10 hours of deployment (Figure 9). This matches closely with observations made on related benthic harpacticoid copepods, in that colonization of similar artificial mesh screens began only at midnight (Hauspie & Polk, 1973). That experiment involved significant labor investment, requiring operators to deploy and collect screens throughout the night, as well as sample processing and counting of attached copepods. Meanwhile, the utility of the SuMOS is clearly demonstrated here, involving a single deployment and retrieval. It should be noted, the small sample size used here means that it is advisable that more deployments be carried out to make ecological determinations as to the diel patterns of the amphipod. Nevertheless, the utility of the SuMOS for studying biological activity in-situ, coupled with its ease of use and deployment, cannot be overstated.

Use in Benthic HAB Monitoring

The SuMOS was deployed for testing in a coral reef environment, in conjunction with researchers from Universiti Malaya. SuMOS units were deployed off the shore of Perhentian

Island, Malaysia using diving weights to anchor and secure the camera. Two initial deployments were carried out, in August 2024 and March 2025. These deployments were able to demonstrate rapid TEP deposition over the course of a day, with images in Figure 10A and B showing the extent after 18 hours of deployment. More notably, the recorded timelapse provides researchers a highly time-resolved study of the deposition, with images recorded every minute for the entire period.

Additionally, the deployments were able to capture colonization of the substrate by discrete organisms. Figure 10C shows a single brown organism moving along the substrate, likely a benthic *Gambierdiscus* cell based on the shape, color, and size. Improved resolution would improve identification of smaller organisms but would come at the expense of field of view, and by extension amount of sample collected, and such moving forward experimental necessities have to be carefully considered for modifying the design.

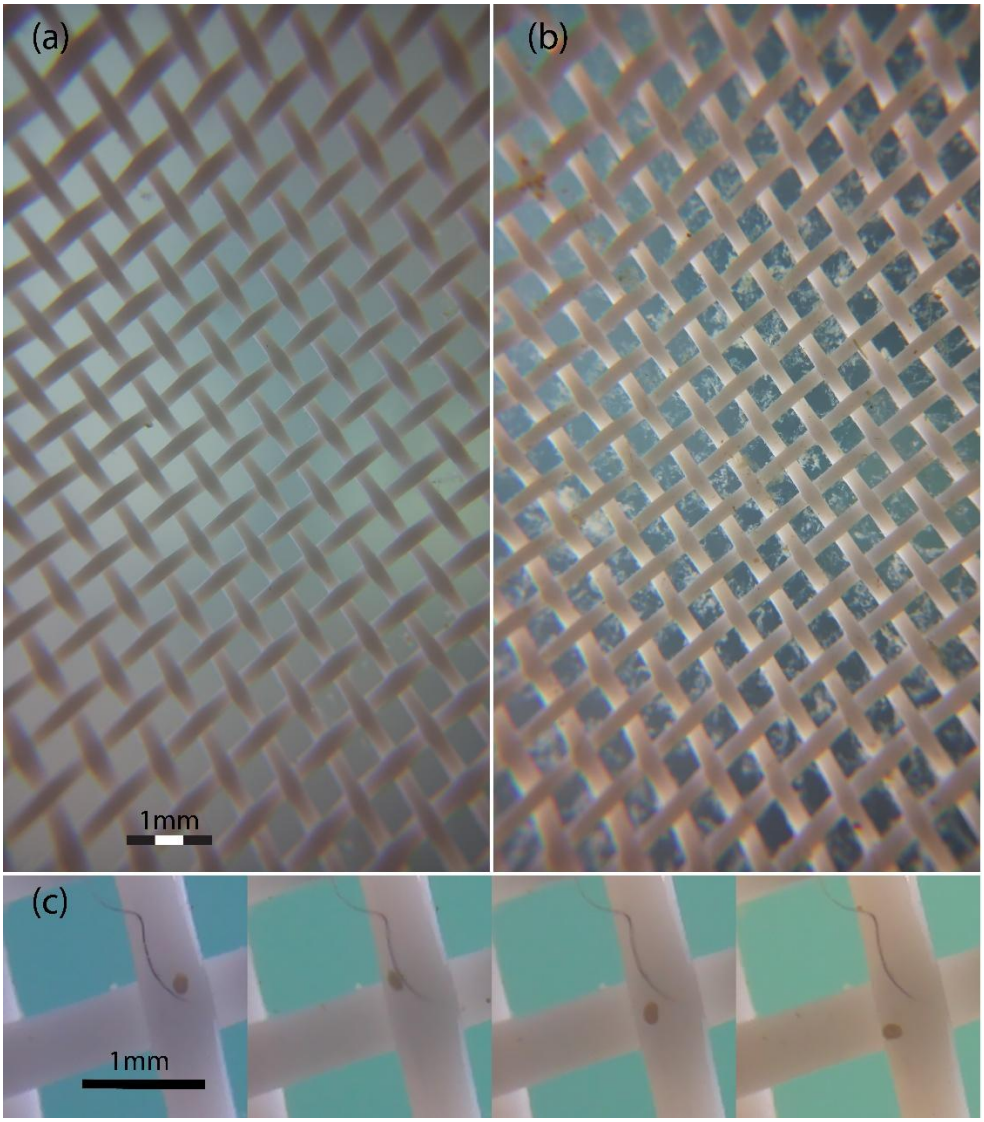

Figure 10: Example photos taken from in-situ deployment of the SuMOS in a coral reef environment surrounding Perhentian Island. (A) before and (B) after, taken 18 hours apart, showing significant TEP deposition over the experimental period. (C) Montage showing a benthic dinoflagellate, possibly *Gambierdiscus*, moving along the substrate. Images are taken one minute apart.

The ability of the device to image and identify shows promise as a method for reducing laborious benthic HAB sampling methods, involving collection and manual processing of the samples, either natural algal samples or artificial substrates (Kassim et al., 2025; Tester et al., 2022). The replacing of manual sampling, processing, and counting with a deployable system, combined with automated annotation and labeling systems in development, promises to reduce bias, improve throughput, and increase accuracy. However, this design is still in its infancy, with

data processing methods lagging. In addition, a larger working dataset is required in order to produce labeled datasets to utilize machine learning techniques for automated labeling and annotation.

Long Term Culture Monitoring Apparatus

Instrument in Context

Studying organismal movement and behavior is an important task, as movement shapes how an organism interacts its environment (Allen et al., 2018; Miyata et al., 2020). The task of tracking and following movement has observed many advances, from high-resolution microscopes with environment-controlled chambers, to animal pose tracking and movement methods for separating movement types from raw displacement, highlighting an important field of innovation (*EVOS Onstage Incubator - US*, n.d.; Gulyás et al., 2016; Soneji et al., 2024). Leveraging on these innovations, aquatic benthic organismal behavior studies has been advanced with the ability for scientists to create fit-for-purpose experimental designs that suit experimental needs, such as two channel fluorescence scanning for diatom behavioral experiments (Morelle et al., 2024).

This section details the creation of hardware originally designed for monitoring culture flasks of *Gambierdiscus* dinoflagellates. These are large lenticularly shaped cells, approximately 60-100µm in diameter, with human health importance that will be addressed in later chapters (Chinain et al., 1999; Nascimento et al., 2015). The hardware – a culture monitoring apparatus, is designed for the timelapse imaging of a large area of culture, over extended time periods, over varying lighting conditions. The apparatus is also meant to be extensible, with the lighting and image acquisition parameters easily programmable to be used in different experimental setups.

Several commercial options exist for microscopic culture monitoring using imaging, but these are often built around full-fledged microscopy platforms and motion control systems (*EVOS Onstage Incubator - US*, n.d.; *Okolab - Leica H301-LG-DLS*, n.d.). These features make them cost prohibitive and make larger fields of view difficult. The culture monitoring apparatus described here provides a low cost, fit for purpose alternative to many of these systems, for the purpose of studying movement of hundreds of individual cells in culture.

This work also includes an automated segmentation and single particle tracking pipeline, as well as a framework for training new segmentation models to be used in the automated segmentation pipeline. The resulting trajectories can be subjected to other forms of analysis, as is described in later chapters. The processing and analysis of video microscopy data is an ongoing and active field of research (Maška et al., 2023; Zimmer et al., 2006). Particle and cell tracking algorithms have become more widespread and accessible in an effort to expand access for various experimental designs (Berg et al., 2019; Ershov et al., 2022; Tinevez et al., 2017). To transform the videos into a form of data that is amenable for analysis, objects in the video usually have to be segmented from the background, and detected objects in consecutive frames are linked together and assigned to individuals (Ershov et al., 2022; Maška et al., 2023; Zimmer et al., 2006).

Many of the available software packages prioritize ease of use and adaptability of the software stack for users to accommodate a wide array of experimental designs and compute resource constraints, at the expense of performance and fine-grained control of the analysis (Tinevez et al., 2017). Due to the large amount of data involved at full resolution (~120GB per 12hr video), a custom software pipeline was implemented to reduce processing time. This

current pipeline also utilizes parallel computation, hardware accelerated deep learning, and asynchronous data transfers for optimization (*Parallel Computing Toolbox Documentation*, n.d.).

Hardware Description

The culture monitoring apparatus as described here is mechanically simple, imaging the bottom surface of a culturing vessel, over extended time periods, in programmable lighting conditions. Cameras, lighting, and samples are mounted to a frame constructed using aluminum 2020 t-slot extrusion rails. The cameras are mounted on a single movable arm on the frame, and samples platforms mounted above, as with an inverted microscope. Lighting panels are attached on the top of the frame to provide transmission lighting, but additional panels can be added in the orthogonal direction to measure the effect of directed light. 3D-printed holders are used to attach cameras and platforms for the sample holders to the t-slot frame rails. A 3D rendering of the setup is found in Figure 11.

The imaging and lighting components are controlled using a MATLAB script that allows for controllable photoperiod and imaging schedule, using generic interfaces that allows a variety of hardware components to be chosen. Lighting is synchronized to the camera acquisition using controllable relays controlled via serial over USB (12V SainSmart), and camera acquisition parameters via the GenTL interface over USB3.0. The components described in this section are an example configuration that is used in later sections of this dissertation for the study of *Gambierdiscus* movements, large cells 80-100µm in diameter.

For imaging, two Basler Pulse 2592x1944 pixels (5 megapixels) USB3.0 color cameras (Basler puA2400-14um) are used. The USB3 Vision standard is used for control of the imaging, so different cameras utilizing the same standards can be used. The cameras are mounted with a 25 mm F1.8 C-Mount lens (Serounder) with a minimum working distance of 25 cm. A 10 mm C-

Mount spacer is added, bringing the minimum working distance to approximately 11 cm. Using this optical setup, the minimum field of view (FOV) of 25.0 mm x 15.5 mm. With a sensor size of 5.7 x 4.3 mm and pixel pitch of 2.2 μm, this gives an optical magnification of approximately 0.25X and a per pixel size of 8 μm.

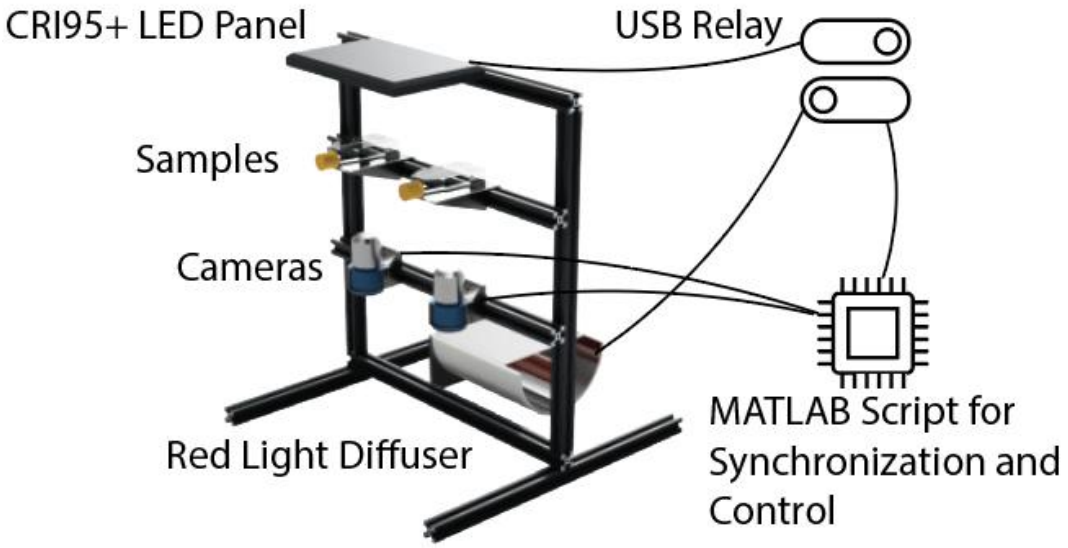

Figure 11: A three dimensional rendering of experimental setup showing the different components mounted to a 2020 aluminium t-slot T-frame.

Lighting for the day period is provided by a dimmable photography LED Panel (Viltrox) with a Color Rendering Index of 95+ mounted onto the frame above the samples, with distance used to control the light intensity cultures receive. For dark periods, samples are illuminated using a narrow band LED light by a low power programmable LED strip wrapped around a pipe and mounted within a half-pipe reflector capped with a diffuser sheet (Figure 11). For this study, dark illumination used red light (630 nm peak, 20nm FWHM) based on the absorption spectra of *Amphidinium carterae*, another benthic dinoflagellate, and evidence of a blue light cryptochrome driving the division circadian rhythm in *Karenia brevis* (Hotos & Bekiari, 2023; Stephanie A. et al., 2007). Light measurements in the night photoperiod segment did not exceed 1 μmol m^{-2} s^{-1}.

Segmentation and Analysis Pipeline

Segmentation of cells used a semantic segmentation deep learning model. Different models should be trained for either the day or night period, both of which are trained similarly. Each video frame is passed through the corresponding day or night neural network model, which generates a binary mask for cell or background pixels. The binary masks is then processed to identify and segment individual blobs. Doublet blobs are further processed classified using an support vector machine (SVM) algorithm trained on features such as shape, eccentricity, size, and aspect ratio, to identify blobs that contained multiple cells. Finally, those objects are split using a watershed algorithm, and final cell centroids are determined. MATLAB 2023B implementations of the above algorithms and methods were used in the original implementation.

Cell tracking matches cell positions across frames by solving the linear assignment problem, with a cost matrix based on Euclidean distance between points in consecutive frames, while also employing a memory window, which enables tracking of cells that sporadically drop out of view due to a variety of reasons such as random noise (Kuhn, 1955). The resulting trajectories are then smoothed by applying a locally estimated scatterplot smoothing (LOESS) on the X and Y coordinates of the cell positions across time before further analysis.

Focal Depth Determination

The start and end of trajectories in the middle of a recording period are an indicator of cells moving vertically, with cells swimming onto or leaving the substrate respectively. This is due to the limited depth of focus in microscopy, where cells outside the focal plane cannot be tracked.

The depth of the focal plane was measured in order to determine how far off the surface cells were before they were no longer detectable using the analysis workflow used for the experiments. The static stage was replaced with an adjustable translating stage with a 0.1mm

resolution, and a culture of *G. belizeanus* placed on the stage. The camera was adjusted so that the bottom of the culture flask with the cells was in focus. The stage was then moved in 0.5mm intervals, and images were taken at each interval. The images were then processed using the same detection workflow as described, and quantified.

The quantification results show a sharp dropoff in the cell detections starting at 2mm (orange line), with the size of the objects detected as cells decreasing with increasing distance from the focal plane (Figure 12). Although not a formal determination of the focal plane thickness, this provides a functional estimate of how far above the focal plane cells would need to be to no longer be detected.

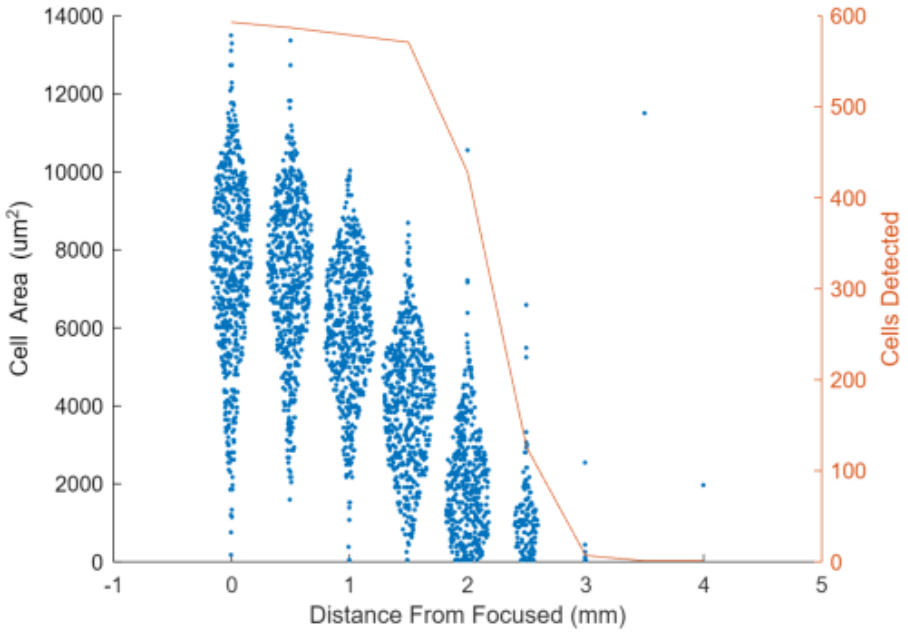

Figure 12: Violin plot of the size of the objects detected as cells (blue points), and number of objects detected (orange line, right axis)

Culture Monitoring Apparatus in Use

The culture monitoring apparatus is used extensively for the tracking of *Gambierdiscus* movements, for which a tuned analysis method and results are discussed in the next chapter. The device was able to be used for extended periods of up to 10 days, after which culture health

became a limiting factor for the length of time the experiments could be conducted. A second limiting factor is storage, although this can be alleviated by storing the active recording period on the recording device, and asynchronously transferring completed recordings onto a larger attached storage device, such as a Network Attached Storage. The simple modular nature of the apparatus also allowed for different types of experiments, such as utilizing different light colors or modified light regimes, be carried out with minimal modifications. Results also showed the ability to track upwards of 800 cells simultaneously, the highest density of cells that were tested. The apparatus was deemed to fit the required purposes, and the results in scientific context follow in the next chapter.

Chapter 3: Shedding Light on Gambierdiscus Behavior: Characterizing the Movement Behavior of the Benthic Harmful Dinoflagellate

Introduction

This chapter focuses on the movement of *Gambierdiscus*, including the movement capability, diel movement patterns, and circadian movement rhythms. *Gambierdiscus* is a genus of large benthic dinoflagellates with 19 described species and at least one described ribotype, globally distributed in tropical and subtropical regions (Litaker et al., 2010; Parsons et al., 2011; Richlen et al., 2024). These species are public health hazards because they produce potent neurotoxins known as ciguatoxins (CTXs) and maitotoxins (MTXs) (Loeffler et al., 2021; Yasumoto, 1978). These toxins accumulate in the food web, causing ciguatera poisoning (CP) when tainted fish or shellfish are consumed. CP is the most commonly reported marine biotoxin-related illness globally, with 10,000 to 50,000 cases reported annually (Chinain et al., 2010, 2021; Dickey & Plakas, 2010; Friedman et al., 2008). Incidence rates are greatly underreported because these neurotoxins produce a broad range of gastrointestinal and neurological symptoms that resemble other illnesses, as well as the lack of consistent diagnostic criteria (Dickey & Plakas, 2010; Friedman et al., 2008).

Gambierdiscus species are found in shallow (<50m), nearshore regions of tropical and sub-tropical oceans. They are found attached to a variety of substrates, including algal turfs, macroalgae, coral rubble, seagrasses, and sand (Munir et al., 2011; Parsons et al., 2011; Sheng et al., 2010; Yasumoto, 1978; Yasumoto et al., 1977). For this reason, these large-celled species (diameter 60 to 100 μm) are considered epibenthic because, though largely benthic, they are capable of using their dual flagella to swim and enter the water column (Fenchel, 2001; Sheng et al., 2010).

The epibenthic nature of cells, and the heterogeneous, highly structured characteristics of the benthos where they occur has hampered efforts to develop standardized sampling methods for these dinoflagellates (Durham et al., 2013; Erickson et al., 2012; Lobel et al., 1988; Parsons et al., 2011; Tester et al., 2022; Vassalli et al., 2018; Yasumoto, 1978; Yasumoto et al., 1977). Unlike in pelagic environments—where large volumes of water can be sampled using towed devices, net tows, or even indirectly measured via sonar— assessing *Gambierdiscus* abundances has focused on manually collecting and quantifying cell numbers from only one or a few substrate types such as macroalgae (Lobel et al., 1988; Meroni et al., 2018; Tester et al., 2022, p. 20; Villareal & Morton, 2002; Yong et al., 2018). Such approaches may not provide an accurate integrated estimate of overall cell abundances in these environments.

Recent research has used artificial substrates suspended near the benthos as a settlement surface for free-swimming cells, as a means of estimating environmental cell populations (Jauzein et al., 2016; Lee et al., 2020; Tester et al., 2014, 2022; Yong et al., 2018). Results have indicated strong correlation between cell numbers settling on artificial substrates, and those collected from nearby macroalgal substrates (Kassim et al., 2025; Lee et al., 2020; Tester et al., 2022). A sampling method that can be deployed anywhere, agnostic of local macroalgal conditions and composition, shows strong potential to be part of a cell population–based public health early warning system for assessing CP risk, which has been a research goal (Lobel et al., 1988; Tester et al., 2022; Vassalli et al., 2018).

Despite extensive research on the influence of external environmental factors such as light, temperature, salinity, and nutrients on the growth and large-scale distribution of *Gambierdiscus* (Bomber et al., 1988; Chateau-Degat et al., 2005; Fernández-Zabala et al., 2022; Kibler et al., 2012; Lee et al., 2020; Litaker et al., 2010; Loeffler et al., 2021; Tester et al., 2014;

Villareal & Morton, 2002; Xu et al., 2016; Yong et al., 2018), our understanding of the "why, where, and how" of their movement – essential aspects in the study of movement ecology, remains woefully incomplete (Mustapa et al., 2019; Nathan et al., 2008; Parsons et al., 2011; Tester et al., 2014).

Sampling studies have inferred that *Gambierdiscus* may exhibit diel migration, but it has not been directly observed or quantified (Nathan et al., 2008; Tester et al., 2022). No studies have specifically examined the movements of the different *Gambierdiscus* species and whether they vary over the diel period, or between species. This information is important for refining artificial substrate sampling protocols and identifying additional studies that may be needed. Additionally, no other studies have examined diel behavior in benthic/epibenthic dinoflagellate species. Consequently, these data have the potential to illuminate differences and similarities in the diel behavior of benthic species, which often form an important component of the benthic microbial community in shallow water oceanic environments, versus those of pelagic dinoflagellate species (Durán-Riveroll et al., 2019).

Materials and Methods

Cell Culturing and Experimental Conditions

Cultures of *Gambierdiscus* were raised in K33 media in untreated T25 culture flasks and maintained at 27 ºC on a 12-hour light:dark photoperiod at 75 μmol m^{-2} s^{-1} of light provided by a CRI95+ LED panel with a color temperature of 5600K. Species and strains used, with isolation location can be found in Table 1.

For water column swimming speeds and characterization, cells were imaged using a digital holographic microscope (DHM). For measuring diel movement patterns, cultures were

imaged using the culture monitoring apparatus described earlier, under the same lighting conditions.

Table 1: List of *Gambierdiscus* cultures used in this study, with isolation locations and strain names. All cultures were provided by Chris Holland of NOAA's Beaufort Laboratory.

Species	Strain ID	Isolation Location
G. australes	NOAA 25	Honolulu Hawaii, USA
G. belizeanus	CCMP339	St. Barthelemy, Caribbean
	Curacao9	Curacao, Caribbean
	Keys Gam2	Florida, USA
G. caribaeus	Divelfa	Carrie Bow Cay, Belize
	ST1C5	St Thomas, Caribbean
	Turks Gam4	The Turks and Caicos, Atlantic
G. carpenteri	GT4	Carrie Bow Cay, Belize
G. carolinianus	Kenny6	North Carolina, USA
	Jamaica alg2 gam22	Ocho Rios, Jamaica, Caribbean
	RROV5	Puerto Rico, USA
G. excentricus	Pulley Ridge	Florida, USA
	St Croix	St Croix, Caribbean

Characterizing *Gambierdiscus* Swimming in the Water Column with Digital Holographic Microscopy (DHM)

To measure the swimming speed of *Gambierdiscus* in the water column, a digital holographic microscope (DHM) was used. DHM is an imaging technique that uses a coherent light source for illumination, and records interference patterns. The interference patterns can be reconstructed digitally to capture three-dimensional information, overcoming the limited depth of focus in traditional light microscopy, enabling instantaneous imaging of volumes and simultaneous tracking of potentially hundreds of particles (Katz & Sheng, 2010). While DHM has been used to study the swimming behavior of pelagic dinoflagellates, it has not been used for benthic dinoflagellates such as *Gambierdiscus* (Lewis et al., 2006; Sheng et al., 2010).

This study used an in-line DHM setup with a 633nm 2mW He-Ne laser (LASOS), a spatial filter for cleaning up the laser profile (Thor Labs), and a 10X infinity-corrected

microscope objective (Nikon). Image recording was done with a global shutter 10GigE camera (Imperx) paired with a 105mm prime DSLR lens (Nikon) set to focus at infinity (Sheng et al., 2007). Cells were transferred to a standard 10mm path length cuvette, allowed to acclimate for 30 minutes, and then imaged at 20 frames per second (fps) after acclimation in the cuvette for 45-min. The imaging plane is the XZ plane as illustrated in Figure 13.

For each set of images, the XYZ centroid coordinates of each cell were extracted using the following workflow. The in-plane X and Z coordinates of the cells were determined from a minimum intensity projection of the volume, using a Sobel edge detection kernel and thresholding routine. The Y coordinates (out-of-plane) was then determined using an autofocusing routine that detects the location of the cells based on maximum image gradient (Katz & Sheng, 2010; M. K. Kim, 2010). Swimming speeds were calculated by pairing cells across consecutive frames using a linear assignment algorithm, computing the Euclidean distance traveled between frames, and dividing this distance by the time interval between frames. A probability distribution function (PDF) for the swimming speeds is calculated by binning the calculated speeds and normalizing the frequency counts, representing the likelihood of observing a cell at a given speed.

In this experiment, the swimming speeds of three species (*G. belizeanus* CCMP 339*, G. caribaeus* ST1C5*,* and *G. excentricus* Pulley Ridge, Table 1) were measured. Between 80 and 100 tracks were counted for each species over a recording period of 150s.

Lateral movement and diel pattern measurements

To measure the lateral movement of *Gambierdiscus* on the surface of the culture flask across multiple diel periods, the culture monitoring apparatus described in Chapter 2 was used. To measure the regular diel movement patterns, cells were imaged under the same 12-12 light-

dark photoperiod in which cells were cultured. Trajectories were extracted using the described video and cell position analysis described in Chapter 2.

The culture monitoring system detection noise and background drift were measured by using 75-90 µm polystyrene microbeads (1.35 g/mL, Cospheric), which served as non-motile control particles. A dilute suspension of microbeads was prepared in K33 media and placed in untreated T25 cell culture flasks to match the conditions used for *Gambierdiscus* recordings. The flasks were then imaged in the culture monitoring apparatus for a continuous 6-hour period under the same illumination, frame rate (0.2 fps), and field of view parameters. Microbead trajectories were extracted using the same workflow as for the live *Gambierdiscus* experiments. Any apparent motion in the microbead trajectories was attributed to system noise, drift, or tracking artifacts, serving to estimate a baseline used to distinguish true motility from noise in the *Gambierdiscus* recordings.

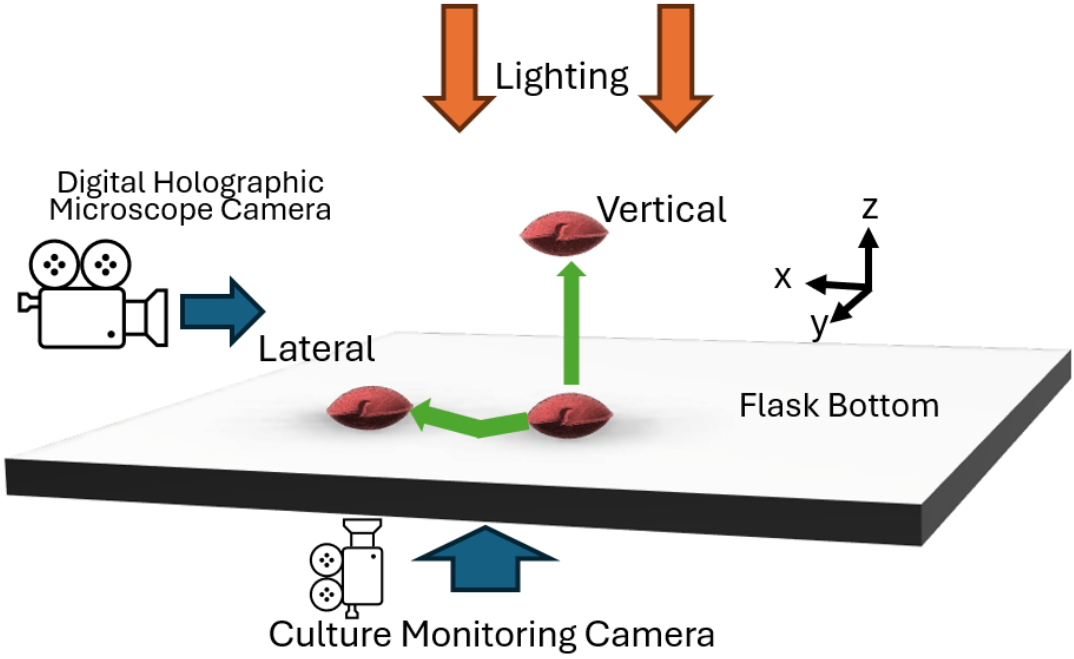

Figure 13. Schematic showing the orientation of imaging apparatuses used in the experiments. The coordinate triad (X, Y, Z axes) serves as a reference frame throughout this study. Specifically, the XY plane is coplanar with the flask bottom or water surface, and the Z axis is orthogonal to the flask bottom. Cells moving along the x-y plane are referred to as moving laterally, while cells moving in the z-direction are described as moving vertically. The

Gambierdiscus model for illustration was taken from (*Interactive Graphics and 3D Models – Harmful Algal Blooms*, n.d.).

Trajectory Analysis

For the instantaneous lateral movement speeds, the mean movement for the population at each time point *t* ($\mu_{spd,t}$), represents the average swimming speed of all cells actively tracked between time *t*-1 and *t*. It is computed by summing the speed of all cells moving between two consecutive frames and dividing by the number of active trajectories at that time point. More formally $\mu_{spd,t}$ is given by the formula

$$\mu_{spd,t} = \frac{\sum_{k=1}^{n} \sqrt{(x_{k,t} - x_{k,t-1})^2 + (y_{k,t} - y_{k,t-1})^2}}{n}$$

Where $x_{k,t}$ and $y_{k,t}$ is the *x* and *y* position of individual cell *k* in frame *t*, and *n* is the number of cells observed in frame *t*. Since the frames are captured at regular intervals, the distance moved between frames corresponds to the average cell movement over that period.

The culture monitoring system has a short depth of focus (2 mm), which means it cannot directly observe vertical movement. Instead, vertical movement was inferred from the disappearance of cells from the focal plane; trajectories that ended prematurely were attributed to cells that had moved off the surface more than 2 mm. (Figure 1). These were considered to have entered the water column and were moving vertically. The proportion of cells leaving the water surface as in relation to the total number of cells observed on the surface at a given time will be referred to as the swim metric (swimMetric).

Population Aggregate Measurements

To compare movement across species during each 12-hour photoperiod segment (day or night), two metrics were quantified for individual cells during each 12-hour photoperiod segment (day or night): average distance traveled and average displacement. Each 12-hour recording is

treated as a single observation. To calculate the average distance traveled for each observation, the total trajectory lengths of all tracked cells weas summed and divided by the number of cells. The average displacement was calculated by measuring the straight-line distance between the start and end positions of each cell, summing these values across all cells, and then dividing by the number of cells tracked. Both metrics were visualized using violin plots to illustrate their distributions across observations. For trajectories that did not span the full 12-hour period, both distance and displacement were extrapolated to the full duration by scaling linearly based on the proportion of time the cell was tracked.

To determine the proportion of the population that did not leave the surface during each recording period (day or night), the number of complete 12 hour trajectories was counted and divided by the average number of trajectories present across each recording period. Due to the recording architecture, trajectories were not extended between videos.

Linear Mixed Effects Model to Correlate Vertical and Lateral Movement

The relationship between lateral and vertical cell movements was correlated using a linear mixed effects model with the form:

$$swimMetric_{s,t,j} = \beta_{0,s} + \beta_{1,s}\,\mu_{spd,s,t,j} + \beta_{2,s}\,(diel\ time)_{s,t,j} + \varepsilon_{s,t,j}$$

In this model, β_1 represents the linear correlation between the two movement types, while β_2 accounts for seasonality correlations between the diel time and vertical swimming.

Where:

- The subscript *s* denotes the species, *t* represents time since experiment start, *j* represents the replicate number.
- *swimMetric* is the proportion of cells leaving the surface at time t, which is binned across ten minutes

- $dielTime_{s,t,j}$ denotes the diel time, or time since the start of the 24-hr diel photoperiod, starting with the light period.
- $\beta_{1,s}$ and $\beta_{2,s}$ are the fixed-effect coefficients for μ_{spd} and *dielTime*, respectively, for each species
- And $\varepsilon_{s,t,j}$ represents the residual error.

Principal Coordinate Analysis of Diel Movement Periods

Principal Coordinate Analysis (PCoA) of the diel movement periods was conducted to visualize similarities in the diel movement patterns of the cells. The instantaneous population movement speed μ_{spd} at each time step *t* across a single 24-hour diel photoperiod is considered a single observation. Pairwise Euclidean distances between these time series were calculated, and PCoA was applied to the resulting distance matrix to generate a lower-dimensional representation of the variation across observations (Bakker, 2023; Javed et al., 2020). Since a Euclidean distance metric was used in the PCoA, this result is equivalent to performing principal component analysis (PCA) on the data (Bakker, 2023; Javed et al., 2020).

More formally, with *n* observations across all species and strains, each observation i is a 24-hr time series for μ_{spd} with T timepoints representing a full light/dark photoperiod represented as $x_i \in \mathbb{R}T$. The full dataset can then be described as $X \in \mathbb{R}n \times T$. The distance matrix used for the PCoA $D \in \mathbb{R}n \times n$ is defined as:

$$\boldsymbol{D} = [d_{i,j}]_{i,j=1}^{n}$$

Where the pairwise distance ($d_{i,j}$) between two diel periods x_i and x_j is given by the equation:

$$d_{i,j} = \| \boldsymbol{x_i} - \boldsymbol{x_j} \|_2 = \sqrt{\sum_{t=1}^{T} (\mu_{spd,i,t} - \mu_{spd,j,t})^2}$$

The resulting PCoA plot provides a visual representation of the relative similarity between movement patterns over diel periods, enabling comparisons across species, strains, or experimental conditions.

Hierarchical Clustering of Diel Movement Periods

Hierarchical clustering was conducted using the UPGMA (unweighted pair group method with arithmetic mean) method for aggregating clusters. This method groups observations based on the pairwise Euclidean distance matrix D as defined above. UPGMA iteratively merges clusters by minimizing the average pairwise distance (average linkage) between all elements in the two clusters being considered. The clusters are then visualized using a dendrogram with each leaf representing one sample, and the branch length representing the average Euclidean distance at which the clusters are joined. Both PCoA and hierarchical dendrograms reveal relationships between the diel movement patterns in the cells, allowing identification of groups of similar movement profiles across species, strains, and experimental replicates.

Image processing and data analysis were carried out in MATLAB (R2023a), except for the linear mixed effects model, which was calculated in R (4.4.2) using the *nlme* package.

Gambierdiscus Circadian Rhythm Measurements

To measure the presence of an endogenous circadian rhythm regulating movement, cultures of *G. australes*, *G. belizeanus* and *G. carolinianus* were imaged using the cell culture monitoring apparatus under free-running 24 hour lights on or off conditions. For each experiment, two periods of 12-hour light/dark cycles were recorded to ensure that the behavior of cells matched the regular diel cycle measurements, before changing the photoperiod to full 24-hour light (L) or dark (D) periods.

Impact of Light Color on Movement Behavior

To measure the impact of different light levels on the movement patterns of the cells, the CRI95+ LED full spectrum white light panel was replaced with an RGB selectable panel, with 488, 532, or 633nm LED lights (Viltrox RB10). Light flux levels were maintained at the same 75µmol m^{-2} s^{-1} as with the white light. *Gambierdiscus australes*, *G. belizeanus* and *G. carolinianus* were imaged under red (633nm), blue (488nm), and green (532nm) light during the day conditions. For image segmentation of the cells in the day or lights on recording period, the different lighting colors were adjusted to the same color by scaling the mean of the red, green, and blue channels to an 8-bit value of 128, providing a roughly grayscale image, before image segmentation using similar methods to above. The remainder of the analysis remains the same.

Literature Survey of *Gambierdiscus* Cell Morphometrics

To compare movement behavioral patterns with morphology for the *Gambierdiscus* species studied, published measurements for *Gambierdiscus* cell dimensions from 8 peer-reviewed studies were compiled (Bravo et al., 2019; Chinain et al., 1999; Fraga et al., 2011; Litaker et al., 2009; Nascimento et al., 2015; Ramos-Santiago et al., 2024; Tudó et al., 2020; Vacarizas et al., 2018). The dorso–ventral depth, transdiameter width, and apical–antapical length, as well as standard deviation in measurements were recorded. Due to the dorso-ventral flattening of *Gambierdiscus* and how they rest on surfaces during measurement, fewer length measurements were obtained from the literature (Bravo et al., 2014). For visualization, the depth and width measurements, along with standard deviations, were plotted in a scatter plot. A 3D scatter plot was used to visualize samples where length was also available.

Results

Characteristic Movement Behaviors and Gallery of Movement

This section presents representative trajectories of individual *Gambierdiscus* cells and characterizes their movement. Digital holographic microscopy (DHM) observations revealed anteroposteriorly compressed lenticular *Gambierdiscus* swims using two different methods. The first swimming style has a helical swimming path, where net displacement is along the central axis, and the apical/antapical axis of the cell is orthogonal to the direction of displacement. This helical swimming path had a helix pitch of -330µm, with the negative sign indicating a left-handed helix, and a radius of 120µm, but the low swimming frequency made getting population aggregates difficult. The second swimming mode is a more direct linear swimming trajectory coupled with axial rotation, where the cell's apical/antapical body axis is aligned with the path of motion (Figure 14A) (Bravo et al., 2014; "Trouble in the Tropics," n.d.).

Using the culture monitoring apparatus, cells on the surface of the flasks can also move in one of two modes: a lateral movement along the surface, or a vertical movement into the water column. Examples of the helical swimming, lateral, and vertical motions exhibited by *Gambierdiscus* are illustrated in Figure 14A-C respectively. Supplementary videos further illustrate the different movement modes (Appendix 4 - Appendix 7).

The movement speeds of three species, *G. belizeanus, G. caribaeus, and G. excentricus* in the water column based on DHM (Figure 14D) and lateral movement speed in the flask based on the culture monitoring apparatus (Figure 14E) are presented as probability distribution functions (PDF). The PDF shows a long-tailed log-normal distribution for water column swimming speed, which is expected for swimming organisms (Lisicki et al., 2019). In contrast, the lateral surface movement speed distribution reflects that while the cells appear almost

stationary at any given moment, they are slowly moving along the surface over time. Figure 14F, G demonstrates increased net displacement time periods relative to non-motile microbeads, indicating movement.

There were marked differences in the amount of lateral movement and displacement between the day and night periods in some species (*G. australes, G. belizeanus, G. carolinianus* and *G. carpenteri*). In contrast, others showed little movement (*G. caribaeus* and *G. excentricus*) (Figure 14F, G). Most species exhibited more lateral movement in the day except for *G. carolinanus* (Figure 14F).

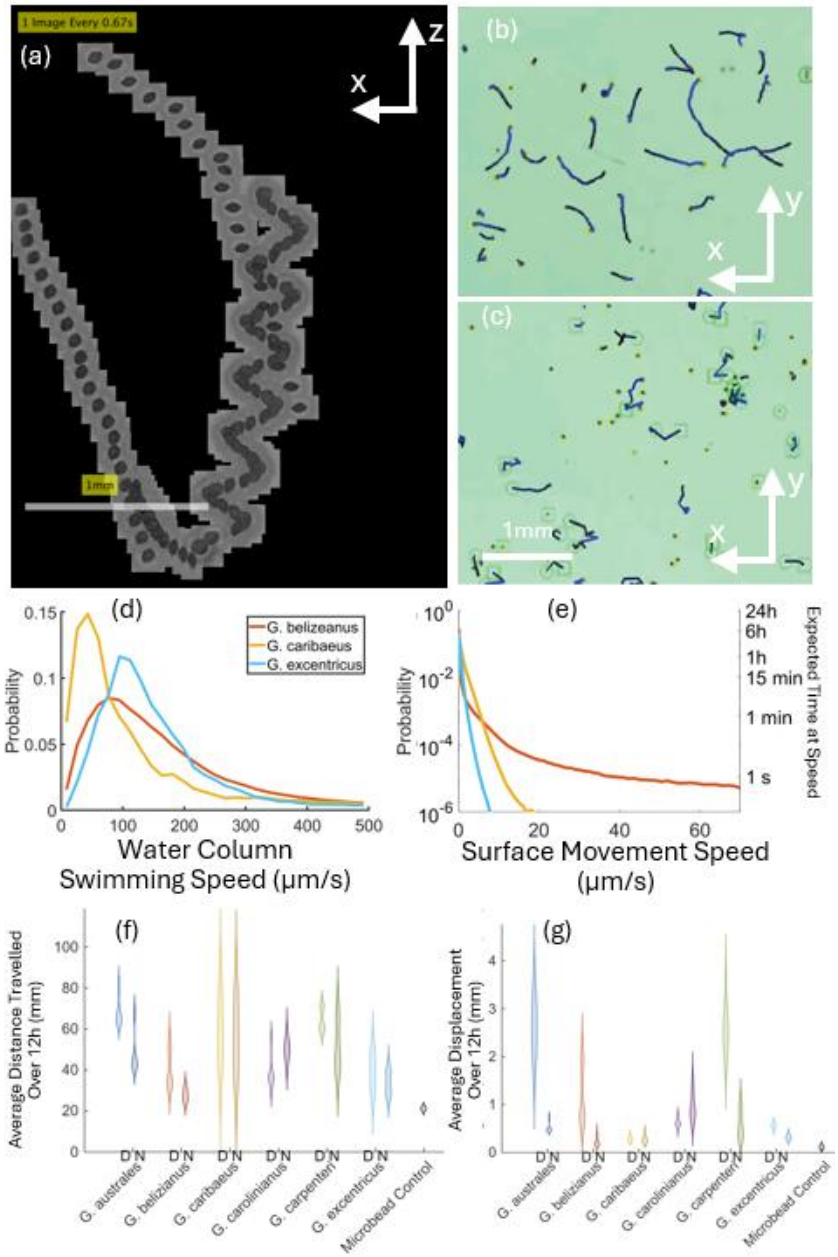

Figure 14: Gallery of movement for *Gambierdiscus*. (A) Montage of *G. caribaeus* cells swimming as captured by digital holographic microscopy, illustrating distinct swimming modes—helical and linear. Each sub-image represents a digital reconstruction of the hologram at the cell's out-of-plane location, taken at 0.67-second intervals. Sub-images are overlaid on a black background to show the temporal progression of individual cells. (B) Lateral movement of *G. carolinianus* as captured by the long-term culture monitoring apparatus. Blue lines are the cell trajectories over a maximum of 150s. The long smooth tracks indicate that cells were captured travelling over the bottom surface of the flask. (C) Vertical cell movements of *G. belizeanus* were captured similarly to B. The shorter and more broken-up blue lines indicate cells moving quickly and then leaving the surface, exiting the focal plane of the imaging system, around 3mm off the surface. The green circles and squares indicate track starts and ends respectively, indicating cells entering or leaving the focal plane. (D) Probability distribution function (PDF) for movement speed of cells swimming in the water column as measured by digital holographic microscopy. (E) PDF for the movement speed of cells moving laterally on the flask surface as measured by the culture monitoring apparatus. For additional context, the secondary y-axis provides the estimated time that a cell would spend moving at the corresponding speed on the x-axis over the course of a 24-hour day. (F) Violin plot of average distance

traveled by individual cells during each 12h recording period. The D and N labels indicate the lighting condition (Day or Night respectively). (G) Violin plot of average displacement observed for individual cells during each 12h recording period.

Diel Movement Patterns

Using a long-term cell culture monitoring apparatus, cultures were monitored for up to seven full diel days with regular day/night cycles. There were distinct patterns in both lateral and vertical cell movement (Figure 15). For example, several species—including *G. australes*, *G. carpenteri*, and *G. excentricus*—exhibited increased lateral movement during the latter part of the light period, although the magnitude varied among species. While there was some interspecies variation in total movement, the values were generally within the same order of magnitude (Figure 14F, G). Notably, cells traversed centimeter-scale distances through lateral movement alone within a single 12h recording period (Figure 14F, G).

The most marked changes in movement immediately followed transitions between light and dark conditions. For instance, *G. carolinianus* began moving laterally shortly after both the light-to-dark (L/D) and dark-to-light (D/L) transitions. In contrast *G. belizeanus* began moving laterally only after the D/L transition. Furthermore, the data indicate that both *G. belizeanus* and *G. carpenteri* increased their vertical movement following the D/L transition (Figure 15), and that *G. australes*, *G. belizeanus*, and *G. carpenteri* showed an increased tendency to move before the transitions, especially the L/D transition.

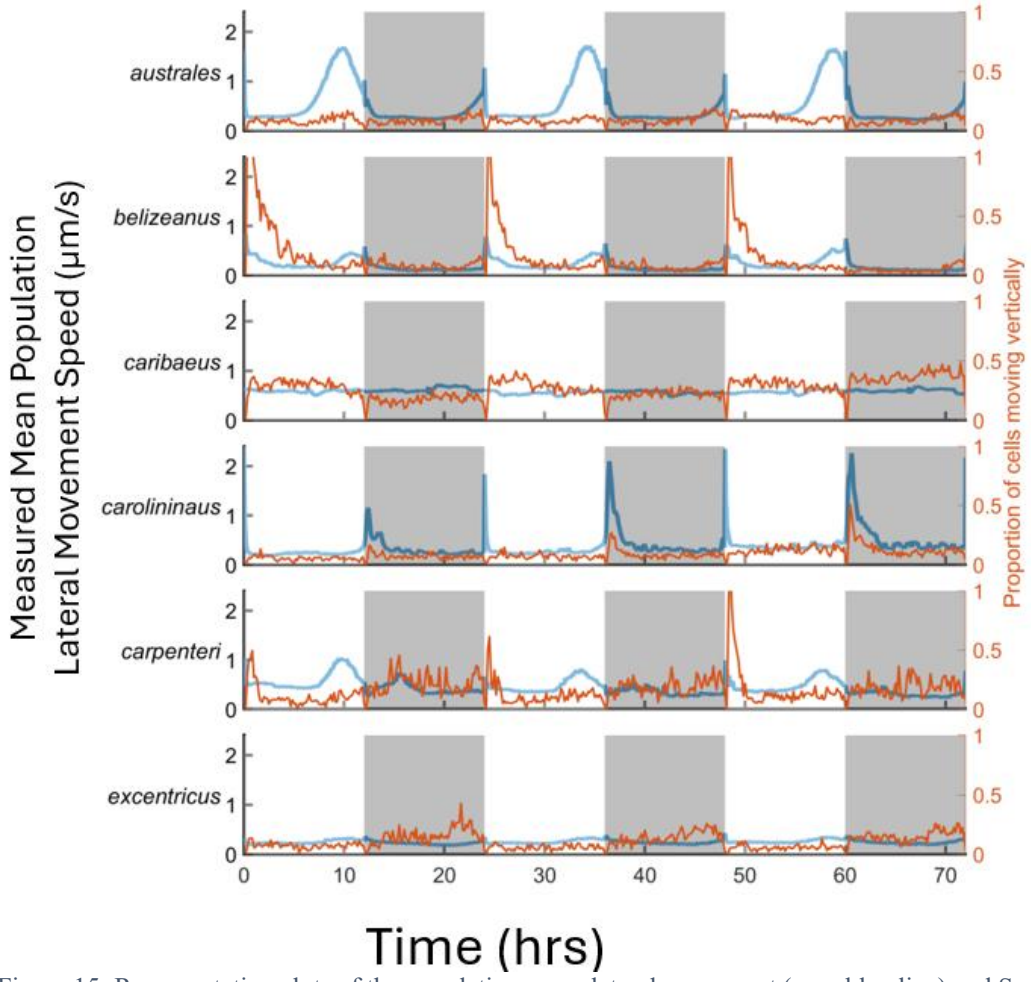

Figure 15: Representative plots of the population mean lateral movement (μ_{spd}, blue line) and Swim Metric, the proportion of total cells entering the water column, as defined as 3mm above the flask bottom, within a 10-minute window (orange line) across three days for all six *Gambierdiscus* species. The dark areas indicate the dark period of a 24 h photoperiod.

There were also differences between species in the proportion of cells that did not leave the surface between the species, as well as whether they preferred to leave the surface during the day or night photoperiod (Figure 16). Species like *G. carolinianus* and *G. excentricus* had the lowest proportion of cells leaving the surface across the recording periods, with more than 80% of cells not leaving the surface across each 12-hour recording period, while *G. belizeanus* had more than half the cells leaving the surface during the day.

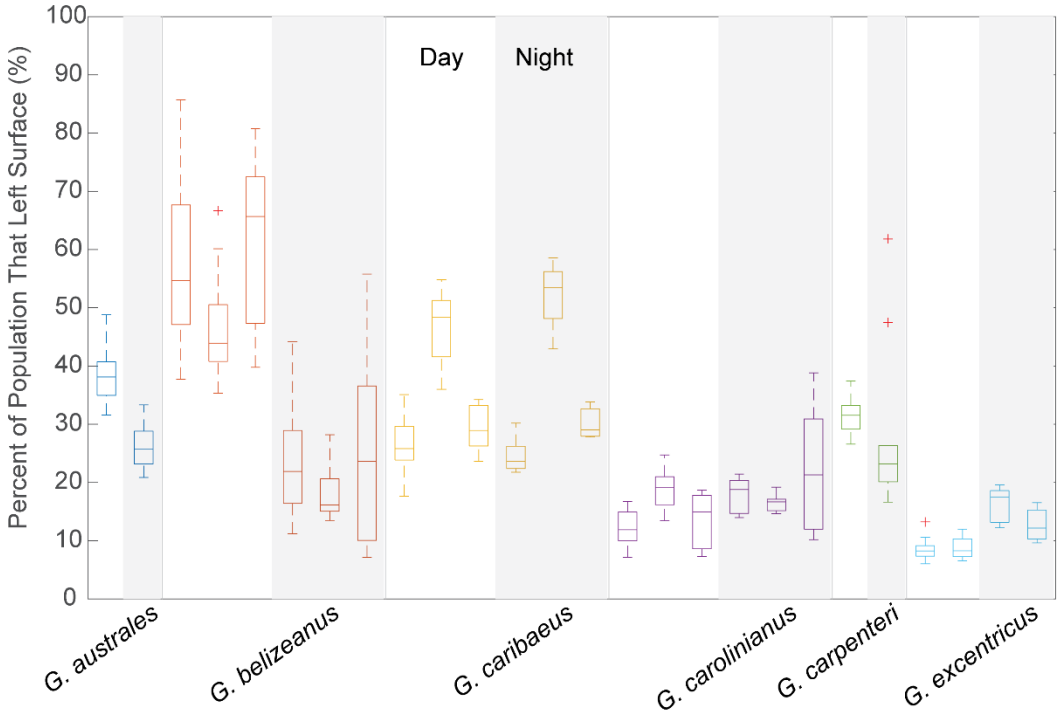

Figure 16: Boxplot of the percentage of cells that left the surface across each 12h recording period. The different species are listed in order, split into individual strains within each species. Each boxplot shows n=10 recording periods across 2 biological replicates over 5 days. Day and night recording periods are split into white and dark patches, respectively.

The linear mixed effect model analysis revealed marked differences in the β1 coefficients among species (Table 2, Figure 17). A positive β1 indicates that an increase in lateral movement is associated with an increase in the proportion of cells leaving the surface. Furthermore, a steeper slope indicates that a smaller change in lateral movement corresponds to a larger shift in vertical movement, and vice versa.

Table 2: Slope coefficient (β1) and significance of the mixed-linear effects model between the proportion of cells swimming and lateral movement speeds of cells swimming binned within 10-minute windows. The different coefficients for the species suggest that the linear correlation differs across species.

Species	**β_1 Slope Coefficient**	**Significance (p)**
G. australes	0.028	>0.001
G. belizeanus	2.101	>0.001
G. caribaeus	0.056	0.18
G. carolinianus	0.111	>0.001

G. carpenteri	0.511	>0.001
G. excentricus	-0.025	>0.001

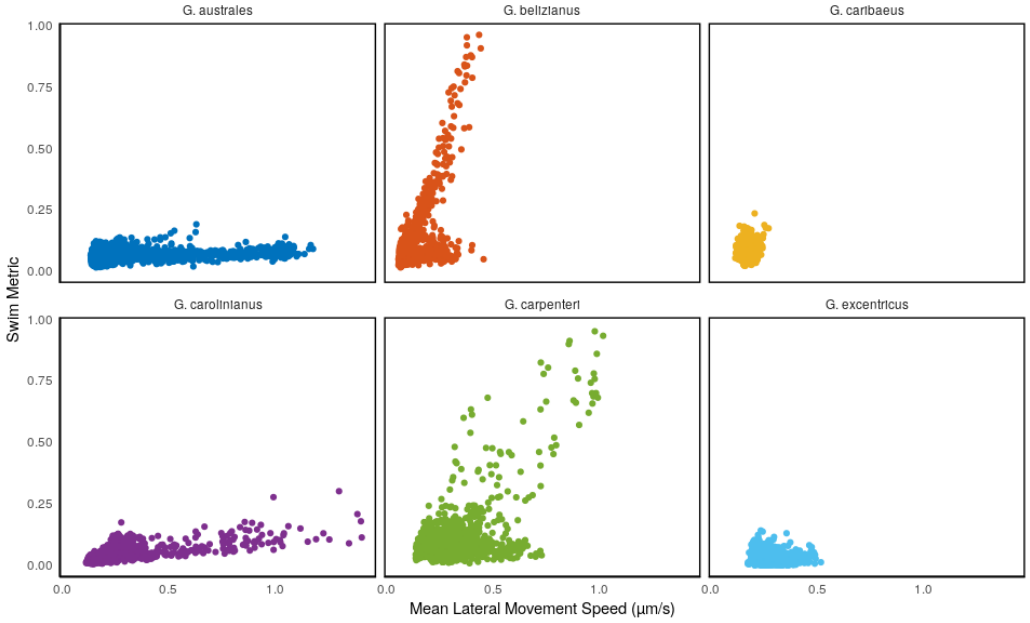

Figure 17. Scatter plots showing correlation between mean lateral movement and proportion of cells leaving surface, binned across 10-minute windows.

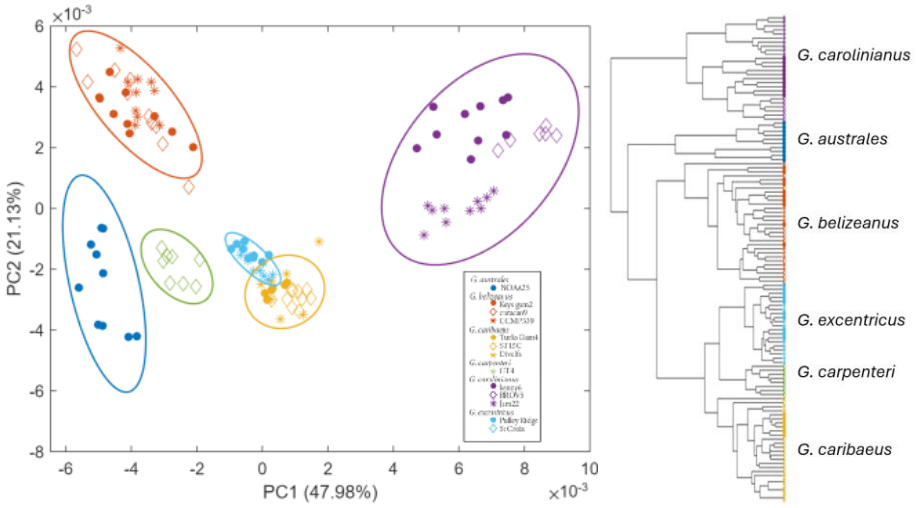

Figure 18: Clustering of the movement patterns. (A) Principal Coordinates Analysis (PCoA) of diel movement patterns, using a Euclidean distance metric for time series. Points closer together have more similar patterns in movement, highlighting the interspecies differentiation and intraspecies clustering. Ellipses indicate the 95% confidence intervals for the clusters. (B, right), Dendrogram showing the results of hierarchical clustering of the diel movement patterns.

The differences in the diel movement patterns were visualized using a Principal Coordinates Analysis (PCoA), and hierarchical clustering on the time series data (Figure 18A, B). Four out of the six species exhibited distinct, non-overlapping 95% confidence intervals in

the PCoA space, with only *G. caribaeus* and *G. excentricus* showing some overlap (Figure 18A). In the dendrogram, each species formed its own cluster. Among the four species that were tested with multiple strains (*G. belizeanus, G. caribaeus, G. carolinianus, and G. excentricus*), only *G. carolinianus* exhibited notable inter-strain clustering. Still, the species cluster remained clearly distinct from the other species - the hierarchical clustering shows no distinct clades for the different strains, except in *G. carolinianus* (Figure 18B). This suggests that inter-strain differentiation is smaller than inter-species differentiation, indicating that the behavioral changes are likely to be consistent within the species, and not linked to strain or isolation geography (Table 1).

Circadian Rhythm Regulation In Absence of Photoperiod *Zeitgebers*

All three species showed changing movement patterns even in free-running lighting conditions, where cells are not given light cues for time. All three species showed strong periodic increases in movement under 24-hour dark conditions, but only *G. carolinianus* continued strong periodic movement under constant light conditions. *Gambierdiscus australes* and *G. carolinianus* began cyclic movement within the first "missed" light period, but *G. belizeanus* took an additional 24 hours to begin the cycle (Figure 19).

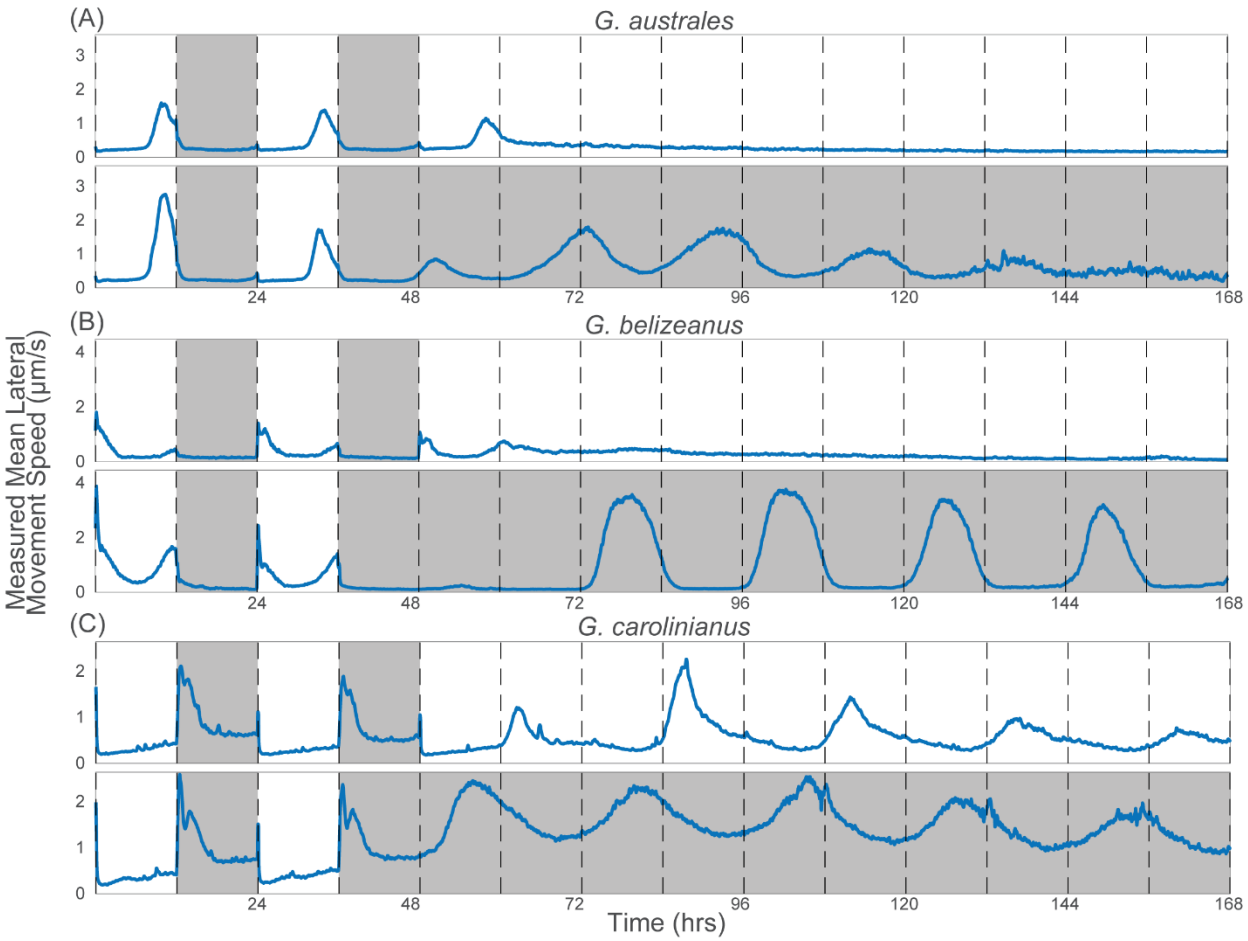

Figure 19: Movement patterns of three *Gambierdiscus* species across free-running light conditions with (A) *G. australes*, (B) *G. belizeanus*, (C) *G. carolinianus*. The first 48 hours are the baseline for the amount of movement over the diel period, where the light and dark panels indicate the day or night recording conditions, and the dotted lines indicate the start and end of each 12-hour recording period.

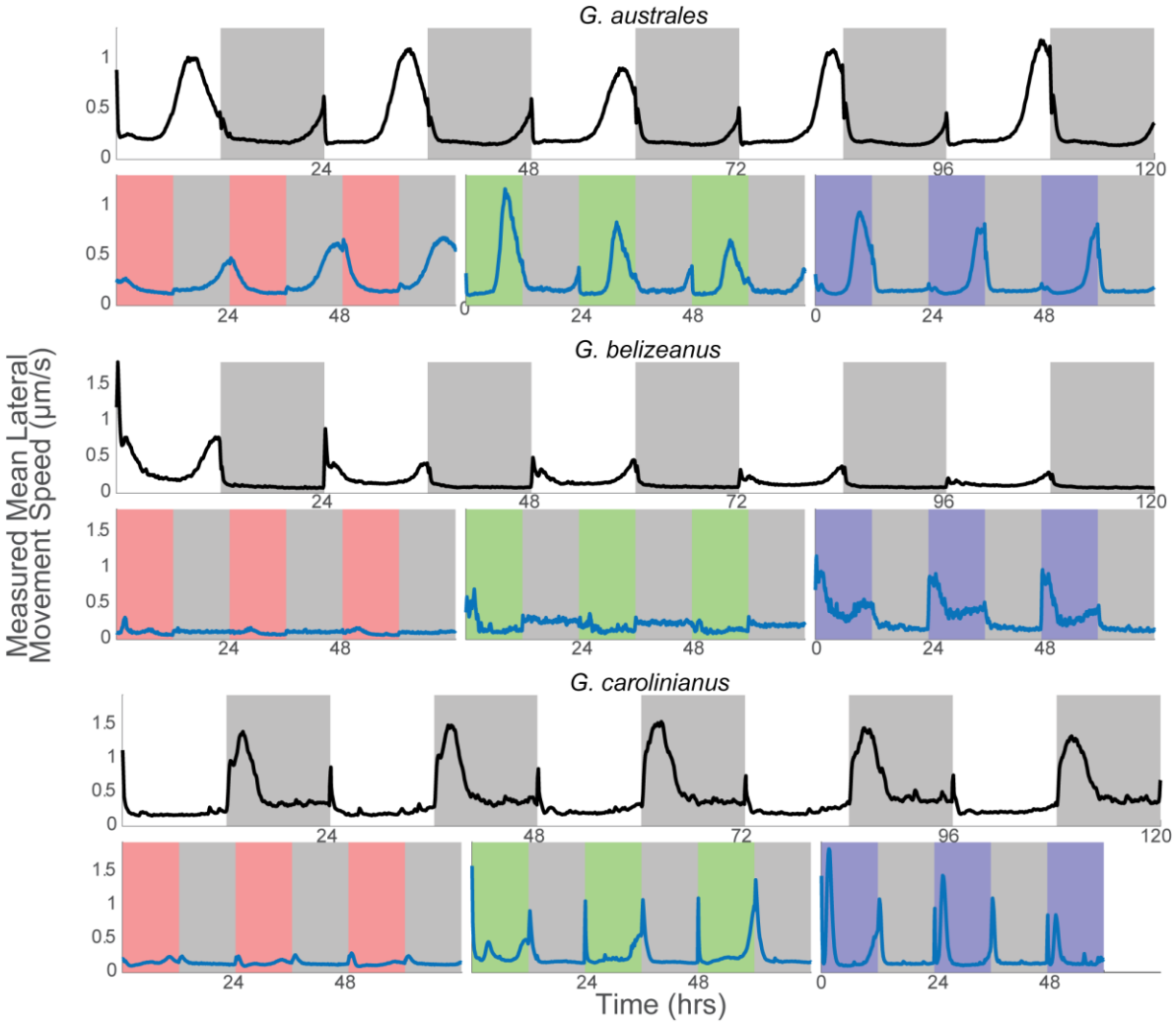

Figure 20: Impact of different light colors on movement of three *Gambierdiscus* species, (A) *G. australes*, (B) *G. belizeanus*, and (C) *G. carolinianus*. Results from the full spectrum white light controls are shown with the white panels, and the red, green, and blue panels correspond to the red, green, and blue light conditions respectively.

The impact of different light colors on the three species showed a consistent decrease in movement during the day period with red light, although this impact was slightly reduced in *G. australes*, which still maintained movement during the dark period. Green light did not shift the movement timing of *G. australes* and *G. carolinianus*, but *G. belizeanus* appeared to stop moving, as in red light. Blue light showed little behavioral change for *G. australes* and *G. belizeanus*, but in *G. carolinanus* it elicited an additional burst of movement 2-3 hours after the onset of each blue light period (Figure 20).

Discussion

Gambierdiscus Movement Capability

This study characterizes the water column swimming speed of *Gambierdiscus* species (Figure 14E). These speeds tend toward the lower end of speeds found for other dinoflagellates, which can range from 100-500µm/s(Kamykowski, 1986; Kamykowski et al., 1992; Lewis et al., 2006; McKay et al., 2006). Given the relatively larger size of *Gambierdiscus* cells compared to other dinoflagellates (from 60-100µm in diameter, Figure 21), these cells are notably slow swimmers when considering the body lengths travelled per unit time (Litaker et al., 2009).

Two Observed Swimming Modes in Gambierdiscus

Gambierdiscus cells exhibit two distinct swimming modes, as illustrated in Figure 14B. In the linear swimming mode, the cell maintains the typical dinoflagellate swimming orientation, travelling in a direction aligned with the epicone and orthogonal to the plane of the cingulum (Fenchel, 2001; H. Jiang et al., 2018; Kamykowski et al., 1992; Lewis et al., 2006; Sheng et al., 2007). This swimming mode, however, loses the "whirling" helical trajectory for which dinoflagellates are eponymous, instead travelling in an almost straight path while retaining its rotation (Fenchel, 2001). In contrast, the larger helical rotation preserves the helical trajectory, yet reorients the cell so that the sulcus faces the direction of travel and the epicone points normal to the helix's center—a marked departure from the orientation seen in other dinoflagellates (Fenchel, 2001).

Like other dinoflagellates, *Gambierdiscus* possesses two dissimilar flagella: the transverse and longitudinal flagella arising from the cingulum and sulcus respectively (Durand-Clement, 1987; Xu et al., 2021). In most dinoflagellate swimming, the transverse flagellum's circular beating provides propulsion, while the longitudinal flagellum steers the cell (Leblond &

Taylor, 1976; Miyasaka et al., 2004). Recently in *Dinophysis,* it was observed that the longitudinal flagella are likely to provide propulsion for the cell, as motility stopped when beating of the flagella did (H. Jiang et al., 2018). Here, although not directly observed, it can be hypothesized that the two modes of swimming arise from use of the different flagella, with the transverse flagellar beating generating the linear swimming, and the longitudinal flagellum in use when swimming the larger helical paths (Miyasaka et al., 2004).

From an ecological standpoint, the larger helical path has been seen in many protists as a way for cells to better sense and respond to chemical gradients in the environment by means of helical klinotaxis, while the straighter linear swimming may be a more efficient method of displacing the cell from one place to another (Abdelgalil et al., 2022; Fenchel, 2001; Long et al., 2003). Our results were inconclusive as to whether the cell uses either preferentially.

Lateral Movement on Surfaces for Gambierdiscus

Gambierdiscus cells move significantly more slowly when traversing laterally along a substrate than when swimming through the water column (Figure 14E, F). Still, this lateral movement should still not be discounted, since from our direct observations (Figure 15A) and previous experiments (Mustapa et al., 2019; Nakahara et al., 1996; Parsons et al., 2011), *Gambierdiscus* cells predominantly reside on surfaces, with only bursts of movement into the water column.

The intermittent movement behavior extends to lateral movement, occurring only in bursts during the day, while the cells spend most of the day with minimal observed activity (Figure 15A). Cells were measured to be able to traverse centimeter-scale distances (Figure 15C), and given that microscale heterogeneity of the benthos can result in highly variable local microhabitats in terms of light, nutrients, and flow, movement at this scale can be expected to

strongly affect the cell's environment (Brakel, 1979; Kiih & Jorgensen, 1994; Schenone et al., 2024). This finding is supported by field observations, which show that *Gambierdiscus* cells attached to the same piece of macroalgal substrate exhibit non-uniform photosynthetic yield and experience different levels of light stress (Villareal & Morton, 2002). This illustrates that the lateral movement, though small in terms of absolute scale, is still ecologically relevant to the cells. We also note that *G. excentricus* appears to be relatively inactive, both in terms of lateral and vertical movements(Figure 15, Figure 16, Figure 17F). This is in line with previous observations, that *G. excentricus* is a more sessile species (Fraga et al., 2011, personal communications with Chris Holland).

Gambierdiscus Attachment and Leaving the Boundary Layer

In our experiments, cells were rarely observed to firmly attach to the substrate or form mucus layers—except in older cultures nearing senescence or in rare instances, where cells exhibited circular trajectories indicating tethering (personal observations). Previous studies have established that *Gambierdiscus* species are not obligate epiphytes, do not always attach to substrates, and that factors such as fluid shear or algal host type may influence attachment (Nakahara et al., 1996; Parsons et al., 2011; Rains & Parsons, 2015). Although the circular trajectories have been documented previously, their frequency has not been well characterized; in our study, such behavior was observed only sporadically over weeks (Nakahara et al., 1996; Rains & Parsons, 2015). In our studies, cells were in still water and allowed to rest on a flat surface, which may have precluded the need for firm attachment, but that does not explain why cells in senescent cultures attached via a mucus film. Future studies might explore whether nutrient stresses trigger mucosal attachment, and whether cellular behavior shifts depending on whether cells are in a mucosal matrix.

The proportion of cells that did not leave the surface over the course of each 12h photoperiod varied from species to species, with *G. belizeanus* leaving the surface almost daily, while only a small proportion of cells from species like *G. excentricus*, *G. carolinianus* and *G. caribaeus* would leave (Figure 16). Similarly, the relationship between lateral and vertical movement differs among species (Figure 17 and Table *2*). These findings suggest that cells exhibit distinct preferences regarding whether they move predominantly along the substrate or detach and enter the water column. Data from this study shows the differences in the species' motility, with species like *G. excentricus* and *G. caribaeus* exhibiting less lateral movement than *G. australes* and *G. carolinianus,* or less vertical movement than *G. belizeanus* and *G. carpenteri* (Figure 17). Such differences in motility further distinguish the species in terms of their behavioral capabilities.

In this study, cells were characterized as having left the substrate when they traveled approximately 2–3 mm above the flask surface, thereby leaving the focal plane of the imaging system. This distance exceeds both the previously reported tether lengths for *Gambierdiscus* (Nakahara et al., 1996), and the typical flow boundary layer thickness observed in reef environments under low to medium flow (Larkum et al., 2003; Martins et al., 2024). Although the static, still-water conditions in the laboratory experiments did not produce a boundary layer, our results suggest that cells leaving the surface were capable of leaving the substrate and entering into bulk flow that could facilitate their dispersal. In future studies it would be useful to examine how the presence of shear forces in flow-through chambers and variations in algal substrate influence the attachment and detachment dynamics of *Gambierdiscus* cells.

Diel Movement Patterns

Our results reveal that *Gambierdiscus* exhibited distinct species-specific diel movement patterns (Figure 15A). Diel vertical migration (DVM) in pelagic dinoflagellates is well established in both field and laboratory experiments, as has the daily migration of benthic diatoms within the vertical layers of the substrate (Baek et al., 2009; Barnett et al., 2020; Haro et al., 2019; Hasle, 1950; Heaney & Furnass, 1980; Kamykowski et al., 1998). This study represents the first quantitative assessment of diel movement on and away from a substrate for the genus *Gambierdiscus*.

The DVM in multiple species across a wide variety of taxa has been linked to different ecological and survival strategies, including responses to temperature and salinity stresses, reduced inter-species competition, and predator avoidance. DVM is also an example of how movement behavior during the day affects the ecology of an organism (Bollens et al., 2012; de Souza et al., 2014; Ji & Franks, 2007).

Species-Specific Differences

The results demonstrated that the six *Gambierdiscus* species studied exhibited distinct movement patterns. Specifically, differences emerged in lateral movement patterns, amounts(Figure 15, Figure 18), and the frequency and timing of cells moving away from the bottom surface of the experimental chamber (Figure 3, Figure 17). In other dinoflagellates, *Ceratium furca, C. tripos,* and *C. fusus,* pelagic co-occurring species from the same genus, different swimming abilities, responses to salinity gradients, and DVM schedules are thought to confer different competitive advantages based on prevailing environmental conditions, and the potential for niche differentiation (Baek et al., 2009; Jephson & Carlsson, 2009). Although the

ecological benefits of these movement behaviors in *Gambierdiscus* remain to be fully understood, our results suggest that similar mechanisms may be operative.

The intra-species clustering demonstrated how strongly the six species used in this study can be separated purely on the basis of lateral movement timing (Figure 18). By treating each diel day as its own time series, our approach enabled effective clustering, dimensionality reduction, and visualization of the data. This approach also provides a method to quantitatively measure differences between them (Ahmed et al., 1975; Castells et al., 2005; Javed et al., 2020). This established our methods as a strong framework for identifying shifts in movement behavior across different species, photoperiods, and environmental parameters.

Schedule of Movement Across the Diel Periods

Several *Gambierdiscus* species initiated movement several hours before the L/D (light-to-dark) transition, suggesting the presence of an intrinsic molecular clock (Figure 15A). Timekeeping mechanisms have been demonstrated in *Gambierdiscus* and other dinoflagellates, although the exact mechanisms have not yet been established due to the enigmatic biology of dinoflagellates (Christianson & Sweeney, 1972; Judd & Place, 2022; Stephanie A. et al., 2007; van Dolah et al., 1995).

We compared the movement patterns of *Gambierdiscus* with other potential influencing factors, but no clear pattern or correlation emerged. In particular, cell shape was not clearly correlated with the movement patterns. Published cell lengths, depths, and widths for the six species (Figure 21) indicate that aspect ratios for cells in the apical view are similar, with cell depth and length showing slight variation (Figure 21A). Greater variability is observed in the degree of anteroposterior compression, with *G. australes* and *G. excentricus* being the most compressed, and *G. caribaeus* and *G. carolinianus* being the least (Figure 21B). Despite these

differences, the pairs did not exhibit similar movement schedules (Figure 21)**.** Although cellular morphology in *Gambierdiscus* is highly variable—even within a single strain—consistent movement schedules were observed within each species across multiple replicates and strains. (Bravo et al., 2014; Fraga et al., 2011; Ramos-Santiago et al., 2024). This suggests the observed movement behaviors are not strongly dependent on cell morphology.

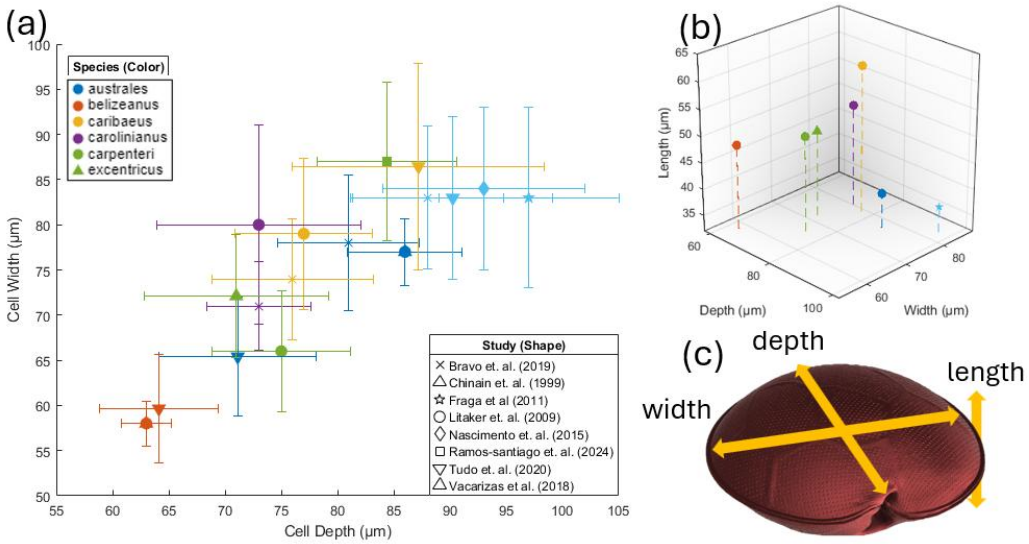

Figure 21: Cell morphometrics for the *Gambierdiscus* species studied. (A) Cell depth (dorso/ventral distance) and width (transdiameter) measurements available from the literature (Bravo et al., 2019; Chinain et al., 1999; Fraga et al., 2011; Litaker et al., 2009; Nascimento et al., 2015; Ramos-Santiago et al., 2024; Tudó et al., 2020; Vacarizas et al., 2018). Markers indicate mean measured value, and error bars are standard errors as published within the corresponding studies. (B) Cell measurements, including length measurements (apical/antapical distance) where available, were taken from (Chinain et al., 1999; Fraga et al., 2011; Litaker et al., 2009). (C) diagram illustrating the different measurements on the anteroposteriorly compressed *Gambierdiscus* cell. 3D model taken from (*Interactive Graphics and 3D Models – Harmful Algal Blooms*, n.d.).

Furthermore, species within the same phylogenetic clade based on ribosomal DNA (*G. australes* and *excentricus* in clade IV, *G. caribaeus* and *carpenteri* in clade II) did not exhibit similar movement patterns compared to those across clades (Ott et al., 2022). Similarly, species that had similar metabolomes by hierarchical clustering (*G. excentricus* and *G. carolinianus*) displayed markedly different movement behaviors (Yon et al., 2024). The timing of cell division was also considered; however, literature indicates that, like most dinoflagellates, *Gambierdiscus* divides during the latter part of the night, and no species-level differences in division timing have

been reported (Baek et al., 2011; Bravo et al., 2012, 2014; Figueroa et al., 2007; Jephson & Carlsson, 2009; Jia et al., 2019; Stephanie A. et al., 2007; van Dolah et al., 1995; W, 1981). This phased division was also observed to be maintained for years without the need for synchronization (Bravo et al., 2014). Without evidence of species level differentiation in cell division timing and responses, it cannot account for the differences in movement schedules.

Our observations also noted different responses to the light/dark transitions among species (Figure 15A). While some of these responses might be attributed to startle reactions to changing light conditions—a phenomenon previously documented by Nakahara et al. where illumination caused cells to detach and swim freely (Nakahara et al., 1996), this work was done before more species of *Gambierdiscus* were recognized, and thus this startle response may not be consistent across the genus (Faust, 1995; Litaker et al., 2009; Nakahara et al., 1996).

At present, no clear pattern has emerged from the literature or our data regarding the factors driving the different movement schedules in *Gambierdiscus*. Further studies are required to elucidate the ecological implications of these diel movement patterns, which will ultimately enhance our understanding of the species' biology and environmental adaptations.

Impact on Sampling

The presence of a diel migration cycle in *Gambierdiscus* strongly supports the idea that sampling methodologies utilizing artificial substrates require a full 24-hour period of deployment (Tester et al., 2014). This data also aligns with previous results showing that cell counts tend to plateau after a 24-hour period (Tester et al., 2014). Since the majority of cell movement occurs near dawn (*G. belizeanus*) or dusk periods (the majority of species tested), sampling and collection of both artificial (AS) and natural (NS) substrates during the midday is likely to avoid the most active periods, maximizing uptake and reducing biases between species. This is

fortunately when sampling is most convenient due to logistical constraints, and the low movement periods lasting most of the day may provide some flexibility in deployment/collection hours.

Differential swimming abilities, times, and preferences among species may also lead to inconsistencies in sampling *Gambierdiscus* cells for environmental monitoring efforts (Parsons et al., 2021). On the one hand, slower swimming species like *G. caribaeus,* or species that are less likely to swim like *G. carolinianus,* might be less likely to colonize a new substrate than cells that are faster swimmers or more likely to leave the surface, like *G. belizeanus* (Figure 17, Table 2). This might cause the former species to be underrepresented over the latter when sampling freshly introduced substrates such as artificial substrates, or potentially even fast-growing natural substrates (Parsons et al., 2021; Tester et al., 2014). Should these differences prove significant under field conditions, the relationship between AS and NS *Gambierdiscus* counts at the genus level would remain correlated linearly as has been determined in many field experiments (Kassim et al., 2025; Lee et al., 2020; Tester et al., 2014, 2022), while species composition shifts between the two sampling methods.

Most studies assessing the community composition of benthic dinoflagellates have classification limited to the genus level (Lee et al., 2020; Mustapa et al., 2019; Tester et al., 2022), mainly because species-level identification using light microscopy remains challenging (Pitz et al., 2021; Vandersea et al., 2012). The importance of species composition cannot be understated given the high variability in toxicity across species, best illustrated on a small French Polynesian island, where only areas with high *G. polynesiensis* counts produced ciguatoxic *Tectus niloticus* gastropods (Darius et al., 2018; Yon et al., 2024). Advances have been made for developing quantitative methods that can discriminate cells to the species level, including

fluorescence in-situ hybridization, qPCR, and recombinase polymerase amplification. Still, widespread adoption has not yet been achieved (Gaiani et al., 2021; Kassim et al., 2025; Kretzschmar et al., 2019; Pitz et al., 2021; Tester et al., 2022; Vandersea et al., 2012). As of this writing, no studies comparing AS and NS methods have been carried out, but shifts in species composition have been demonstrated for macroalgal samples sampled within the same locale, and at different depths within the same region (Fernández-Zabala et al., 2022; Funaki et al., 2022; Pitz et al., 2021).

Despite the above-discussed possibility, it is important to note that laboratory conditions are a great simplification of the field environment. In nature, detachment and proliferation are influenced not only by a cell's inherent behavior but also by factors such as grazing, water movement, and inconsistent light regimes (Tester et al., 2022). Thus, more work is required to determine whether motility behavior of cells directly affects the species composition across different sampling methods, or if other factors, such as wave action and forced detachment, play a more dominant role in *Gambierdiscus* settling dynamics.

Endogenous Circadian Rhythms Regulating Movement in *Gambierdiscus*

Our results indicate that *Gambierdiscus* cells, even in a steady environment devoid of environmental cues like light-dark transitions, cells time their lateral movement. This is indicative that movement is regulated by an endogenous circadian rhythm, an internal molecular clock that tracks time without external cues, and can pre-empt environmental *zeitgebers*, or time-givers, such as the diel or tidal cycles (Cohen & Golden, 2015; Dagenais-Bellefeuille & Morse, 2013; Hardeland & Nord, 1984; Jadhav et al., 2022). Circadian rhythm regulation has been implicated in the control of many cellular processes in dinoflagellates, such as cell division and DNA replication (Vicker et al., 1988), photosynthesis (Sweeney, 1986), nitrogen assimilation

(Dagenais-Bellefeuille & Morse, 2013), and most famously bioluminescence (Hastings, 2007). Many of these have clear ecological roles, such as the futility of bioluminescence during the day or of photosynthesis at night (Cohen & Golden, 2015; Hastings, 2013; Jadhav et al., 2022; Vicker et al., 1988).

Diel vertical migration and movement patterns in pelagic dinoflagellates such as *Lingulodinium* (previously *Gonyaulax*), have also been shown to be regulated by an endogenous circadian rhythm, with behavioral changes in anticipation of the onset of light or dark periods (Roenneberg et al., 1989). In this context, the entrainment of movement behavior by a circadian rhythm enables cells to move toward more favorable conditions ahead of environmental *zeitgebers*, maximizing benefit to the cell (Roenneberg et al., 1989). That *Gambierdiscus* species maintain their movement behavior on a similar endogenous circadian rhythm system suggests that pre-emptive movement in response to changes in photoperiod may offer similar advantages. However, a comprehensive understanding of how these circadian rhythms interact with environmental cues to shape cell behavior awaits further investigation (Dagenais-Bellefeuille & Morse, 2013).

The different responses of the three species tested in free-running light conditions point to different oscillator systems that entrain the circadian rhythms. Simply the differing responses to light, for example with only *G. carolinianus* maintaining bursts of movement during full light exposure, or *G. belizeanus* only initiating the bursts of movement after missing a full diel period, indicate that the mechanisms underlying the circadian rhythms demonstrate some divergence between the species (Figure 19). Previous studies regarding the regulation of bioluminescent behavior on circadian rhythms have pointed to multiple "quasi-independent oscillators" within a single cell or species, showing the breadth of oscillator systems that may be present in

dinoflagellates, but our results also demonstrate species-specific oscillator systems that maintain the same outward phenotype of movement timing (Hastings, 2013). What appears to be three different responses in three different species in *Gambierdiscus* may indicate either a highly modular oscillator system tuned for each species' needs as has been hypothesized in polyketide synthesis, or entirely unique clock mechanisms within each species (Haq et al., 2023; Williams et al., 2021).

Molecular clocks capable of timekeeping have been well characterized in other algae, and even been expressed *in vitro* (P. Kim et al., 2020). However, the exact mechanisms by which they occur in dinoflagellates is still enigmatic, lacking canonical TTFL oscillators from eukaryotes or *Kai* oscillator genes from prokaryotes, and some species may have multiple oscillator systems each regulating a single or several systems (Hastings, 2013; Jadhav et al., 2022). A blue-light receptive cryptochrome was implicated in entraining the circadian rhythm of the cell cycle in *Karenia brevis*, but few targeted searches have since been conducted on the signaling pathways responsible, or other proteins involved in discrete rhythms (Stephanie A. et al., 2007).

Light Color Impact on Timing of Movement and Circadian Rhythm

The impact of light color on a circadian rhythm can provide hints about the identity of the proteins responsible for entrainment, but it also points to the potential ecological reason for the circadian rhythm (Roenneberg & Merrow, 2002; Sorek & Levy, 2012). The differential responses to exposure to the different light colors indicate different entrainment responses of the circadian rhythms, possibly stemming from different circadian rhythm oscillator mechanisms (Figure 20). This echoes the different circadian rhythm behaviors shown in the free-running experiments (Figure 19).

There also appear to be multiple overlapping effects arising from the exposure to the single wavelength light aside from the entrainment of the circadian rhythm, such as the strong diminishment of movement in the red light, as well as the additional burst of movement in *G. carolinianus* 2-3 hours after initiation of the light (Figure 20). Several hypotheses are plausible regarding the diminishment of movement in red light, in addition to the likely suppression of the circadian rhythm. First is an ecological reason, where red light indicates that cells are nearer the surface, which is a location they may prefer. An alternative hypothesis may be that photosynthetic coupling may yield a different signaling state, reducing the capacity for motility, although this does not account for why *G. australes* movement does not diminish as significantly. The burst of movement in the blue light for *G. carolinianus,* however, is more mysterious, potentially the action of a saturated photoreceptor. Further studies are required to verify these hypotheses or identify others, as well as identify the identities of the proteins involved in light reception that trigger these behaviors.

Chapter 4: Comparative Analysis of Canonical and Non-Canonical Rhodopsins in Amphidinium carterae and Karlodinium veneficum

Introduction

Identifying the proteins behind a cellular function is not a trivial task, but is even more difficult in dinoflagellates stemming from their enigmatic biology as described earlier (Wang et al., 2011, 2014). A significant part of that challenge is the highly divergent nature of their proteome, as well as a large number of genes providing a massive potential search space, compounded with multiple homologs for a single protein family (Haq et al., 2023; Stephens et al., 2018; Williams et al., 2021). This chapter focuses on a comprehensive survey of microbial rhodopsins from the transcriptomes of two species of dinoflagellates, *Amphidinium carterae* and *Karlodinium veneficum*. The two species were chosen due to the existence of relatively well-characterized transcriptomes, as well as notable similarities and differences, and microbial rhodopsins are a well-characterized protein family with highly conserved structural features and residue motifs that make targeted review and analysis accessible (Bachvaroff, 2019; Bulzu et al., 2022; Judd & Place, 2022). This chapter also highlights some of the aforementioned difficulties currently faced with the annotation of proteins in dinoflagellates.

The target proteins, rhodopsins, are membrane-bound proteins with seven transmembrane helices and a pocket for a retinal chromophore bound by a lysine residue in helix 7, forming a Schiff base (Bayley et al., 1981; Ernst et al., 2014; Slamovits et al., 2011). Absorbed light causes a conformational change in the chromophore and protein, which performs functions such as ion-pumping and intracellular signaling (Bayley et al., 1981; Bergo et al., 2006; Luecke et al., 2001; Subramaniam & Henderson, 2000). Since the original discovery of proton-pump bacteriorhodopsin in *Halobacterium halobium*, characterization of the functional and

phylogenetic rhodopsin families has greatly expanded (Ernst et al., 2014; Govorunova et al., 2017; Kandori, 2015; Oesterhelt & Stoeckenius, 1971, 1973). These include sodium pumping and halorhodopsins that pump sodium and chloride ions, respectively, sensory rhodopsin that binds a transducer protein for downstream signaling, proteorhodopsins that act as protein pumps and might drive a large portion of marine phototrophy, channelrhodopsins that act as ion channels, and heliorhodopsins that regulate other proteins (Bergo et al., 2006; Cho et al., 2022; de la Torre et al., 2003; Inoue et al., 2013; Kandori, 2015, 2015; Kato et al., 2012; Kolbe et al., 2000; Luecke et al., 2001; Sieradzki et al., 2018). The rhodopsin backbone has found potential well beyond its natural roles, serving as an optogenetic tool in neuroscience, a molecular switch in synthetic biology, and a model scaffold for protein engineering (Alekseev et al., 2022; Brown et al., 2018; Davison et al., 2022; Tu et al., 2024).

Dinoflagellate rhodopsins have been implicated in several facets of their lifestyle, including phototaxis (movement towards or away from light), heterotrophy (digestion), and even in the enigmatic eye-like ocelloid organelles in the warnowiid dinoflagellates (Aihara et al., 2019; Hartz et al., 2011; Hayakawa et al., 2015; Slamovits et al., 2011; Westermann et al., 2023). However, these studies have relied on conservative identification strategies and are dependent on methods built on non-dinoflagellate sequences, which may not capture the full diversity of dinoflagellate rhodopsins (Hayakawa et al., 2015; Shi et al., 2015; Zhang et al., 2024).

By combining iterative profile-based searches, structural modeling, functional motif-based annotation, and phylogenetic analysis on the transcriptomes of *A. carterae* and *K. veneficum*, we uncover both putative canonical rhodopsins—including a proteorhodopsin and, for the first time in dinoflagellates, a heliorhodopsin—as well as divergent rhodopsins with noncanonical motifs and extensive accessory domains.

Methods and Materials

Putative Rhodopsin Identification

HMM-based initial screening: An initial superset of potential dinoflagellate rhodopsins was identified from a database of 63 dinoflagellate transcriptomes using an iterative Hidden Markov Model (HMM) search method. The dinoflagellate transcriptomes were compiled by Williams *et al.* in a prior study, using six-frame translations for each transcript (Williams et al., 2021). The *HMMER* suite of tools was used to screen transcripts that matched known HMM profiles employing *hmmsearch* against Pfam domains associated with rhodopsins: PF00001 (7tm_1), PF01036 (Bac-rhodopsin), PF10413 (Rhodopsin_N), PF18761 (HeR), and PF20684 (Fung_rhodopsin) (Potter et al., 2018). Transcript sequences with matches to these domains were extracted and used to construct custom HMMs (*hmmbuild*) for each domain of interest. These custom HMMs were then scanned using *hmmsearch* against the candidate coding regions for transcriptomes of *Amphidinium carterae* CCMP1314 and *Karlodinium veneficum* CCMP1975 (Bachvaroff, 2019; Judd & Place, 2022). Candidate coding regions were identified using *TransDecoder*, using the universal genetic code setting (*TransDecoder/TransDecoder*, 2015/2025).

Filtering by Rhodopsin Specific Functional Motifs: The resulting sequences formed a preliminary set of candidate sequences of potential rhodopsins, with an expected high proportion of false positives. To enrich for true rhodopsins, candidates were filtered by alignment to sets of reference rhodopsins to identify the conserved Lys216 residue, essential for covalent bonding to the retinal chromophore (Bayley et al., 1981). All named positions and residues are referred to with respect to the equivalent position in bacteriorhodopsin (PDB 1FBB) (Bayley et al., 1981). Due to the generally low sequence identity, both structural and sequence-based alignments were

employed in parallel. Sequences for which both alignment approaches identified Lys216 were retained as likely rhodopsins; transcripts where the methods disagreed were subjected to manual review of structural alignments. The resulting sequences formed a set of putative rhodopsins which were used for further analysis, including retinal binding pocket alignment to further ascertain the protein's ability to bind the retinal chromophore.

Structural Alignment: For structural alignment, candidate sequence structures were predicted using *OmegaFold*, which was selected due to its ability to predict *de novo* structures without the need for multiple structural alignments (MSA) against known databases (Wu et al., 2022). The predicted structures were aligned to high-resolution crystal structures of a diverse group of microbial rhodopsins: bacteriorhodopsin (BR; PDB 1FBB), proteorhodopsin (PR; 4JQ6), halorhodopsin (HR; 1E12), channelrhodopsin (ChR; 3UG9), sensory rhodopsin (SR; 1JGJ), and heliorhodopsin (HeR; 6SU4). Alignments were performed with *FoldMason* using the easy-msa workflow, generating a separate multiple structural alignment (MSTA) for each candidate against all six reference structures simultaneously (Gilchrist et al., 2024).

Multiple Sequence Alignment: For the sequence alignment, candidate sequences were aligned against a reference of compiled rhodopsin sequences taken from the reduced representative tree generated by Bulzu *et al.* (Bulzu et al., 2022). The reference set was first filtered by removing sequences that produced unique insertions of more than 10 amino acids in the other sequences, resulting in an MSA profile with 810 microbial rhodopsins, all of which had the Lys216 motifs aligned. Candidate sequences were aligned individually against the MSA profile using *mafft* with the *--add* parameter (Katoh et al., 2002). Transmembrane (TM) helix locations were predicted using *DeepTMHMM* (Hallgren et al., 2022), and candidate sequences

were only considered to be putative rhodopsins if the aligned Lys residue was determined to be within a transmembrane helix.

Locating the Rhodopsin and Accessory Domains: Because many putative rhodopsin sequences contained long N- and C-terminal extensions, the boundaries of the transmembrane (TM) rhodopsin domain were determined, and the terminal extensions separated. The TM region was identified programmatically using three criteria: (1) the location of Lys216, which forms the Schiff base with retinal and was assumed to lie within TM7; (2) the positions of predicted TM helices from *DeepTMHMM*; and (3) the local structural confidence scores, as given by the predicted local distance difference test (pLDDT) from the *OmegaFold* predictions.

To define domain boundaries sites outside of the TM helices, the first derivative of a 10–amino acid moving mean of pLDDT scores was calculated. The most prominent local maxima (N-terminus) and minima (C-terminus) were taken as approximate domain boundaries. Although the pLDDT derivative does not necessarily reflect true structural borders, it provides a computationally reproducible proxy that captures the transition from highly structured TM helices (high pLDDT) to flexible loop or extension regions (low pLDDT) (Binder et al., 2022). Terminal extensions were only retained for downstream analysis if they exceeded 50 amino acids. The starting location of the domains in the intra- or extracellular space was predicted using the *DeepTMHMM* results, taking into account the end location of the last helix before cropping.

Once the boundaries for cutting were determined, the sequences and protein structures were isolated using *BioPython's SeqIO* and *PDBParser* modules, respectively (Cock et al., 2009). Structures were cropped directly from the larger protein structure file to preserve the "native" predicted conformation. Both the rhodopsin domains and N/C accessory terminal

domains were stored separately for further analysis. All protein structures were visualized using *ChimeraX* (Pettersen et al., 2021).

Rhodopsin Color Tuning Prediction

Color tuning of the rhodopsin proteins was predicted using *OpsiGen,* which utilizes geometric deep learning to predict the wavelength of the rhodopsins based on sequences and structural predictions (Sela et al., 2024). A local installation of the software was created, and a pipeline was used to run each structure and sequence pair through the prediction pipeline, predicting the peak absorption wavelength of each candidate.

Putative Rhodopsin Sequence Phylogeny

Putative rhodopsin sequences were placed in a reference tree using SATe-enabled Phylogenetic Placement (SEPP), based on references described by Bulzu *et al*., which were roughly annotated to families of rhodopsins (Bulzu et al., 2022; Mirarab et al., 2012). The SEPP workflow constructs an Ensemble of HMMs to represent the MSA of the reference tree, dividing the MSA into smaller pieces. It then computes a broader placement in the alignment by aligning the query sequence against the best fitting HMM. Then, *pplacer* was used to place the query sequence in the input tree (Matsen et al., 2010). This strategy reduces alignment error relative to global methods and allows each putative rhodopsin to be treated independently, preventing large numbers of query sequences from distorting the placement.

Functional Motif Identification

For the identification of key motifs likely to be involved in the function of the molecule and retinal binding on the putative rhodopsins, multiple structural and sequence alignments from the preliminary filtering were reused. Key motifs were identified from a literature review of

known function-defining residues in rhodopsins, and the aligned residues were extracted from the MSAs and MSTAs.

For transcripts where motif identity did not agree between the two alignment methods, manual review of the motif and residue location was carried out using the 3D coordinates of the residues in the predicted protein structure, emphasizing that the residues of interest should be facing the inside of the channel, nearer to the Lys216 residue. The Euclidean distance of the Cα for each residue from the Cα of Lys216 was calculated and used to determine the orientation of the residue along the helix. This was compared with the appropriate positions in BR (1FPP) for the final determination of the residues occupying the function-defining positions in reference rhodopsins.

Annotation of Accessory Domains

The N and C-terminal extensions past the 7 TM region of rhodopsin are putative accessory domains with potential functionality. Domain sequences were scanned against multiple databases using *InterProScan* to identify homologous domains at the sequence level (Blum et al., 2025). In parallel, predicted structures of these domains were compared against the AlphaFold Database (AFDB) using the DALI webserver to search for more distant structural homologs (Holm, 2022; Holm et al., 2023; Varadi et al., 2024). DALI hits were scored using the z-score and length of alignment metrics to determine the quality and extent of the alignments.

Phototaxis Measurements

For measuring phototaxis in the cells, a multi-well chamber was designed and 3D-printed. Lanes were 40mm long, 5mm wide at the narrowest point, and 5mm tall, with additional circular wells on each side, allowing the volume of the chamber to exceed 1mL. The lanes can be

separated using a plug stopper that separates each lane into two volumes. Chambers and stoppers were printed on a consumer fused filament fabrication 3D printer (FLSUN V400) in PLA (Polymaker Polyterra), using matte black to reduce internal reflections. Each piece was printed at 100% infill.

For the experiments the chambers were placed in a box to block out external light, and a high color rendering index (CRI95+) photography LED panel light (Viltrox L116T) was set at 5600K and placed horizontally to the wells. Light levels were measured using a light meter placed in the middle of the well facing the light source and adjusted to 75 μmol m^{-2} s^{-1} by changing the distance from the LED. Then, 1 mL of cell culture was placed via pipette into the middle of each lane, and the cells were allowed to swim for 3 hours. At the end of the experimental period, chambers were plugged and removed from the box. Cells on each end of the lane were counted using a handheld cell counter (Scepter 3.0, Millipore Sigma) with a 40μm aperture sensor.

A phototaxis metric is calculated for each lane, derived from cell counts, as given by

$$Phototaxis\ Metric\ = 2\left(\frac{n_L}{n_L + n_D}\right) - 1$$

Where n_L is the number of cells in the well nearer to the light, n_D is the number of cells in the well away from the light. The metric sums the cells closer to the light over the total number of cells, with a normalization that scales the possible outputs from -1 to +1, where +1 indicates 100% cells were in the well closer to the light (positive phototaxis), -1 indicates 100% cells were in the well away from the light (negative phototaxis), and zero indicates cells were equally distributed (no phototaxis response). Tests were carried out in three biological replicates, and pairwise t-tests with unequal variances were carried out between the phototaxis metrics of the different species and the microbead control.

Cells of *K. veneficum* CCMP1975, *A. carterae* CCMP1314, and *A. carterae* CCMP2980 were tested, alongside a microbead control. Two strains of *A. carterae* were tested since CCMP1314 has been in culture for more than 70 years, while CCMP2980 is a more recent isolation (2009), and the loss of phototactic ability in cultured dinoflagellates has been observed over extended periods (Hulburt, 1957; Morten et al., 2013; Scorzetti et al., 2009).

Results

The initial iterative *hmmer* search workflow yielded a preliminary pool of 35 protein sequences for *Amphidinium carterae* and 43 for *Karlodinium veneficum*. Of these preliminary proteins, 18 *A. carterae* and 10 *K. veneficum* sequences retain an aligned Lys216 residue, with a majority of the sequences having agreement between the structural and sequence alignment methods (Figure 22A).

Protein length ranged between 200 and 800 AA, with the *A. carterae* sequences having a longer median length of 520 AAs versus *K. veneficum*'s 302 AAs (Figure 22B). Additional accessory domains were found outside of the core rhodopsin domain, which were cropped using methods described above (Figure 22C, D). Following the cropping of additional domains N or C terminal to the main rhodopsin domain, all but 1 of the 28 additional domains were intracellular, with the range and size of these additional domains being similar between *A. carterae* and *K. veneficum* (Figure 22E). A number of these domains exceeded the length of the rhodopsin domains themselves. The predicted color tuning of the rhodopsins was similar across species, with *A. carterae* showing a slight bias towards greener, higher-wavelength light (Figure 22F).

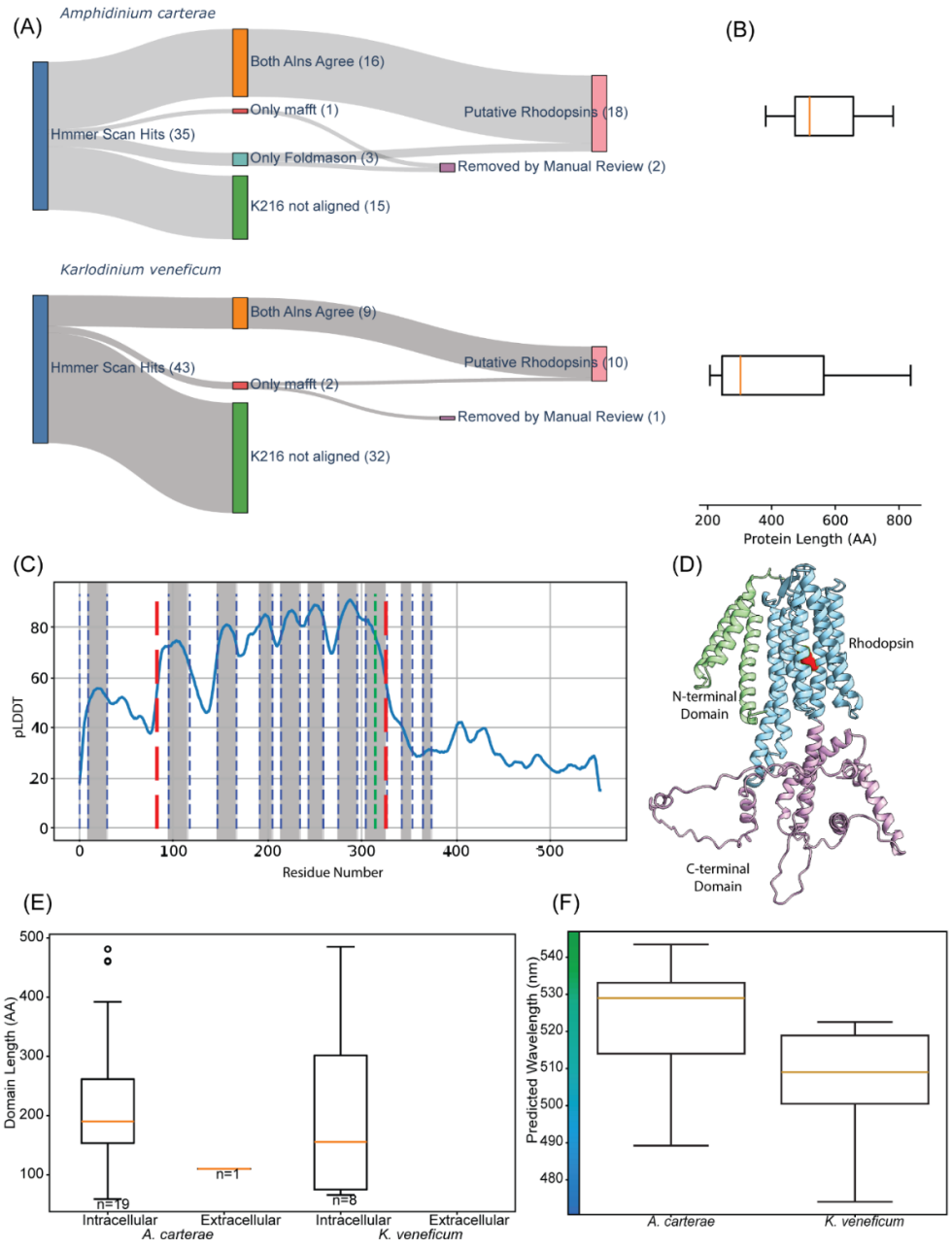

Figure 22: Summary of putative rhodopsin sequences. (A) Sankey diagram of the number of predicted proteins at the different workflow steps for *A. carterae* and *K. veneficum*. (B) Boxplot of protein lengths. (C) pLDDT plot, also showing transmembrane helix regions (grey with blue borders), Lys216 location (green line), and boundaries of the N and C terminal domains (heavy red lines). (D) OmegaFold predicted structure of protein from panel A, showing the corresponding domain separations. The Lys216 residue atoms are highlighted in red. (E) Domain lengths for intra- and extracellular domains, and (F) predicted color tuning for the rhodopsin absorption maximum.

Conserved Rhodopsin Structural Features

These 28 putative sequences showed substantial z-score similarity with the set of reference rhodopsins used for alignments (Figure 23A), as well as high coverage with low root mean square distance (RMSD), a measure of structural deviation between two aligned proteins (Figure 23B). Eight key binding pocket residues were identified in the literature search, in helices C, F, and G (Table 3, Figure 23C). These residues show strong conservation for the eight selected binding pocket residues with the 800+ rhodopsins curated by Bulzu *et al*., as can be seen in the logo sequence plot in Figure 23D (Bulzu et al., 2022).

Table 3: Key motifs in rhodopsins as obtained from literature review. Residue numbers are the corresponding positions in bacteriorhodopsin

Motifs	**Location**	**Functions**	**Sources**
Asp85 – Thr89 – Asp96	Helix C	"DTD" motif, enables proton pumping in BR, with some variability in the final D96. "DTE" in PR, "NTQ" for HR, enabling chloride pumping, "NDQ" in sodium pumping rhodopsins.	(Ernst et al., 2014; Inoue et al., 2013, 2016; Kandori, 2015; Kolbe et al., 2000; Otto et al., 1989)
Arg82 – Tyr 83 – Trp86 – Trp182 – Tyr185 – Pro 186 – Trp189	Helix C (82-86), Helix F (remainder)	Rhodopsin binding pocket for all-trans-retinal.	(Bulzu et al., 2022; Heyne et al., 2000; Luecke et al., 2000; Malakar et al., 2024)
Asp212	Helix G	Counter ion for protonated retinal chromophore, key for proton pumping. Asp212Asn in sodium-pumping rhodopsins, Asp212Ser for HeR.	(Bulzu et al., 2022; Ernst et al., 2014; Inoue et al., 2013)
Lys216	Helix G	Forms covalent protonated Schiff base with retinal chromophore.	(Bayley et al., 1981)

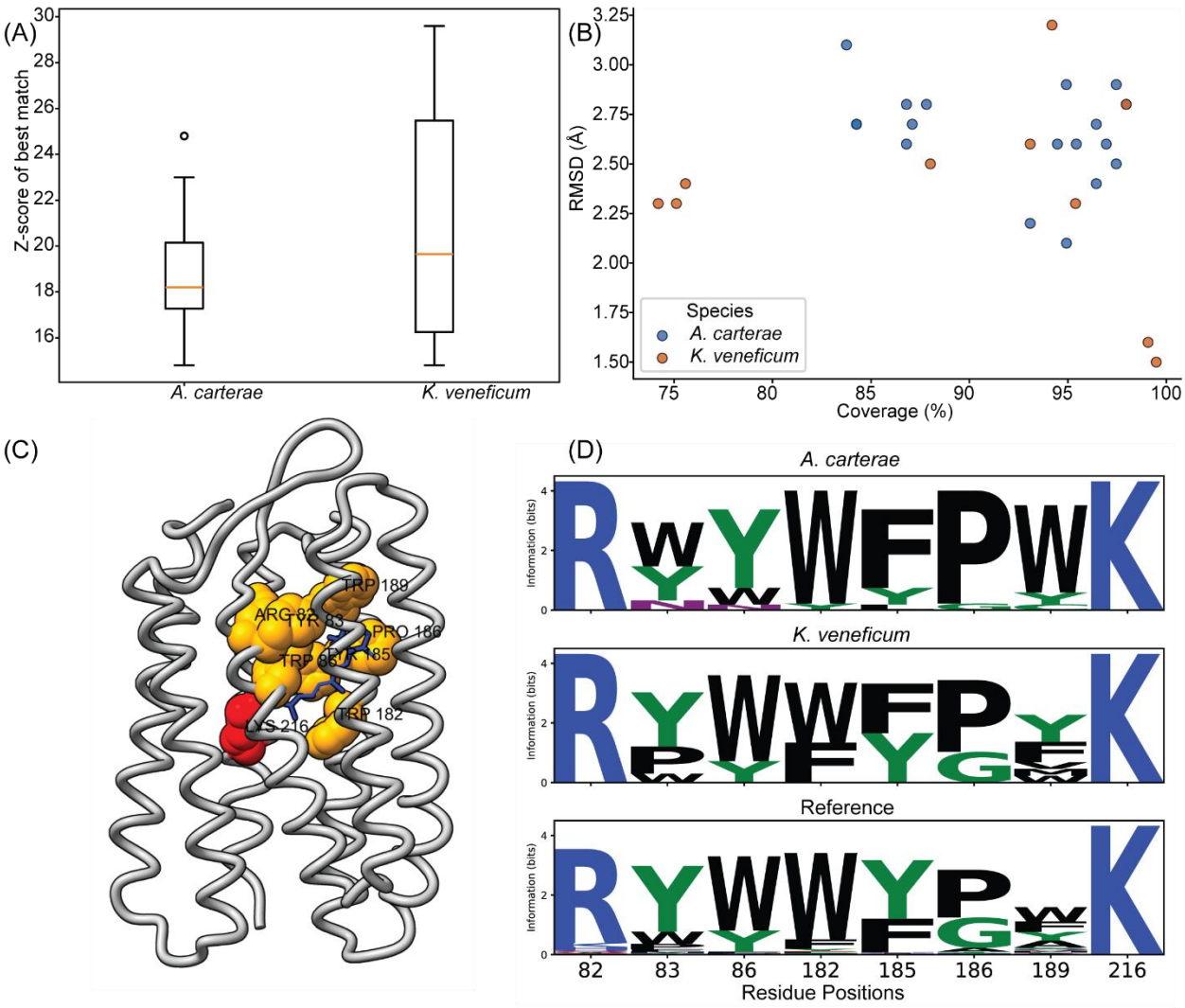

Figure 23: Conserved features of putative rhodopsin sequences to known references. (A) Boxplot of z-scores for pairwise comparisons of candidate putative rhodopsin regions against high-resolution structures of six rhodopsins. Only the best z-score is kept. (B) RMSD versus alignment coverage of the reference subject rhodopsin. An alignment coverage of 100% indicates that the subject (reference rhodopsin structure) is fully aligned with the query (putative rhodopsin structure). (C) Structure of bacteriorhodopsin, with retinal (blue) bound to Lys216 (red). The yellow residues highlighted make up the rhodopsin binding pocket, as defined in Table 3. (D) Sequence logo plot of the binding pocket, showing strong conservation between the *A. carterae*, *K. veneficum*, and reference binding pockets.

Putative Rhodopsins in Phylogenetic Context

Comparing the putative rhodopsin sequences with the broader rhodopsin literature, the phylogenetic tree with the *A. carterae* and *K. veneficum* sequences shows candidates falling into five clades across different rhodopsin families (Figure 24A). The *K. veneficum* sequences had a heliorhodopsin and a proteorhodopsin that fit well in the corresponding clade.

A majority of the sequences (12 *A._carterae*, 4 *K. veneficum*) fell into a clade populated only by dinoflagellate sequences (Bulzu et al., 2022) (Figure 24A). In this clade, the Asp212 residue, largely conserved in rhodopsins, has a higher occurrence of substitution with asparagine (Asn).

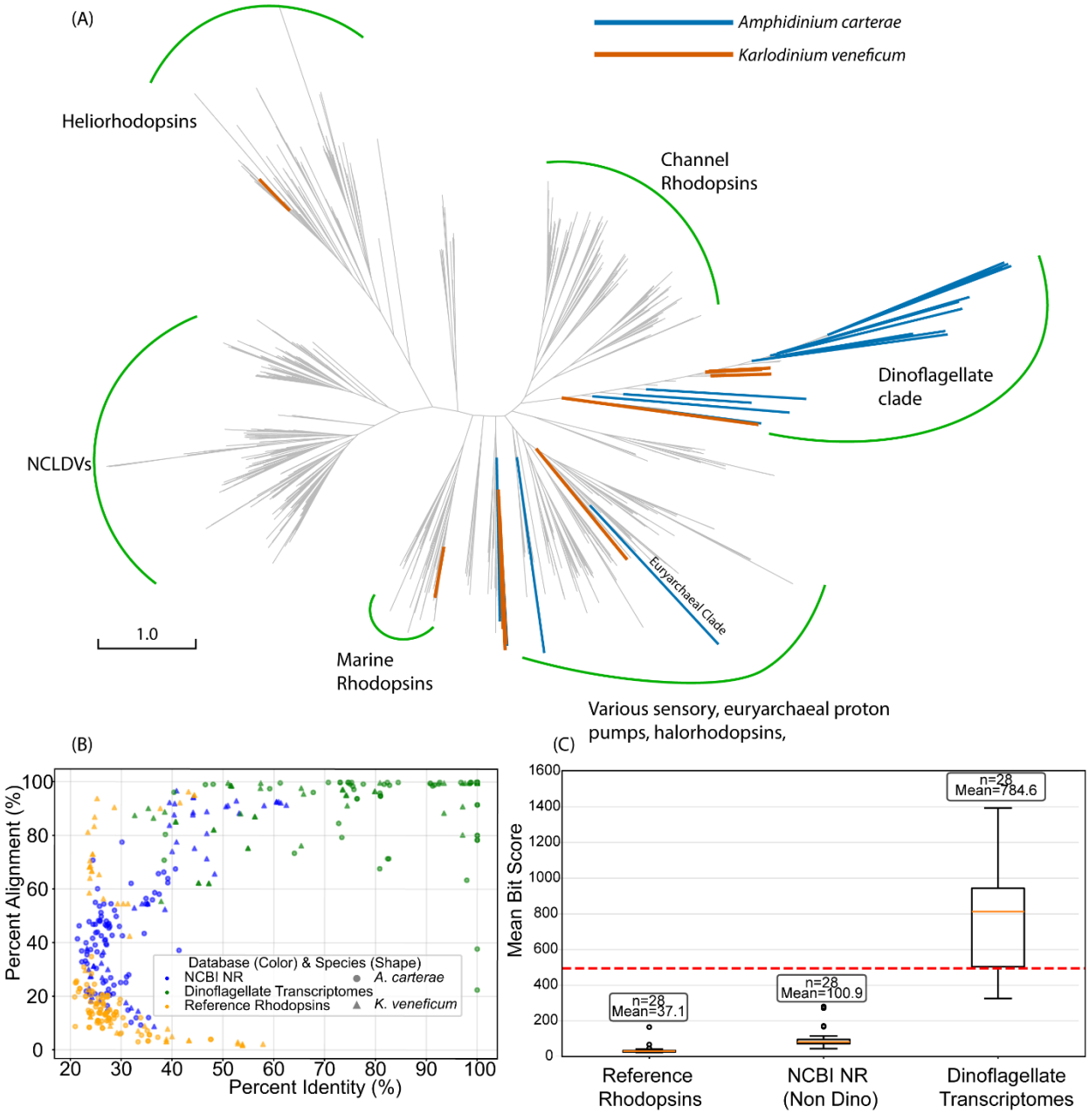

Figure 24: Candidate sequences in relation to the broader context of microbial rhodopsins. (A) Unrooted phylogenetic tree, with parent alignment and annotations taken from Bulzu et al. *Amphidinium carterae* and *K. veneficum* sequences are highlighted in blue and orange, respectively. (B) Scatter plot of percent alignment versus

percent identity, and (C) boxplot of bitscore for the 5 best protein BLAST hits for each candidate sequence against a curated set of well-characterized rhodopsins, the NCBI NR database excluding dinoflagellates, and the dinoflagellate transcriptomes, showing poor conservation of the rhodopsins outside of the dinoflagellate phyla.

The protein BLAST results for the putative rhodopsin sequences against three datasets (20 reference rhodopsins, the NCBI NR (non-redundant) database excluding dinoflagellate sequences, and 61 dinoflagellate transcriptomes) highlight their poor conservation outside of dinoflagellates (Figure 24B,C). Percent alignment and identity for the BLAST comparisons against the reference rhodopsins were either low percent identity or alignment in the bottom left, while the NR comparisons did not exceed 65% alignment (Figure 24B). In contrast, BLAST comparisons against the dinoflagellate transcriptomes yielded higher identity and alignment. The same trend is reflected in the bitscore distributions. The curated reference of 20 rhodopsins had a mean bitscore of 30, compared to 495 for a perfect self-match for a 249 AA proteorhodopsin. The NCBI NR dataset showed slight improvement with a mean of 113, but this was much lower than that for the dinoflagellate transcriptomes with 784. Bitscores can exceed the proteorhodopsin perfect self-match of 495 due to the longer protein lengths, where longer alignments yield higher bit scores.

InterProScan results of the 28 putative rhodopsins assigned only 18 of these sequences to rhodopsin family proteins (9 *A. carterae*, 9 *K. veneficum*), with the remaining 10 sequences yielding no hits. Of these hits, many e-value results were not low, with only 6 sequences meeting a lenient e-value cutoff below 1e-5 (Appendix 8).

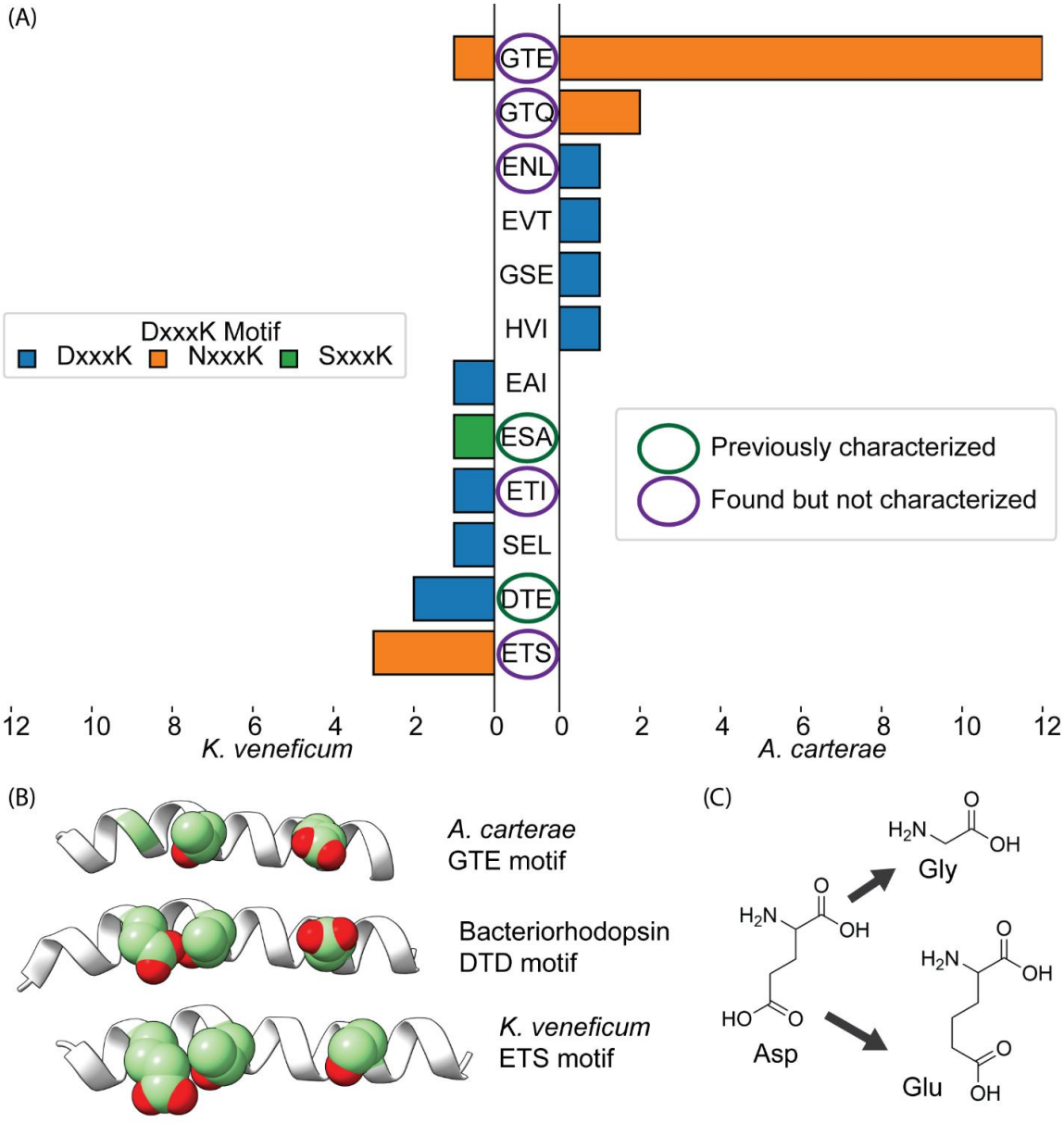

Figure 25: Helix C motifs and structures. (A) Distribution of helix C DTD-equivalent motifs in *A. carterae* and *K. veneficum*, colored according to the corresponding helix G DxxxK-equivalent motif. (B) Structural models of helix C from *A. carterae* transcript DN1475 (GTE motif), bacteriorhodopsin (BR; DTD motif, PDB 1FBB), and *K. veneficum* transcript comp4819 (ETS motif). Residues of the motif are shown as spheres (carbon in light green, oxygen in red). (C) Amino acid substitutions in the Asp85 BR equivalent, showing Gly for *A. carterae* and Glu for *K. veneficum*. Panels B and C highlight the significant shift in likely function for *A. carterae*, but the possibly conserved function in *K. veneficum*.

In helix C the DTD motif (positions 85, 89, 96 in bacteriorhodopsin) is a critical determinant of ion-pumping activity in microbial rhodopsins, as laid out in Table 3. Even a

single amino acid substitution can modify the ion specificity (Inoue et al., 2016; Kurihara & Sudo, 2015). The residues in these positions are intensely involved in moving ions across the membrane by sequential electronic bonding and release of the ion as the protein undergoes light-driven conformational shifts (Subramaniam & Henderson, 2000). There is substantial diversity in the composition of this DTD motif in the putative rhodopsins, with 12 unique motifs amongst 28 putative transcripts.

Two motifs in *K. veneficum* match previously characterized known rhodopsin types. The DTE motif in proteorhodopsins, a proton pump-type rhodopsin, and the ESA motif in heliorhodopsins, a light-driven regulator of secondary proteins (Bamann et al., 2014; Kovalev et al., 2020). The transcripts with those corresponding motifs are the same transcripts placed in the proteorhodopsin and heliorhodopsin clades by phylogenetic analysis (Figure 24A). The latter sequence also retained the Asp212Ser substitution characteristic of heliorhodopsins (Bulzu et al., 2022; Kovalev et al., 2020).

In the broader survey of 2000 rhodopsins compiled by Bulzu *et al*., several of the motifs found in the putative rhodopsins were also observed - ENL in *A. carterae*, and ETI, ETS in *K. veneficum*, with ETS being the most common form in *K. veneficum*. The GTE and GTQ motifs have also been observed in surveys of channel rhodopsins (Govorunova et al., 2021). The remaining five motifs have not been observed in other published rhodopsin sequences.

Most importantly, *A. carterae* and *K. veneficum* show largely non-overlapping motif sets, sharing only the GTE motif which appears in a single *K. veneficum* transcript but in more than ten *A. carterae* sequences. Notably, *K. veneficum* has residues consistent with proton-pumping ability. In contrast, the most common motifs in *A. carterae*, GTE, and GTQ have the Asp85Gly substitution in the first motif position (Figure 25B). The loss of the amino acid sidechain, and

critically the electronegative carboxylate group, disrupts the ability of the protein to serve as a proton acceptor (Figure 25B). The Asp85Glu substitution in *K. veneficum* ETS motif changes the stereochemistry slightly with a one-carbon longer sidechain. However, the functional carboxylate is still maintained, while the Asp96Ser substitution has been observed in proton-pumping rhodopsins, indicating a single electrochemically similar substitution from a known proton-pumping motif (Figure 25C) (Suzuki et al., 2022).

Annotation of Accessory Domains

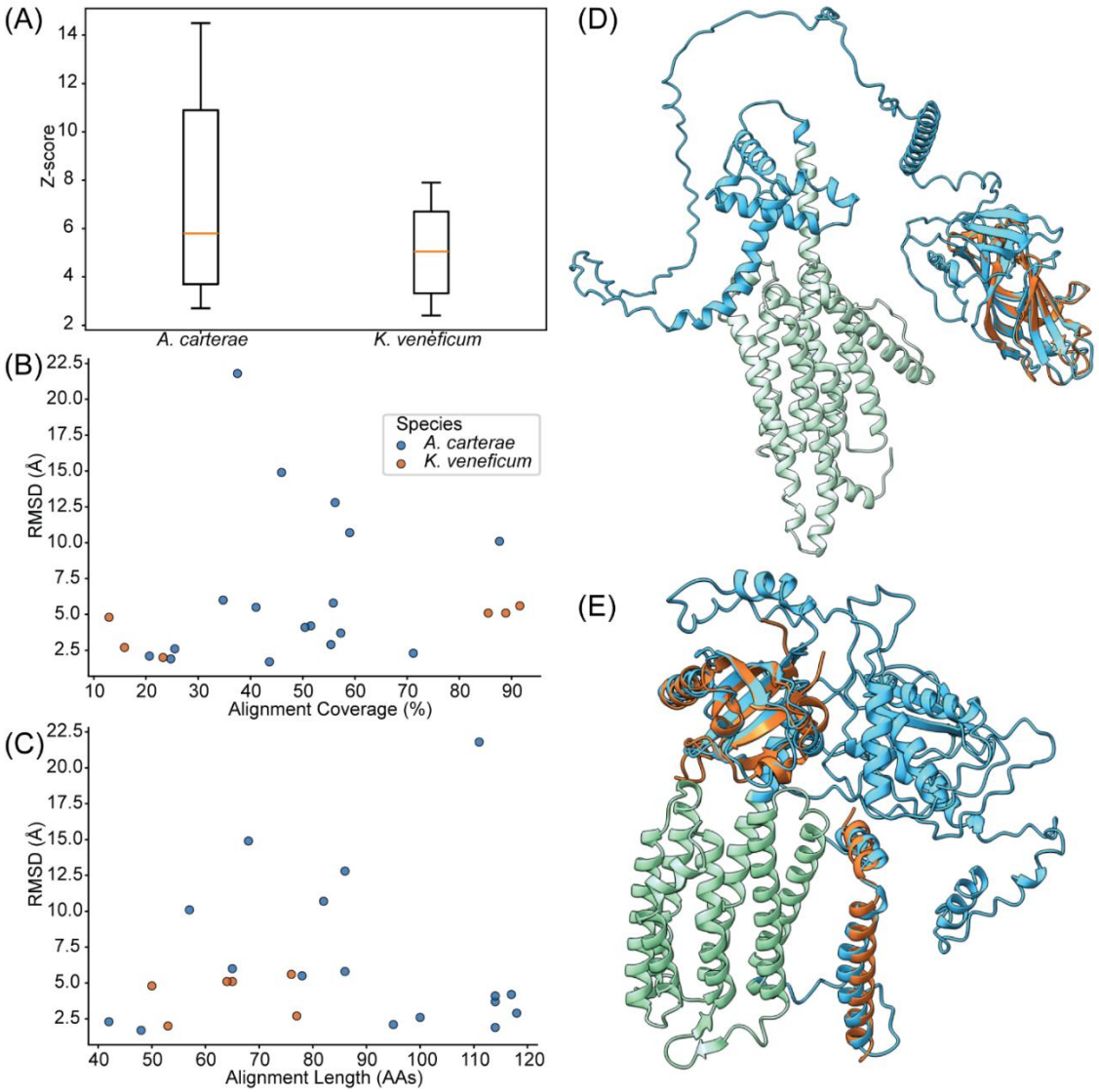

Figure 26: Results from domain annotation using DALI against the complete AlphaFold structural DataBase (AFDB). (A) boxplot of z-scores for the annotated domains. (B) RMSD against % coverage of query. (C) RMSD against total alignment length. (D) Structure of *A. carterae* transcript DN23874, with rhodopsin domain in light green, and cropped domain in light blue. The best-scoring aligned protein is in orange (4IHB, dysferlin) with a z-score of 14.5. (E) Structure of *A. carterae* transcript DN7146, with both N and C terminal domains. The N-terminal domain shown is the shorter alignment, with the two helices (9FNN, cellulose synthase catalytic subunit chain X, z-score 3.7). In contrast, the C terminal is the longer domain, matching 4XT2 (aryl hydrocarbon receptor nuclear translocator, z-score 11.7). Both Panel D and E demonstrate the incomplete structural matches of even the best-matching domains.

The 28 accessory domains returned no results in searches against multiple family, domain, and site databases (CDD, HAMAP, NCBIfam, PANTHER, PRINTS, Pfam, PISRF, SMART, CATH-Gene3D, and SUPERFAMILY). Structural homology comparisons using DALI against the AlphaFold Database (AFDB) showed structural homologs for 23 out of the 28 accessory domains. The median z-score for both species was under 6, with *A. carterae* having four sequences with z-scores greater than 8 (Figure 26A), indicating a substantial structural similarity (Holm et al., 2006). However, the quality of the hits shows that even the best hits were usually incomplete, with low percentage coverage against the accessory domains (Figure 26B, D). Many of the sequences yielded poor RMSD results, a measure of structural deviation between two sequences, with 12 out of 23 having an RMSD greater than 5Å. An RMSD of less than 3Å for alignments greater than 100AAs, is considered similar (Holm et al., 2006). For sequences with high percentage coverage and low RMSD, the alignment length was short, leading to low z-scores (Figure 26C). This last category features small domains and cannot be considered substantial evidence. An example of this last category is shown in Figure 26E, where the N-terminal accessory domain aligns with two helices, providing coverage of most of the query domain, but with a low z-score of 3.7.

Phototaxis Measurements

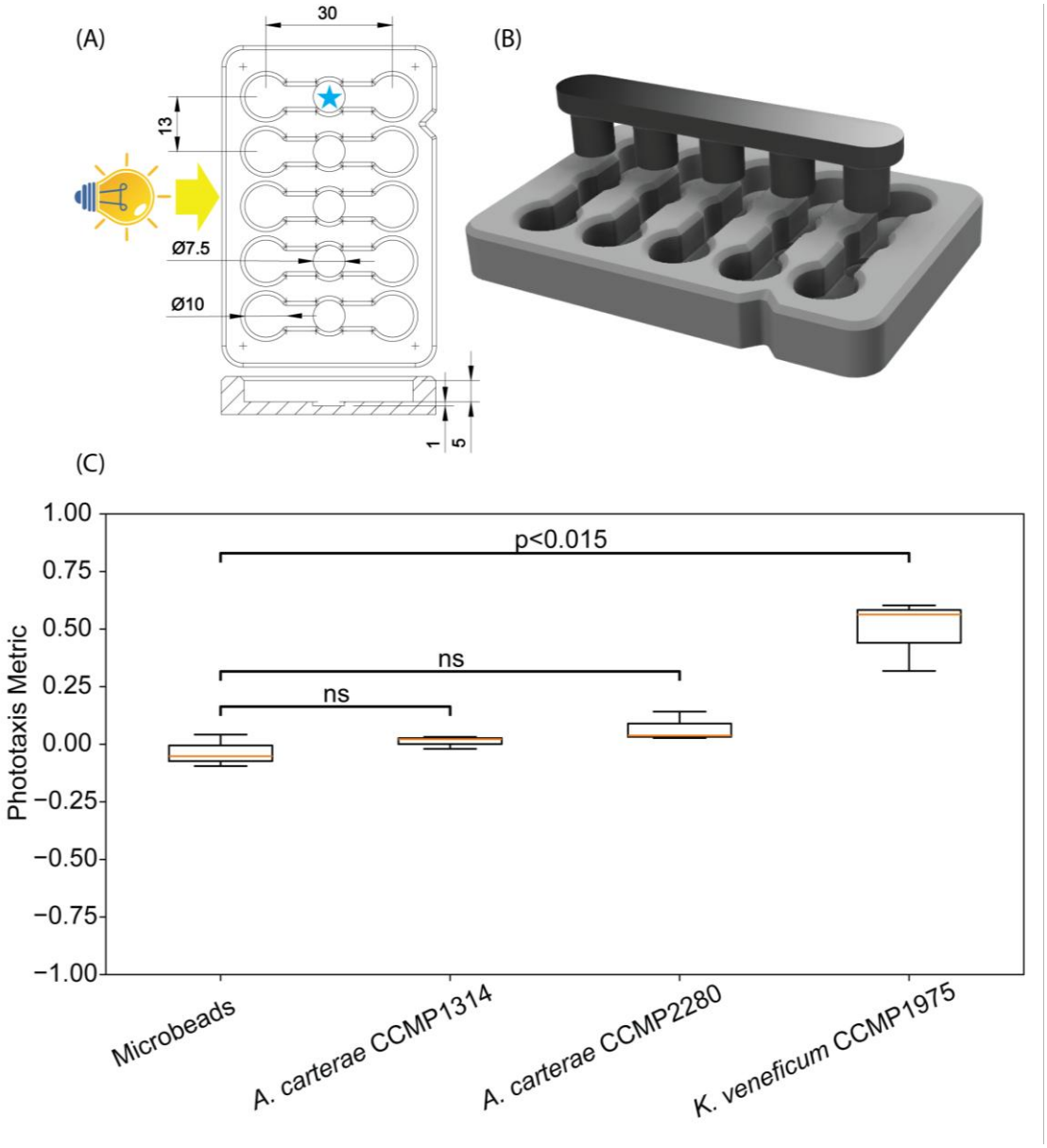

Figure 27: Phototaxis assay overview. (A) Schematic drawing of the assay chamber. Dimensions are in millimeters, with the bottom projection being the side profile of a single lane. The yellow arrow indicates the direction of light, and the blue star indicates the position in the well where cells are added. (B) 3D render also showing the plug stopper for use in separating the two chambers at the conclusion of the movement time. (C) Results of phototaxis assay at 75 µmol m^{-2} s^{-1}. A +1.0 phototaxis metric indicates 100% of cells were in wells closer to the light, -1.0 indicates 100% of cells were in wells further from the light, and zero indicates cells were equally distributed between the two wells. The results of the pairwise t-test comparisons between the microbead control and cell cultures are annotated by the square brackets, with "ns" indicating $p>0.05$.

The schematic drawing, orientation of the light, and 3D rendering of the phototaxis assay chambers are shown in Figure 27A, B, with the plug stopper also shown in the 3D rendering. The

results of the phototaxis assays showed that after 3 hours of exposure to a directional light source, *A. carterae* distributions were not significantly different from the microbead control, regardless of strain (CCMP1314 or CCMP2980), while *K. veneficum* showed phototaxis towards the light at 75 μmol $m^{-2}s^{-1}$, indicating a positive phototactic response (Figure 27C).

Discussion

The Rhodopsin Repertoires of *Amphidinium carterae* and *Karlodinium veneficum*

This study provides a comprehensive view of the rhodopsin complement in complete transcriptomes from two core, free-living dinoflagellates: *A. carterae* and *K. veneficum*. Both species are athecate dinoflagellates of similar size (about 10μm in diameter)(Bachvaroff et al., 2014; Janouškovec et al., 2017). Both species are facultative mixotrophs, capable of photosynthesis and consuming other organic matter, like bacteria and other protists, produce highly similar polyketide sterolysin secondary metabolites, and both are responsible for regular blooms associated with fish mortality worldwide (S. A. Murray et al., 2015; Place et al., 2024; Sheng et al., 2007; Tornberg, 2019; Wellkamp et al., 2020). The two species exhibit different lifestyles, where *A. carterae* is a largely benthic sand-dwelling species that will sometimes leave the benthos, while *K. veneficum* is a pelagic and estuarine species (S. Murray & Patterson, 2002; Sheng et al., 2007). The two species have different chloroplast types and origins, indicating an early divergence within the dinoflagellate tree (Yoon et al., 2002; Zapata et al., 2012).

Our survey yielded 18 and 10 putative rhodopsin transcripts in *A. carterae* and *K. veneficum* respectively, based on the iterative HMM screening followed by rhodopsin-specific motif filtering (Figure 22A), yielding high structural similarities to high resolution structures of known rhodopsins (Figure 23A, B), and finally strong conservation of key retinal binding pocket

residues crucial to rhodopsin's function as a light receptor (Figure 23C, D) (Bulzu et al., 2022; Heyne et al., 2000; Luecke et al., 2000; Malakar et al., 2024). Comparisons to non-dinoflagellate rhodopsins and the NCBI non-redundant databases reveal poor sequence identity between our rhodopsin candidates and non-dinoflagellate sequences, and existing annotation methods like InterProScan fail to detect rhodopsins from within our candidate group (Figure 24B, C, Appendix 8). Our results show that recent advances in *in silico* methods now allow for a broader and inclusive identification of candidate sequences, capturing greater diversity without the need for references while still enabling confident filtering and annotation (Bulzu et al., 2022; Ma et al., 2020; Zhang et al., 2024).

Phylogenetic Context of Putative Dinoflagellate Rhodopsins

Phylogenetic placement of the putative rhodopsins into a larger database of known rhodopsins, as collected by Bulzu *et al.,* showed placement in diverse families (Appendix 8). Several algae surveyed exhibit similar breadth; the *Chlamydomonas reinhardtii* genome encodes up to 12 opsins, but only two have been characterized (Greiner et al., 2017; Nagel et al., 2002, 2003). *Symbiodinium* genomes and transcriptomes encode for a similar number of rhodopsin sequences, and these were also distributed across a large portion of the rhodopsin tree (Aihara et al., 2019; González-Pech et al., 2021).

Two of the sequences identified in this study align cleanly within other well-defined clades: a proteorhodopsin and a heliorhodopsin, both from the *K. veneficum* transcriptome (Figure 24A). The functional motifs and structural alignments similarly place the corresponding transcripts into the aforementioned rhodopsin families, with the proteorhodopsin sequence having the DxxxK and DTE motif, and heliorhodopsin with the SxxxK and ESA motif (Figure 25A). The predicted membrane topology of the latter sequence further supports its classification

as a heliorhodopsin, characterized by an extracellular C-terminus, opposite to the cytoplasmic termination typical of other rhodopsins (Kovalev et al., 2020). To the best of our knowledge, this represents the first time a heliorhodopsin sequence has been found in a dinoflagellate.

The function of proteorhodopsins has been established to be a light driven proton pump, while heliorhodopsins have a less distinct function, having recently been found to bind and regulate other proteins such as glutamine synthetase and DNA photolyases (Bamann et al., 2014; Cho et al., 2022; de la Torre et al., 2003; Frigaard et al., 2006; Shim et al., 2022). Proteorhodopsins have been found by other studies in *K. veneficum*, as well as other dinoflagellates, where possible uses include light-driven digestion of food particles in vacuoles (Lin et al., 2010; Meng et al., 2019; Shi et al., 2015; Westermann et al., 2023; Zhang et al., 2024). However, unlike most dinoflagellate proteorhodopsin sequences that fall within the xanthorhodopsin clade of proteorhodopsins, the putative *K. veneficum* proteorhodopsin did not (Lin et al., 2010). Instead, both dinoflagellate sequences are most similar to bacterial homologs (Appendix 8), suggesting they may have originated through horizontal gene transfer (HGT), which has been shown to be prevalent and drivers of gene innovation in dinoflagellates (Moszczyński et al., 2012; Wisecaver et al., 2013).

Several sequences fell into a more ambiguous and functionally diverse clade of rhodopsins, that did not fit cleanly into defined families and functional groups (Figure 24A). The broader clade encompasses several known ion pumps, including halorhodopsins, sodium pumps, and sensory rhodopsins. However, the phylogenetic placement of most of these sequences could not be reconciled with their functional motifs (Appendix 8) (Bulzu et al., 2022; Inoue et al., 2015). The ion pump capacity of a rhodopsin is strongly determined by TM helix C, with even single residue modifications being able to select for proton and not chloride ions (Ernst et al.,

2014; Hayashi et al., 2020; Inoue et al., 2016; Kandori, 2015). For example, KV_comp61380 and AC_DN39985 both fall in a clade with multiple bacteriorhodopsin sequences (Appendix 8), but the *K. veneficum* sequence with a DTE motif is far more likely to preserve a proton-pumping functionality than the *A. carterae* sequence with a GSL motif (Appendix 9).

Unsurprisingly, a large number of our putative dinoflagellate rhodopsin sequences cluster well with the dinoflagellate clade, where the Asp212 in the DxxxK motif is replaced by Asn, and accessory domains are present (Bulzu et al., 2022). The Asp212 residue is a counterion to the protonated retinal Schiff base, but substitution is not entirely detrimental to the proton pump ability of the rhodopsin (Kovalev et al., 2020; Marti et al., 1991; Needleman et al., 1991; Watari et al., 2019).

Some studies suggest the Asp212Asn modification slightly red-shifts the rhodopsin's absorption spectra. This might be responsible for the slightly red-shifted absorptions of the *A. carterae* sequences as compared to the *K. veneficum* (Figure 22D). Many of the sequences within this clade also contained the GTE motif at the helix C locations we analyzed. Govorunova et. al. encountered this GTE motif in metagenomic dinoflagellate rhodopsin sequences (mgdChR1) and, based on a highly conserved TCP motif at positions 89-91 on BR (TTP in BR), classified these sequences as channelrhodopsins (ChR) (Govorunova et al., 2021). In their analysis, these sequences formed a distinct clade from other channelrhodopsins, but their analysis was limited to the channelrhodopsin family. Our predicted proteins with the GTE motif similarly contained the TCP motif in the same location, but fell outside of the channelrhodopsin clade, similarly substituting the conserved Asp212 with Asn. These metagenomic mgdChR1 were shown to have weak ion channel ability, and removal of the C-terminal accessory domain increased the ion-moving ability of the protein (Govorunova et al., 2021).

Chimeric Proteins Represent Likely Novel Functions in Dinoflagellate Rhodopsins

The presence of large cytoplasmic accessory domains outside of the 250-300 amino acid core domain suggests that dinoflagellates may utilize rhodopsins in ways that go beyond canonical functions (Bayley et al., 1981; Kato et al., 2012; Kolbe et al., 2000; Kovalev et al., 2020; Luecke et al., 2001; Ran et al., 2013; Subramaniam & Henderson, 2000). The cytoplasmic location of these domains suggests an internal signaling or enzymatic role as opposed to an external sensing role. In recent years, other eukaryotic lineages have been found to co-opt the rhodopsin backbone, forming chimeras that utilize the light-receptive properties of rhodopsin (Bulzu et al., 2022; Nagata & Inoue, 2021). Fungal BeGC1 combines a core Type 1 microbial rhodopsin, a coiled coil linker domain, and a guanylyl cyclase domain for visual perception (Avelar et al., 2014). In the choanoflagellate *Salpingoeca rosetta*, Rh-PDE is a fusion of a rhodopsin and a cyclic nucleotide phosphodiesterase domain, characterized as a rhodopsin-mediated light-dependent regulator of cell messaging (Watari et al., 2019). In green alga *Chlamydomonas reinhardtii* and *Vovlox carteri*, 2C-Cyclops have a rhodopsin core flanked by cytosolic N- and C-termini domains, an architecture also seen in some sequences found in this study (Awasthi et al., 2020; Tian et al., 2018). This gene fusion of accessory domains may represent the dinoflagellates co-opting the rhodopsin backbone, shifting away from ion-pumping function towards functioning as a light-regulated protein with other primary functions (Avelar et al., 2014; Awasthi et al., 2020; Tian et al., 2018; Watari et al., 2019).

However, given that sequence and structural homology tools were insufficient to further elucidate the identity or function of the accessory domains (Figure 26), these regions represent novel folds or highly divergent adaptations specific to dinoflagellates (Blum et al., 2025; Varadi et al., 2024). Further annotation of these proteins will require approaches beyond *in silico*

prediction, moving back toward functional studies—such as structural determination, biochemical assays, and expression experiments—that can both clarify protein roles and help expand the databases on which computational methods rely, but may also provide novel insights and mechanisms for optogenetics (Awasthi et al., 2020; Roberts et al., 2011; Schnoes et al., 2013).

Tentative Association between Phototaxis and Ion-Pumping Capacity

Our results also demonstrate phototaxis in *K. veneficum,* and little to no phototactic behavior in *A. carterae.* Phototaxis is commonly found in many dinoflagellates, but our data showing that *A. carterae* is not phototactic is also in line with prior studies (Eggersdorfer & Häder, 1991; Forward, 1973; Halldal, 1958; Kamykowski et al., 1998). Following prior observations that dinoflagellates may lose their phototactic capacity after extended culture periods, a more recently isolated strain was tested (CCMP2980) (Hulburt, 1957; Morten et al., 2013; Scorzetti et al., 2009). *Karlodinium veneficum* CCMP1975 was isolated more recently than *A. carterae* CCMP1314, but 15 years before CCMP2980, while still maintaining its capacity for phototaxis. These results suggest that the absence of phototaxis in *A. carterae* is unlikely to be an artifact of long-term culture history (Li et al., 2000). The benthic nature of *A. carterae* does not preclude phototaxis capability, since several benthic alga, including *Gambierdiscus*, a benthic dinoflagellate, demonstrate phototaxis (Liefer et al., 2021; Morelle et al., 2024). The phototactic capacity of *K. veneficum* has not been described in prior literature.

The differences in rhodopsin repertoire between *A. carterae* and *K. veneficum*, particularly with respect to the ion-pumping capacity, may explain the contrasting phototactic behaviors (Figure 27C). Should *A. carterae* still maintain a light-driven ion pump rhodopsin, it would likely represent a novel rhodopsin ion-pumping pathway, while *K. veneficum* has at least

one canonical proteorhodopsin, as well as several other rhodopsins with motifs that may retain ion-pumping capacity (Hayashi et al., 2020; Slamovits et al., 2011; Subramaniam & Henderson, 2000; Suzuki et al., 2022). Ion transport by channelrhodopsins and other rhodopsins can directly influence membrane potential and flagellar responses, providing a plausible mechanism for phototaxis, as has been established in *Chlamydomonas* (Baidukova et al., 2022; Foster et al., 1984; Sineshchekov et al., 2002). Rhodopsins have also been linked to phototaxis in dinoflagellates such as *Oxyrrhis marina* and *Symbiodinium* (Aihara et al., 2019; Hartz et al., 2011). Together, these findings present a highly targeted avenue for further functional and characterization studies to identify the mechanisms of phototaxis in dinoflagellates and highlight the use of *in silico* bioinformatic tools as a vital starting point for bridging sequence-based predictions with phenotype.

Chapter 5: Conclusion

Thus, this dissertation has come to a rest where it began, with the helical, purposeful movements of dinoflagellates. This work set out to expand upon our understanding of movement behavior in dinoflagellates, an important field of study due to their economic, environmental, and human health impacts. Movement behavior is a pivotal part of the life history strategy of any organism and is likely a key contributor to the dinoflagellates' long-standing success in the environment. As established earlier, it also informs sampling methods for studies and monitoring, and understanding triggers for behaviors helps us predict and mitigate their impacts.

The first part of this dissertation focused on developing hardware and software methods for studying movement over the diel periods. This includes a fully programmable cell culture monitoring apparatus capable of tracking cell movement on the surface of culture flask, and a deployed submersible microscope (SuMOS) for observing microbial attachment kinetics *in-situ*. By focusing on open-source methods and low-cost, easily available hardware components, this work makes replicating these studies accessible. This is not just a step towards democratizing behavioral studies not limited to dinoflagellates, but by decreasing the barrier to entry, also enables increased adoption of standardized methods.

The SuMOS is a low-cost submersible microscope that images a replaceable substrate, with infra-red lighting to allow for deployment in low visibility or low light conditions, and is fully self-contained, using replaceable battery packs and storage, to allow for unmanned, untethered deployments lasting more than 24 hours. The SuMOS was successful in observing benthic amphipod colonization and swimming times in the Chesapeake Bay, closely matching prior manual studies on benthic copepod colonization of similar mesh screens, while significantly reducing labor requirements. The SuMOS was also deployed in a marine reef

environment, where TEP deposition and attachment of cells was directly observed, although more work on calibration and a larger dataset is required for the SuMOS to replace existing sampling methods for benthic HAB monitoring.

The second part of the dissertation successfully used the cell culture monitoring apparatus in movement studies of *Gambierdiscus*, the causative agent of ciguatera and a primary driver of this work. It enabled the measurement of movement patterns in six *Gambierdiscus* species across multiple diel periods, revealing that each species exhibits distinct peaks of movement activity at different times of day. These differences were found to be maintained across different strains independent of location of isolation, and showed no correlation with morphology, phylogenetics, or metabolomic profiles.

In addition, the analysis revealed that the different species exhibit different biases towards movement on and off the surface in the water column, as well as the percentage of cells that leave the surface daily. The swimming speeds of three species were also measured using digital holography, showing that the *Gambierdiscus* cells are slow swimmers relative to their body size. These behaviors impact the cells' proliferation as well as nutrient and light environment heavily but also have implications as to how future studies sample and monitor for them. The presence of diel patterns in movement, as well as different movement timing indicates that deployed artificial substrate samplers should be deployed for periods in excess of 24 hours, while natural substrate sampling methods need to take into account the behavior of the local species composition when designing sampling schedules.

In addition to diel movement patterns, the cell monitoring apparatus was used to determine that the movement of three species of *Gambierdiscus* was regulated by an endogenous circadian rhythm, where the bursts of movement would continue in the absence of the light/dark

transitions. The circadian rhythms were also shown to have different initiations and responses to light or dark, indicating they are regulated by different oscillator systems. Repeating the observations using red, green, and blue narrow wavelength light sources tells a similar story, with each species showing different responses to the different wavelengths. The identity of the molecular clock systems, as well as the proteins that entrain them, is still enigmatic, but the presence of what appears to be three systems in three species from the same genus highlights the high degree of divergence that can be found in dinoflagellates. This divergence from the main tree of life, as well as within the dinoflagellate lineage itself, is just another facet in why linking genes to function in these organisms remains such a formidable task.

The third part of this work focused on methods for illuminating a small portion of the dark genes – genes which standard bioinformatic methods are unable to annotate and identify, and that are widespread in the dinoflagellate lineage. To simplify the search space, the work focused on identifying and characterizing microbial rhodopsins, a family of retinylidene proteins with a deep corpus of literature, within two species of core dinoflagellates with deeply sequenced and studied transcriptomes, *Amphidinium carterae* and *Karlodinium veneficum*. Using an annotation method that combined remote homolog detection with functional and structural motif guided filtering, 18 and 10 putative rhodopsins were identified from the transcriptomes of the two species, respectively. Half of these sequences were not identified using regular annotation tools. Of these, we identify two canonical rhodopsins, a proteorhodopsin and heliorhodopsin, the latter being the first finding in a dinoflagellate.

Additional analysis of key functional motifs revealed that *A. carterae* likely retains no canonical ion-pumping capability, whereas *K. veneficum* does, a finding correlated with the phototactic capability of the two species. Structural analysis also revealed extensive gene fusions

of accessory domains with the rhodopsin core, but the accessory domains could not be annotated even with current state-of-the-art remote homolog detection methods. Taken together, this indicates that dinoflagellates may have co-opted the rhodopsin backbone, originally a proton pump, into a switch for other light-gated protein functions, though those functions remain novel and uncharacterized.

In conclusion, this dissertation has shed a light on the behavior and mechanisms that have made dinoflagellates so successful for so long. By developing open-source hardware for behavioral studies, we enable the expansion of these types of studies into different fields and focuses. Using these methods, we characterized the movement of *Gambierdiscus*, demonstrating movement as a part of their ecology, and providing a baseline understanding of their daily schedules for others to build on. We extended this into finding endogenous circadian rhythms that regulate this movement, as well as what appears to be three different oscillator systems and entrainment systems in as many species, though the underlying mechanisms are still enigmatic. In trying to establish links between gene and function, we characterized the rhodopsin repertoires of *A. carterae* and *K. veneficum*, two species with notable similarities and differences, and found few canonical representatives of rhodopsins, as well as a lack of canonical ion-pumping capacity in *A. carterae* coupled with a lack of phototactic capacity. Instead, we find a preponderance of chimeric gene fusions of the rhodopsin backbone with novel accessory domains, indicating a shift away from the original ion-pumping function of rhodopsins into yet undescribed light-gated functionality. Taken together, these studies illuminate new aspects of dinoflagellate biology while also revealing just how much of their complexity remains hidden.

With this, we demonstrate that following advances in technology, computational methods, and scientific techniques, we can take discrete steps into better understanding the

dinoflagellate lineage. And yet more questions remain, with each new insight revealing even deeper layers of uncertainty, reminding us how much remains to be understood about this enigmatic group of algae. Still, dinoflagellates have been around more than twice as long as the dinosaurs. What is a little more time for them to remain our little swimming enigmas?

Appendices

Appendix 1: Bill of Materials for SuMOS Waterproof Housing

Designator	Component	Number	Cost per unit (USD)	Total cost (USD)	Source of materials	Notes
PVC Pipe	*4" Sch80 PVC*	16cm	9	9		
PVC Union	4" PVC Union	1	29.99	29.99	Amazon	
PVC Cap	4" PVC Cap	1	12	12	Amazon	
Acrylic window	¼" clear acrylic panel	1	15	15	Amazon	
Securing Rods	5mm Aluminium Extruded Rod	1	1	1	Amazon	
PLA filament	Polymaker PLA PRO Filament Black	1	25	25	Amazon	
TPU Filament	SpiderMaker SpiderFlex Matte Finish Flexible TPE(TPU)	1	5	5	Amazon	Cost is for weight used.

Appendix 2: Bill of Materials for SuMOS Internal Electronics

Designator	Component	Number	Cost per unit (USD)	Total cost (USD)	Source of materials	Notes
Raspberry Pi Zero 2W	Raspberry Pi Zero 2W	1	15	15	Adafruit	
SD Card	SanDisk 16GB Ultra microSDHC UHS-I Memory Card	1	6	*6*	Amazon	
Camera Module	*Raspberry Pi Camera Module 3 NoIR - 12MP 75 Degree Infrared Lens*	1	25	25	Adafruit	
-Camera Ribbon Cable	Raspberry Pi Zero v1.3 Camera Cable	1	5.95	5.95	Adafruit	
TSL2591	Adafruit TSL2591 High Dynamic Range Digital Light Sensor - STEMMA QT	1	6.95	6.95	Amazon	
-Stemma QT connector	STEMMA QT / Qwiic JST SH 4-pin Cable with Premium Female Sockets	1	0.95	0.95	Adafruit	

IR LED	Adafruit Super-bright 5mm IR LED	2	0.44	0.88	Amazon	
Indicator LED	CHANZON 3mm LED Diode Lights	1	0.06	0.06	Amazon	Any 2-2.2V LED is suitable.
RTC (Real time clock)	DS3231 Real Time Clock Module	1	3	3	Amazon	
Power Bank	Anker PowerCore 10,000 mAh Redux, Power Bank	1	35	35	Amazon	
Power Cable	Cable Matters Right Angle USB Cable	1	4	4	Amazon	Contains two cables, but only one is angled the right direction.
USB Drive	SanDisk 32GB 3-Pack Ultra Fit USB 3.1 Flash Drive	1	6	*6*	Amazon	Other USB devices work, but the SuMOS was designed with this form factor in mind.
USB Data Cable	StarTech.com 5in Right Angle Micro USB to USB OTG Host Adapter M/F	1	3.86	3.86	Amazon	
Macro Lens	Leshareselect Professional 2 in 1 Lens Universal Clip 37mm Mobile Phone Lens 0.45x 49uv Super Wide-Angle + Macro HD Lens for All Smartphones	2	7	14	Amazon	
+10 Diopter Lens	37mm Closeup Filter Set	1	10	10	Amazon	
IR Resistor	56Ω 1/4W Metal Film Resistor	1	0.01	0.01	Amazon	
Indicator Resistor	68Ω 1/4W Metal Film	1	0.01	0.01	Amazon	

Appendix 3: Description of Files in Public Repository for SuMOS.

Name	Description	Link
3D Models	3D models in .F3D format for the housings, wrenches, and mounts	https://osf.io/zhbjf/
divePiSettings.conf	Text file to be placed in USB drive that control the capture parameters of the device	https://osf.io/zhbjf/
Install Scripts	Scripts used for setup, testing, and streaming of the SuMOS	https://osf.io/zhbjf/

Appendix 4: Video of *Gambierdiscus* swimming in UFO swimming mode, available digitally.

Appendix 5: Video of *Gambierdiscus* swimming in spiral swimming mode, available digitally.

Appendix 6: Video of *Gambierdiscus* with many cells leaving surface of imaging flask, available digitally.

Appendix 7: Video of *Gambierdiscus* moving laterally on surface of flask, available digitally.

Appendix 8: Annotated PhyloXML file for phylogenetic tree of rhodopsins, with *A. carterae* sequences colored in blue and *K. veneficum* in orange. Available digitally.

Appendix 9: Sequences, motifs, and domain boundaries of the putative rhodopsin transcripts. Available digitally.

Bibliography

Abdelgalil, M., Aboelkassem, Y., & Taha, H. (2022). Sea urchin sperm exploit extremum seeking control to find the egg. *Physical Review E*, *106*(6), L062401. https://doi.org/10.1103/PhysRevE.106.L062401

Ahmed, N., Milne, P. J., & Harris, S. G. (1975). Electrocardiographic Data Compression Via Orthogonal Transforms. *IEEE Transactions on Biomedical Engineering*, *BME-22*(6), 484–487. IEEE Transactions on Biomedical Engineering. https://doi.org/10.1109/TBME.1975.324469

Aihara, Y., Maruyama, S., Baird, A. H., Iguchi, A., Takahashi, S., & Minagawa, J. (2019). Green fluorescence from cnidarian hosts attracts symbiotic algae. *Proceedings of the National Academy of Sciences*, *116*(6), 2118–2123. https://doi.org/10.1073/pnas.1812257116

Alekseev, A., Gordeliy, V., & Bamberg, E. (2022). Rhodopsin-Based Optogenetics: Basics and Applications. *Methods in Molecular Biology (Clifton, N.J.)*, *2501*, 71–100. https://doi.org/10.1007/978-1-0716-2329-9_3

Alexandre, G. (2010). Coupling metabolism and chemotaxis-dependent behaviours by energy taxis receptors. *Microbiology (Reading, England)*, *156*(Pt 8), 2283–2293. https://doi.org/10.1099/mic.0.039214-0

Alexandre, G., Greer-Phillips, S., & Zhulin, I. B. (2004). Ecological role of energy taxis in microorganisms. *FEMS Microbiology Reviews*, *28*(1), 113–126. https://doi.org/10.1016/j.femsre.2003.10.003

Allen, R. M., Metaxas, A., & Snelgrove, P. V. R. (2018). Applying Movement Ecology to Marine Animals with Complex Life Cycles. *Annual Review of Marine Science*, *10*(Volume 10, 2018), 19–42. https://doi.org/10.1146/annurev-marine-121916-063134

Anderson, D. M., Fensin, E., Gobler, C. J., Hoeglund, A. E., Hubbard, K. A., Kulis, D. M., Landsberg, J. H., Lefebvre, K. A., Provoost, P., Richlen, M. L., Smith, J. L., Solow, A. R., & Trainer, V. L. (2021). Marine harmful algal blooms (HABs) in the United States: History, current status and future trends. *Harmful Algae*, *102*, 101975. https://doi.org/10.1016/j.hal.2021.101975

Artolozaga, I., Ayo, B., Latatu, A., Azúa, I., Unanue, M., & Iriberri, J. (2000). Spatial distribution of protists in the presence of macroaggregates in a marine system. *FEMS Microbiology Ecology*, *33*(3), 191–196. https://doi.org/10.1111/j.1574-6941.2000.tb00741.x

Assun ão, J., Catarina Guedes, A., & Xavier Malcata, F. (2017). Biotechnological and Pharmacological Applications of Biotoxins and Other Bioactive Molecules from Dinoflagellates. *Marine Drugs 2017, Vol. 15, Page 393*, *15*(12), 393. https://doi.org/10.3390/MD15120393

Avelar, G. M., Schumacher, R. I., Zaini, P. A., Leonard, G., Richards, T. A., & Gomes, S. L. (2014). A rhodopsin-guanylyl cyclase gene fusion functions in visual perception in a fungus. *Current Biology: CB*, *24*(11), 1234–1240. https://doi.org/10.1016/j.cub.2014.04.009

Awasthi, M., Sushmita, K., Kaushik, M. S., Ranjan, P., & Kateriya, S. (2020). Novel Modular Rhodopsins from Green Algae Hold Great Potential for Cellular Optogenetic Modulation Across the Biological Model Systems. *Life (Basel, Switzerland)*, *10*(11), 259. https://doi.org/10.3390/life10110259

Bachvaroff, T. R. (2019). A precedented nuclear genetic code with all three termination codons reassigned as sense codons in the syndinean *Amoebophrya sp.* ex *Karlodinium veneficum*. *PLoS ONE*, *14*(2), e0212912. https://doi.org/10.1371/journal.pone.0212912

Bachvaroff, T. R., Gornik, S. G., Concepcion, G. T., Waller, R. F., Mendez, G. S., Lippmeier, J. C., & Delwiche, C. F. (2014). Dinoflagellate phylogeny revisited: Using ribosomal proteins to resolve deep branching dinoflagellate clades. *Molecular Phylogenetics and Evolution*, *70*, 314–322. https://doi.org/10.1016/j.ympev.2013.10.007

Bachvaroff, T. R., & Place, A. R. (2008). From Stop to Start: Tandem Gene Arrangement, Copy Number and Trans-Splicing Sites in the Dinoflagellate *Amphidinium carterae*. *PLOS ONE*, *3*(8), e2929. https://doi.org/10.1371/journal.pone.0002929

Baek, S. H., Shimode, S., Shin, K., Han, M.-S., & Kikuchi, T. (2009). Growth of dinoflagellates, *Ceratium furca* and *Ceratium fusus* in Sagami Bay, Japan: The role of vertical migration and cell division. *Harmful Algae*, *8*(6), 843–856. https://doi.org/10.1016/j.hal.2009.04.001

Baek, S. H., Shin, H. H., Choi, H.-W., Shimode, S., Hwang, O. M., Shin, K., & Kim, Y.-O. (2011). Ecological behavior of the dinoflagellate *Ceratium furca* in Jangmok harbor of Jinhae Bay, Korea. *Journal of Plankton Research*, *33*(12), 1842–1846. https://doi.org/10.1093/plankt/fbr075

Baidukova, O., Oppermann, J., Kelterborn, S., Fernandez Lahore, R. G., Schumacher, D., Evers, H., Kamrani, Y. Y., & Hegemann, P. (2022). Gating and ion selectivity of Channelrhodopsins are critical for photo-activated orientation of *Chlamydomonas* as shown by in vivo point mutation. *Nature Communications*, *13*(1), 7253. https://doi.org/10.1038/s41467-022-35018-6

Bakker, J. (2023). *Applied Multivariate Statistics in R*.

Bamann, C., Bamberg, E., Wachtveitl, J., & Glaubitz, C. (2014). Proteorhodopsin. *Biochimica et Biophysica Acta (BBA) - Bioenergetics*, *1837*(5), 614–625. https://doi.org/10.1016/j.bbabio.2013.09.010

Barnett, A., Méléder, V., Dupuy, C., & Lavaud, J. (2020). The Vertical Migratory Rhythm of Intertidal Microphytobenthos in Sediment Depends on the Light Photoperiod, Intensity, and Spectrum: Evidence for a Positive Effect of Blue Wavelengths. *Frontiers in Marine Science*, *7*. https://doi.org/10.3389/fmars.2020.00212

Bayley, H., Huang, K. S., Radhakrishnan, R., Ross, A. H., Takagaki, Y., & Khorana, H. G. (1981). Site of attachment of retinal in bacteriorhodopsin. *Proceedings of the National Academy of Sciences of the United States of America*, *78*(4), 2225. https://doi.org/10.1073/pnas.78.4.2225

Berdalet, E., Fleming, L. E., Gowen, R., Davidson, K., Hess, P., Backer, L. C., Moore, S. K., Hoagland, P., & Enevoldsen, H. (2015). Marine harmful algal blooms, human health and wellbeing: Challenges and opportunities in the 21st century. *Journal of the Marine Biological Association of the United Kingdom. Marine Biological Association of the United Kingdom*, *2015*, 10.1017/S0025315415001733. https://doi.org/10.1017/S0025315415001733

Berg, S., Kutra, D., Kroeger, T., Straehle, C. N., Kausler, B. X., Haubold, C., Schiegg, M., Ales, J., Beier, T., Rudy, M., Eren, K., Cervantes, J. I., Xu, B., Beuttenmueller, F., Wolny, A., Zhang, C., Koethe, U., Hamprecht, F. A., & Kreshuk, A. (2019). ilastik: Interactive machine learning for (bio)image analysis. *Nature Methods 2019 16:12*, *16*(12), 1226–1232. https://doi.org/10.1038/s41592-019-0582-9

Bergo, V. B., Ntefidou, M., Trivedi, V. D., Amsden, J. J., Kralj, J. M., Rothschild, K. J., & Spudich, J. L. (2006). Conformational Changes in the Photocycle of *Anabaena* Sensory Rhodopsin. *Journal of Biological Chemistry*, *281*(22), 15208–15214. https://doi.org/10.1074/jbc.M600033200

Binder, J. L., Berendzen, J., Stevens, A. O., He, Y., Wang, J., Dokholyan, N. V., & Oprea, T. I. (2022). AlphaFold illuminates half of the dark human proteins. *Current Opinion in Structural Biology*, *74*, 102372. https://doi.org/10.1016/j.sbi.2022.102372

Blasco, D. (1978). Observations on the diel migration of marine dinoflagellates off the Baja California coast. *Marine Biology*, *46*(1), 41–47. https://doi.org/10.1007/BF00393819

Block, B. A., Dewar, H., Blackwell, S. B., Williams, T. D., Prince, E. D., Farwell, C. J., Boustany, A., Teo, S. L. H., Seitz, A., Walli, A., & Fudge, D. (2001). Migratory Movements, Depth Preferences, and Thermal Biology of Atlantic Bluefin Tuna. *Science*, *293*(5533), 1310–1314. https://doi.org/10.1126/science.1061197

Blum, M., Andreeva, A., Florentino, L. C., Chuguransky, S. R., Grego, T., Hobbs, E., Pinto, B. L., Orr, A., Paysan-Lafosse, T., Ponamareva, I., Salazar, G. A., Bordin, N., Bork, P., Bridge, A., Colwell, L., Gough, J., Haft, D. H., Letunic, I., Llinares-López, F., … Bateman, A. (2025). InterPro: The protein sequence classification resource in 2025. *Nucleic Acids Research*, *53*(D1), D444–D456. https://doi.org/10.1093/nar/gkae1082

Bollens, S. M., Quenette, J. A., & Rollwagen-Bollens, G. (2012). Predator-enhanced diel vertical migration in a planktonic dinoflagellate. *Marine Ecology Progress Series*, *447*, 49–54. https://doi.org/10.3354/meps09467

Bomber, J. W., Guillard, R. R. L., & Nelson, W. G. (1988). Rôles of temperature, salinity, and light in seasonality, growth, and toxicity of ciguatera-causing *Gambierdiscus toxicus*

Adachi et Fukuyo (Dinophyceae). *Journal of Experimental Marine Biology and Ecology*, *115*(1), 53–65. https://doi.org/10.1016/0022-0981(88)90189-X

Bowman, R., Müllenbroich, C., Diederich, B., McConnell, G., Faez, S., & Arancio, J. (2024). Open, reproducible hardware for microscopy. *Philosophical Transactions. Series A, Mathematical, Physical, and Engineering Sciences*, *382*(2274), 20230112. https://doi.org/10.1098/rsta.2023.0112

Bowman, R. W. (2023). Improving instrument reproducibility with open source hardware. *Nature Reviews Methods Primers*, *3*(1), 27. https://doi.org/10.1038/s43586-023-00218-x

Brakel, W. H. (1979). Small-Scale Spatial Variation in Light Available to Coral Reef Benthos: Quantum Irradiance Measurements from a Jamaican Reef. *Bulletin of Marine Science*, *29*(3), 406–413.

Bravo, I., Figueroa, R. I., & Fraga, S. (2014). Cellular and nuclear morphological variability within a single species of the toxigenic dinoflagellate genus *Gambierdiscus*: Relationship to life-cycle processes. *Harmful Algae*, *40*, 1–8. https://doi.org/10.1016/j.hal.2014.09.009

Bravo, I., Rodriguez, F., Ramilo, I., Rial, P., & Fraga, S. (2019). Ciguatera-Causing Dinoflagellate *Gambierdiscus* spp. (Dinophyceae) in a Subtropical Region of North Atlantic Ocean (Canary Islands): Morphological Characterization and Biogeography. *Toxins*, *11*(7), Article 7. https://doi.org/10.3390/toxins11070423

Bravo, I., Vila, M., Casabianca, S., Rodriguez, F., Rial, P., Riobó, P., & Penna, A. (2012). Life cycle stages of the benthic palytoxin-producing dinoflagellate *Ostreopsis* cf. *Ovata* (Dinophyceae). *Harmful Algae*, *18*, 24–34. https://doi.org/10.1016/j.hal.2012.04.001

Brown, J., Behnam, R., Coddington, L., Tervo, D. G. R., Martin, K., Proskurin, M., Kuleshova, E., Park, J., Phillips, J., Bergs, A. C. F., Gottschalk, A., Dudman, J. T., & Karpova, A. Y.

(2018). Expanding the Optogenetics Toolkit by Topological Inversion of Rhodopsins. *Cell*, *175*(4), 1131-1140.e11. https://doi.org/10.1016/j.cell.2018.09.026

Bulzu, P.-A., Kavagutti, V. S., Andrei, A.-S., & Ghai, R. (2022). The Evolutionary Kaleidoscope of Rhodopsins. *mSystems*, *7*(5), e00405-22. https://doi.org/10.1128/msystems.00405-22

Castells, F., Mora, C., Rieta, J. J., Moratal-Pérez, D., & Millet, J. (2005). Estimation of atrial fibrillatory wave from single-lead atrial fibrillation electrocardiograms using principal component analysis concepts. *Medical and Biological Engineering and Computing*, *43*(5), 557–560. https://doi.org/10.1007/BF02351028

Chateau-Degat, M.-L., Chinain, M., Cerf, N., Gingras, S., Hubert, B., & Dewailly, É. (2005). Seawater temperature, *Gambierdiscus* spp. Variability and incidence of ciguatera poisoning in French Polynesia. *Harmful Algae*, *4*(6), 1053–1062. https://doi.org/10.1016/j.hal.2005.03.003

Chinain, M., Darius, H. T., Ung, A., Cruchet, P., Wang, Z., Ponton, D., Laurent, D., & Pauillac, S. (2010). Growth and toxin production in the ciguatera-causing dinoflagellate *Gambierdiscus polynesiensis* (Dinophyceae) in culture. *Toxicon: Official Journal of the International Society on Toxinology*, *56*(5), 739–750. https://doi.org/10.1016/j.toxicon.2009.06.013

Chinain, M., Faust, M. A., & Pauillac, S. (1999). Morphology and Molecular Analyses of Three Toxic Species of *Gambierdiscus* (dinophyceae): G. Pacificus, Sp. Nov., G. Australes, Sp. Nov., and G. Polynesiensis, Sp. Nov. *Journal of Phycology*, *35*(6), 1282–1296. https://doi.org/10.1046/j.1529-8817.1999.3561282.x

Chinain, M., Gatti, C. M. I., Darius, H. T., Quod, J.-P., & Tester, P. A. (2021). Ciguatera poisonings: A global review of occurrences and trends. *Harmful Algae*, *102*, 101873. https://doi.org/10.1016/j.hal.2020.101873

Cho, S.-G., Song, M., Chuon, K., Shim, J., Meas, S., & Jung, K.-H. (2022). Heliorhodopsin binds and regulates glutamine synthetase activity. *PLOS Biology*, *20*(10), e3001817. https://doi.org/10.1371/journal.pbio.3001817

Christianson, R., & Sweeney, B. M. (1972). Sensitivity to Stimulation, a Component of the Circadian Rhythm in Luminescence in *Gonyaulax*. *Plant Physiology*, *49*(6), 994. https://doi.org/10.1104/PP.49.6.994

Clayton, S., Chrabot, J., Echevarria, M., Gibala-Smith, L., Mogatas, K., Bernhardt, P., & Mulholland, M. (2024). Diel Vertical Migration Rates of the Dinoflagellate Species *Margalefidinium polykrikoides* in a lower Chesapeake Bay Tributary. *Frontiers in Microbiology*, *15*. https://doi.org/10.3389/fmicb.2024.1378552

Cock, P. J. A., Antao, T., Chang, J. T., Chapman, B. A., Cox, C. J., Dalke, A., Friedberg, I., Hamelryck, T., Kauff, F., Wilczynski, B., & de Hoon, M. J. L. (2009). Biopython: Freely available Python tools for computational molecular biology and bioinformatics. *Bioinformatics*, *25*(11), 1422–1423. https://doi.org/10.1093/bioinformatics/btp163

Cohen, S. E., & Golden, S. S. (2015). Circadian Rhythms in Cyanobacteria. *Microbiology and Molecular Biology Reviews*, *79*(4), 373–385. https://doi.org/10.1128/mmbr.00036-15

Colley, N. J., & Nilsson, D. E. (2016). Photoreception in Phytoplankton. *Integrative and Comparative Biology*, *56*(5), 764–775. https://doi.org/10.1093/ICB/ICW037

Crump, J., McLay, C., & Chambers, S. (1999). Ciguatera fish poisoning. *Postgraduate Medical Journal*, *75*(889), 678–679.

Dagenais-Bellefeuille, S., & Morse, D. (2013). Putting the N in dinoflagellates. *Frontiers in Microbiology*, *4*. https://doi.org/10.3389/fmicb.2013.00369

Darius, H. T., Roué, M., Sibat, M., Viallon, J., Gatti, C. M. iti, Vandersea, M. W., Tester, P. A., Litaker, R. W., Amzil, Z., Hess, P., & Chinain, M. (2018). *Tectus niloticus* (Tegulidae, Gastropod) as a Novel Vector of Ciguatera Poisoning: Detection of Pacific Ciguatoxins in Toxic Samples from Nuku Hiva Island (French Polynesia). *Toxins*, *10*(1), Article 1. https://doi.org/10.3390/toxins10010002

Davison, P. A., Tu, W., Xu, J., Della Valle, S., Thompson, I. P., Hunter, C. N., & Huang, W. E. (2022). Engineering a Rhodopsin-Based Photo-Electrosynthetic System in Bacteria for CO2 Fixation. *ACS Synthetic Biology*, *11*(11), 3805–3816. https://doi.org/10.1021/acssynbio.2c00397

Davy, S. K., Allemand, D., & Weis, V. M. (2012). Cell Biology of Cnidarian-Dinoflagellate Symbiosis. *Microbiology and Molecular Biology Reviews : MMBR*, *76*(2), 229–261. https://doi.org/10.1128/MMBR.05014-11

de la Torre, J. R., Christianson, L. M., Béjà, O., Suzuki, M. T., Karl, D. M., Heidelberg, J., & DeLong, E. F. (2003). Proteorhodopsin genes are distributed among divergent marine bacterial taxa. *Proceedings of the National Academy of Sciences*, *100*(22), 12830–12835. https://doi.org/10.1073/pnas.2133554100

de Souza, K. B., Jephson, T., Hasper, T. B., & Carlsson, P. (2014). Species-specific dinoflagellate vertical distribution in temperature-stratified waters. *Marine Biology*, *161*(8), 1725–1734. https://doi.org/10.1007/s00227-014-2446-2

de Vargas, C., Audic, S., Henry, N., Decelle, J., Mahé, F., Logares, R., Lara, E., Berney, C., Le Bescot, N., Probert, I., Carmichael, M., Poulain, J., Romac, S., Colin, S., Aury, J.-M.,

Bittner, L., Chaffron, S., Dunthorn, M., Engelen, S., … Karsenti, E. (2015). Eukaryotic plankton diversity in the sunlit ocean. *Science*, *348*(6237), 1261605. https://doi.org/10.1126/science.1261605

Dedman, S., Aalto, E. A., Stokesbury, M. J. W., Schallert, R. J., Castleton, M. R., & Block, B. A. (2023). Assignment of tracks from tagged Atlantic bluefin tuna *Thunnus thynnus* to potential stocks using behavioural differences and habitat partitioning. *Frontiers in Marine Science*, *10*. https://doi.org/10.3389/fmars.2023.1165910

Delgado, A., Power, S., Richards, C., Daly, P., Briciu-Burghina, C., Delauré, Y., & Regan, F. (2023). Establishment of an antifouling performance index derived from the assessment of biofouling on typical marine sensor materials. *Science of The Total Environment*, *887*, 164059. https://doi.org/10.1016/j.scitotenv.2023.164059

Dickey, R. W., & Plakas, S. M. (2010). Ciguatera: A public health perspective. *Toxicon*, *56*(2), 123–136. https://doi.org/10.1016/j.toxicon.2009.09.008

Dodge, J. D., & Crawford, R. M. (1969). Observations on the fine structure of the eyespot and associated organelles in the dinoflagellate *Glenodinium Foliaceum*. *Journal of Cell Science*, *5*(2), 479–493. https://doi.org/10.1242/jcs.5.2.479

Domènech, F., Tomás, J., Crespo-Picazo, J. L., García-Párraga, D., Raga, J. A., & Aznar, F. J. (2017). To Swim or Not to Swim: Potential Transmission of *Balaenophilus manatorum* (Copepoda: Harpacticoida) in Marine Turtles. *PLoS ONE*, *12*(1), e0170789. https://doi.org/10.1371/journal.pone.0170789

Durand-Clement, M. (1987). Study of Production and Toxicity of Cultured *Gambierdiscus toxicus*. *Biological Bulletin*, *172*(1), 108–121. https://doi.org/10.2307/1541610

Durán-Riveroll, L. M., Cembella, A. D., & Okolodkov, Y. B. (2019). A Review on the Biodiversity and Biogeography of Toxigenic Benthic Marine Dinoflagellates of the Coasts of Latin America. *Frontiers in Marine Science*, *6*. https://doi.org/10.3389/fmars.2019.00148

Durham, W. M., Climent, E., Barry, M., De Lillo, F., Boffetta, G., Cencini, M., & Stocker, R. (2013). Turbulence drives microscale patches of motile phytoplankton. *Nature Communications 2013 4:1*, *4*(1), 1–7. https://doi.org/10.1038/ncomms3148

Echenique-Subiabre, I., Jackrel, S. L., McCarren, J., James, C. C., Perez-Coronel, E., Tran, C., Perreault, M., Farah, U., White, P. S., Baker, H. K., Wall, C. B., Sager, L., Becker, S., Barton, A. D., & Shurin, J. B. (2025). Traits determine dispersal and colonization abilities of microbes. *Applied and Environmental Microbiology*, *91*(3), e02055-24. https://doi.org/10.1128/aem.02055-24

Eggersdorfer, B., & Häder, D.-P. (1991). Phototaxis, gravitaxis and vertical migrations in the marine dinoflagellate *Prorocentrum micans*. *FEMS Microbiology Letters*, *85*(4), 319–326. https://doi.org/10.1111/j.1574-6968.1991.tb04758.x

Eppley, R. W., Holm-Harisen, O., & Strickland, J. D. (1968). Some Observations on the Vertical Migration of Dinoflagellates. *Journal of Phycology*, *4*(4), 333–340. https://doi.org/10.1111/j.1529-8817.1968.tb04704.x

Erickson, J. S., Hashemi, N., Sullivan, J. M., Weidemann, A. D., & Ligler, F. S. (2012). In Situ Phytoplankton Analysis: There's Plenty of Room at the Bottom. *Analytical Chemistry*, *84*(2), 839–850. https://doi.org/10.1021/ac201623k

Ernst, O. P., Lodowski, D. T., Elstner, M., Hegemann, P., Brown, L. S., & Kandori, H. (2014). Microbial and Animal Rhodopsins: Structures, Functions, and Molecular Mechanisms. *Chemical Reviews*, *114*(1), 126–163. https://doi.org/10.1021/cr4003769

Ershov, D., Phan, M.-S., Pylvänäinen, J. W., Rigaud, S. U., Le Blanc, L., Charles-Orszag, A., Conway, J. R. W., Laine, R. F., Roy, N. H., Bonazzi, D., Duménil, G., Jacquemet, G., & Tinevez, J.-Y. (2022). TrackMate 7: Integrating state-of-the-art segmentation algorithms into tracking pipelines. *Nature Methods*, *19*(7), 829–832. https://doi.org/10.1038/s41592-022-01507-1

EVOS Onstage Incubator—US. (n.d.). Retrieved September 8, 2025, from https://www.thermofisher.com/us/en/home/life-science/cell-analysis/cellular-imaging/evos-cell-imaging-systems/accessories/onstage-incubator.html

Falkowski, P. (2012). Ocean Science: The power of plankton. *Nature*, *483*(7387), S17–S20. https://doi.org/10.1038/483S17a

Falkowski, P. G., Fenchel, T., & Delong, E. F. (2008). The Microbial Engines That Drive Earth's Biogeochemical Cycles. *Science*, *320*(5879), 1034–1039. https://doi.org/10.1126/science.1153213

Faust, M. A. (1995). Observation of Sand-Dwelling Toxic Dinoflagellates (dinophyceae) from Widely Differing Sites, Including Two New Species. *Journal of Phycology*, *31*(6), 996–1003. https://doi.org/10.1111/j.0022-3646.1995.00996.x

Fenchel, T. (2001). How Dinoflagellates Swim. *Protist*, *152*(4), 329–338. https://doi.org/10.1078/1434-4610-00071

Feng, F., Wang, S., Zhang, X., Fang, X., Xu, Y., & Liu, J. (2025). Fine-Grained Identification of Benthic Diatom Scanning Electron Microscopy Images Using a Deep Learning

Framework. *Journal of Marine Science and Engineering*, *13*(6), 1095. https://doi.org/10.3390/jmse13061095

Fernández-Zabala, J., Amorim, A., Tuya, F., Herrera, R., & Soler-Onís, E. (2022). Playing hide and seek: Distribution with depth of potentially harmful epibenthic dinoflagellates of Southern El Hierro Island, Canary Islands (NE Atlantic). *Harmful Algae*, *117*, 102271. https://doi.org/10.1016/j.hal.2022.102271

Field, C. B., Behrenfeld, M. J., Randerson, J. T., & Falkowski, P. (1998). Primary Production of the Biosphere: Integrating Terrestrial and Oceanic Components. *Science*, *281*(5374), 237–240. https://doi.org/10.1126/science.281.5374.237

Figueroa, R. I., Garcés, E., & Bravo, I. (2007). Comparative study of the life cycles of *Alexandrium tamutum* and *Alexandrium minutum* (Gonyaulacales, Dinophyceae) in culture. *Journal of Phycology*, *43*(5), 1039–1053. https://doi.org/10.1111/j.1529-8817.2007.00393.x

Fish along the Florida Keys are spinning in circles until they die—And no one knows why. (2025, September 24). Animals. https://www.nationalgeographic.com/animals/article/spinning-fish-sawfish-florida-toxins-diseases-algae

Fitt, W. K. (1984). The role of chemosensory behavior of *Symbiodinium microadriaticum*, intermediate hosts, and host behavior in the infection of coelenterates and molluscs with zooxanthellae. *Marine Biology*, *81*(1), 9–17. https://doi.org/10.1007/BF00397620

Forward, R. B. (1973). Phototaxis in a Dinoflagellate: Action Spectra as Evidence for a Two-Pigment System*. *PIanta (Berl.)*, *111*, 167–178.

Forward, R. B. (1974). Phototaxis by the dinoflagellate *Gymnodinium splendens* Lebour. *The Journal of Protozoology*, *21*(2), 312–315. https://doi.org/10.1111/J.1550-7408.1974.TB03659.X

Foster, K. W., Saranak, J., Patel, N., Zarilli, G., Okabe, M., Kline, T., & Nakanishi, K. (1984). A rhodopsin is the functional photoreceptor for phototaxis in the unicellular eukaryote *Chlamydomonas*. *Nature*, *311*(5988), 756–759. https://doi.org/10.1038/311756a0

Foster, K. W., & Smyth, R. D. (1980). Light Antennas in phototactic algae. *Microbiological Reviews*, *44*(4), 572–630.

Fraga, S., Rodríguez, F., Caillaud, A., Diogène, J., Raho, N., & Zapata, M. (2011). *Gambierdiscus excentricus* sp. Nov. (Dinophyceae), a benthic toxic dinoflagellate from the Canary Islands (NE Atlantic Ocean). *Harmful Algae*, *11*, 10–22. https://doi.org/10.1016/j.hal.2011.06.013

Francis, D. (1967). On the Eyespot of the Dinoflagellate, *Nematodinium*. *Journal of Experimental Biology*, *47*(3), 495–501. https://doi.org/10.1242/jeb.47.3.495

Friedman, M. A., Fleming, L. E., Fernandez, M., Bienfang, P., Schrank, K., Dickey, R., Bottein, M.-Y., Backer, L., Ayyar, R., Weisman, R., Watkins, S., Granade, R., & Reich, A. (2008). Ciguatera Fish Poisoning: Treatment, Prevention and Management. *Marine Drugs*, *6*(3), 456–479. https://doi.org/10.3390/md20080022

Frigaard, N.-U., Martinez, A., Mincer, T. J., & DeLong, E. F. (2006). Proteorhodopsin lateral gene transfer between marine planktonic Bacteria and Archaea. *Nature*, *439*(7078), 847–850. https://doi.org/10.1038/nature04435

Funaki, H., Gaonkar, C. C., Kataoka, T., Nishimura, T., Tanaka, K., Yanagida, I., Abe, S., Yamaguchi, H., Nagasaki, K., & Adachi, M. (2022). Horizontal and vertical distribution

of *Gambierdiscus* spp. (Dinophyceae) including novel phylotypes in Japan identified by 18S rDNA metabarcoding. *Harmful Algae*, *111*, 102163. https://doi.org/10.1016/j.hal.2021.102163

Gaiani, G., Toldrà, A., Rey, M., Andree, K., Alcaraz, C., Diogène, J., O'Sullivan, C., & Campàs, M. (2021). *Recombinase Polymerase Amplification for* Gambierdiscus *and* Fukuyoa *detection: A step further in the ciguatera risk management*. https://doi.org/10.3390/IECT2021-09168

Gallardo-Rodríguez, J., Sánchez-Mirón, A., García-Camacho, F., López-Rosales, L., Chisti, Y., & Molina-Grima, E. (2012). Bioactives from microalgal dinoflagellates. *Biotechnology Advances*, *30*(6), 1673–1684. https://doi.org/10.1016/j.biotechadv.2012.07.005

Gervasi, A., Cardol, P., & Meyer, P. E. (2022). Automated Open-Hardware Multiwell Imaging Station for Microorganisms Observation. *Micromachines*, *13*(6), 833. https://doi.org/10.3390/mi13060833

Gilchrist, C. L. M., Mirdita, M., & Steinegger, M. (2024). *Multiple Protein Structure Alignment at Scale with FoldMason* (p. 2024.08.01.606130). bioRxiv. https://doi.org/10.1101/2024.08.01.606130

Gómez, F. (2012). A quantitative review of the lifestyle, habitat and trophic diversity of dinoflagellates (Dinoflagellata, Alveolata). *Systematics and Biodiversity*, *10*(3), 267–275. https://doi.org/10.1080/14772000.2012.721021

González-Pech, R. A., Stephens, T. G., Chen, Y., Mohamed, A. R., Cheng, Y., Shah, S., Dougan, K. E., Fortuin, M. D. A., Lagorce, R., Burt, D. W., Bhattacharya, D., Ragan, M. A., & Chan, C. X. (2021). Comparison of 15 dinoflagellate genomes reveals extensive sequence

and structural divergence in family Symbiodiniaceae and genus *Symbiodinium*. *BMC Biology*, *19*, 73. https://doi.org/10.1186/s12915-021-00994-6

Gornik, S. G., Hu, I., Lassadi, I., & Waller, R. F. (2019). The Biochemistry and Evolution of the Dinoflagellate Nucleus. *Microorganisms*, *7*(8), 245. https://doi.org/10.3390/microorganisms7080245

Govender, Y., Jury, M.-R., Govender, Y., & Jury, M.-R. (2024). Environmental controls on bioluminescent dinoflagellate density, in Laguna Grande, Fajardo, Puerto Rico. *Revista de Biología Tropical*, *72*(1). https://doi.org/10.15517/rev.biol.trop..v72i1.56729

Govorunova, E. G., Sineshchekov, O. A., Li, H., & Spudich, J. L. (2017). Microbial Rhodopsins: Diversity, Mechanisms, and Optogenetic Applications. *Annual Review of Biochemistry*, *86*, 845–872. https://doi.org/10.1146/annurev-biochem-101910-144233

Govorunova, E. G., Sineshchekov, O. A., Li, H., Wang, Y., Brown, L. S., Palmateer, A., Melkonian, M., Cheng, S., Carpenter, E., Patterson, J., Wong, G. K.-S., & Spudich, J. L. (2021). Cation and Anion Channelrhodopsins: Sequence Motifs and Taxonomic Distribution. *mBio*, *12*(4), 10.1128/mbio.01656-21. https://doi.org/10.1128/mbio.01656-21

Greiner, A., Kelterborn, S., Evers, H., Kreimer, G., Sizova, I., & Hegemann, P. (2017). Targeting of Photoreceptor Genes in *Chlamydomonas reinhardtii* via Zinc-Finger Nucleases and CRISPR/Cas9. *The Plant Cell*, *29*(10), 2498–2518. https://doi.org/10.1105/tpc.17.00659

Gulyás, M., Bencsik, N., Pusztai, S., Liliom, H., & Schlett, K. (2016). AnimalTracker: An ImageJ-Based Tracking API to Create a Customized Behaviour Analyser Program. *Neuroinformatics*, *14*(4), 479–481. https://doi.org/10.1007/s12021-016-9303-z

Hackett, J. D., Anderson, D. M., Erdner, D. L., & Bhattacharya, D. (2004). Dinoflagellates: A remarkable evolutionary experiment. *American Journal of Botany*, *91*(10), 1523–1534. https://doi.org/10.3732/AJB.91.10.1523

Halldal, I. (1958). Action Spectra of Phototaxis and Relation Problem in Volvocales, Ulva-Gamete and Dinophyceae. *Physiologia Plantarum*, *11*(1), 118–153. https://doi.org/10.1111/J.1399-3054.1958.TB08432.X

Hallgren, J., Tsirigos, K. D., Pedersen, M. D., Armenteros, J. J. A., Marcatili, P., Nielsen, H., Krogh, A., & Winther, O. (2022). *DeepTMHMM predicts alpha and beta transmembrane proteins using deep neural networks* (p. 2022.04.08.487609). bioRxiv. https://doi.org/10.1101/2022.04.08.487609

Hansen, P. (1991). Quantitative importance and trophic role of heterotrophic dinoflagellates in a coastal pelagial food web. *Marine Ecology Progress Series*, *73*, 253–261. https://doi.org/10.3354/meps073253

Haq, S., Oyler, B. L., Williams, E., Khan, M. M., Goodlett, D. R., Bachvaroff, T., & Place, A. R. (2023). Investigating A Multi-Domain Polyketide Synthase in *Amphidinium carterae*. *Marine Drugs*, *21*(8), 425. https://doi.org/10.3390/md21080425

Hardeland, R., & Nord, P. (1984). Visualization of free-running circadian rhythms in the dinoflagellate *Pyrocystis noctiluca*. *Marine Behaviour and Physiology*, *11*(3), 199–207. https://doi.org/10.1080/10236248409387045

Haro, S., Bohórquez, J., Lara, M., Garcia-Robledo, E., González, C. J., Crespo, J. M., Papaspyrou, S., & Corzo, A. (2019). Diel patterns of microphytobenthic primary production in intertidal sediments: The role of photoperiod on the vertical migration

circadian rhythm. *Scientific Reports*, *9*(1), 13376. https://doi.org/10.1038/s41598-019-49971-8

Hartz, A. J. (2010). *Investigating the Ecological Role of Cell Signaling in Free-Living Marine*.

Hartz, A. J., Sherr, B. F., & Sherr, E. B. (2011). Photoresponse in the Heterotrophic Marine Dinoflagellate *Oxyrrhis marina*. *Journal of Eukaryotic Microbiology*, *58*(2), 171–177. https://doi.org/10.1111/j.1550-7408.2011.00529.x

Hasle, G. R. (1950). Phototactic Vertical Migration in Marine Dinoflagellates. *Oikos*, *2*(2), 162–175. https://doi.org/10.2307/3564790

Hastings, J. W. (2007). The Gonyaulax Clock at 50: Translational Control of Circadian Expression. *Cold Spring Harbor Symposia on Quantitative Biology*, *72*, 141–144. https://doi.org/10.1101/sqb.2007.72.026

Hastings, J. W. (2013). Circadian Rhythms in Dinoflagellates: What Is the Purpose of Synthesis and Destruction of Proteins? *Microorganisms*, *1*(1), 26–32. https://doi.org/10.3390/microorganisms1010026

Hauspie, R., & Polk, Ph. (1973). Swimming Behaviour Patterns in Certain Benthic Harpacticoids (Copepoda). *Crustaceana*, *25*(1), 95–103.

Hayakawa, S., Takaku, Y., Hwang, J. S., Horiguchi, T., Suga, H., Gehring, W., Ikeo, K., & Gojobori, T. (2015). Function and Evolutionary Origin of Unicellular Camera-Type Eye Structure. *PLOS ONE*, *10*(3), e0118415. https://doi.org/10.1371/journal.pone.0118415

Hayashi, T., Yasuda, S., Suzuki, K., Akiyama, T., Kanehara, K., Kojima, K., Tanabe, M., Kato, R., Senda, T., Sudo, Y., Murata, T., & Kinoshita, M. (2020). How Does a Microbial Rhodopsin RxR Realize Its Exceptionally High Thermostability with the Proton-Pumping

Function Being Retained? *The Journal of Physical Chemistry B*, *124*(6), 990–1000. https://doi.org/10.1021/acs.jpcb.9b10700

Hays, G. C. (2003). A review of the adaptive significance and ecosystem consequences of zooplankton diel vertical migrations. *Hydrobiologia*, *503*(1), 163–170. https://doi.org/10.1023/B:HYDR.0000008476.23617.b0

Heaney, S. I., & Furnass, T. I. (1980). Laboratory models of diel vertical migration in the dinoflagellate *Ceratium hirundinella*. *Freshwater Biology*, *10*(2), 163–170. https://doi.org/10.1111/j.1365-2427.1980.tb01190.x

Heyne, K., Herbst, J., Dominguez-Herradon, B., Alexiev, U., & Diller, R. (2000). Reaction Control in Bacteriorhodopsin: Impact of Arg82 and Asp85 on the Fast Retinal Isomerization, Studied in the Second Site Revertant Arg82Ala/Gly231Cys and Various Purple and Blue Forms of Bacteriorhodopsin. *The Journal of Physical Chemistry B*, *104*(25), 6053–6058. https://doi.org/10.1021/jp992877u

Holdo, R. M., Holt, R. D., & Fryxell, J. M. (2009). Opposing Rainfall and Plant Nutritional Gradients Best Explain the Wildebeest Migration in the Serengeti. *The American Naturalist*, *173*(4), 431–445. https://doi.org/10.1086/597229

Holm, L. (2022). Dali server: Structural unification of protein families. *Nucleic Acids Research*, *50*(W1), W210–W215. https://doi.org/10.1093/nar/gkac387

Holm, L., Kääriäinen, S., Wilton, C., & Plewczynski, D. (2006). Using Dali for Structural Comparison of Proteins. *Current Protocols in Bioinformatics*, *14*(1), 5.5.1-5.5.24. https://doi.org/10.1002/0471250953.bi0505s14

Holm, L., Laiho, A., Törönen, P., & Salgado, M. (2023). DALI shines a light on remote homologs: One hundred discoveries. *Protein Science*, *32*(1), e4519. https://doi.org/10.1002/pro.4519

Hoppenrath, M. (2017). Dinoflagellate taxonomy—A review and proposal of a revised classification. *Marine Biodiversity*, *47*(2), 381–403. https://doi.org/10.1007/s12526-016-0471-8

Hotos, G., & Bekiari, V. (2023). Absorption Spectra as Predictors of Algal Biomass and Pigment Content of the Cultured Microalgae *Amphidinium carterae*, *Isochrysis galbana*, *Nephroselmis sp.*, and *Anabaena sp. International Journal of Plant Biology*, *14*, 879–895. https://doi.org/10.3390/ijpb14040065

Hulburt, E. M. (1957). The taxonomy of unarmored dinophyceae of shallow embayments on Cape Cod, Massachusetts. *The Biological Bulletin*, *112*(2), 196–219. https://doi.org/10.2307/1539198

Inoue, K., Kato, Y., & Kandori, H. (2015). Light-driven ion-translocating rhodopsins in marine bacteria. *Trends in Microbiology*, *23*(2), 91–98. https://doi.org/10.1016/j.tim.2014.10.009

Inoue, K., Nomura, Y., & Kandori, H. (2016). Asymmetric Functional Conversion of Eubacterial Light-driven Ion Pumps*. *Journal of Biological Chemistry*, *291*(19), 9883–9893. https://doi.org/10.1074/jbc.M116.716498

Inoue, K., Ono, H., Abe-Yoshizumi, R., Yoshizawa, S., Ito, H., Kogure, K., & Kandori, H. (2013). A light-driven sodium ion pump in marine bacteria. *Nature Communications*, *4*(1), 1678. https://doi.org/10.1038/ncomms2689

Institute of Marine Sciences (CSIC), Barcelona, Berdalet, E., Tester, P., Chinain, M., Fraga, S., Lemée, R., Litaker, W., Penna, A., Usup, G., Vila, M., & Zingone, A. (2017). Harmful

Algal Blooms in Benthic Systems: Recent Progress and Future Research. *Oceanography*, *30*(1), 36–45. https://doi.org/10.5670/oceanog.2017.108

Interactive Graphics and 3D Models – Harmful Algal Blooms. (n.d.). Retrieved March 21, 2025, from https://hab.whoi.edu/regions-resources/interactive-graphics-3d-models/

Jadhav, D. B., Sriramkumar, Y., & Roy, S. (2022). The enigmatic clock of dinoflagellates, is it unique? *Frontiers in Microbiology*, *13*. https://doi.org/10.3389/fmicb.2022.1004074

Janouškovec, J., Gavelis, G. S., Burki, F., Dinh, D., Bachvaroff, T. R., Gornik, S. G., Bright, K. J., Imanian, B., Strom, S. L., Delwiche, C. F., Waller, R. F., Fensome, R. A., Leander, B. S., Rohwer, F. L., & Saldarriaga, J. F. (2017). Major transitions in dinoflagellate evolution unveiled by phylotranscriptomics. *Proceedings of the National Academy of Sciences*, *114*(2), E171–E180. https://doi.org/10.1073/pnas.1614842114

Jauzein, C., Fricke, A., Mangialajo, L., & Lemée, R. (2016). Sampling of *Ostreopsis* cf. *ovata* using artificial substrates: Optimization of methods for the monitoring of benthic harmful algal blooms. *Marine Pollution Bulletin*, *107*(1), 300–304. https://doi.org/10.1016/j.marpolbul.2016.03.047

Javed, A., Lee, B. S., & Rizzo, D. M. (2020). A benchmark study on time series clustering. *Machine Learning with Applications*, *1*, 100001. https://doi.org/10.1016/j.mlwa.2020.100001

Jékely, G. (2009). Evolution of phototaxis. *Philosophical Transactions of the Royal Society B: Biological Sciences*, *364*(1531), 2795–2808. https://doi.org/10.1098/rstb.2009.0072

Jephson, T., & Carlsson, P. (2009). Species- and stratification-dependent diel vertical migration behaviour of three dinoflagellate species in a laboratory study. *Journal of Plankton Research*, *31*(11), 1353–1362. https://doi.org/10.1093/plankt/fbp078

Ji, R., & Franks, P. (2007). Vertical migration of dinoflagellates: Model analysis of strategies, growth, and vertical distribution patterns. *Marine Ecology Progress Series*, *344*, 49–61. https://doi.org/10.3354/meps06952

Jia, Y., Gao, H., Tong, M., & Anderson, D. M. (2019). Cell cycle regulation of the mixotrophic dinoflagellate *Dinophysis acuminata*: Growth, photosynthetic efficiency and toxin production. *Harmful Algae*, *89*, 101672. https://doi.org/10.1016/j.hal.2019.101672

Jiang, H., Kulis, D. M., Brosnahan, M. L., & Anderson, D. M. (2018). Behavioral and mechanistic characteristics of the predator-prey interaction between the dinoflagellate *Dinophysis acuminata* and the ciliate *Mesodinium*. *Harmful Algae*, *77*, 43. https://doi.org/10.1016/J.HAL.2018.06.007

Jiang, Y., Chen, F., & Liang, S.-Z. (1999). Production potential of docosahexaenoic acid by the heterotrophic marine dinoflagellate *Crypthecodinium cohnii*. *Process Biochemistry*, *34*(6), 633–637. https://doi.org/10.1016/S0032-9592(98)00134-4

Johnson, C. H., Roeber, J. F., & Hastings, J. W. (1984). Circadian Changes in Enzyme Concentration Account for Rhythm of Enzyme Activity in *Gonyaulax*. *Science*, *223*(4643), 1428–1430. https://doi.org/10.1126/science.223.4643.1428

Juavinett, A. L. (2022). The next generation of neuroscientists needs to learn how to code, and we need new ways to teach them. *Neuron*, *110*(4), 576–578. https://doi.org/10.1016/j.neuron.2021.12.001

Judd, M., & Place, A. R. (2022). A Strategy for Gene Knockdown in Dinoflagellates. *Microorganisms*, *10*(6), 1131. https://doi.org/10.3390/MICROORGANISMS10061131

Kamykowski, D. (1986). The temperature acclimated swimming speed of selected marine dinoflagellates. *Article in Journal of Plankton Research*. https://doi.org/10.1093/plankt/8.2.275

Kamykowski, D., Milligan, E. J., & Reed, R. E. (1998). Relationships between geotaxis/phototaxis and diel vertical migration in autotrophic dinoflagellates. *Journal of Plankton Research*, *20*(9), 1781–1796.

Kamykowski, D., Reed, R. E., & Kirkpatrick, G. J. (1992). Comparison of sinking velocity, swimming velocity, rotation and path characteristics among six marine dinoflagellate species. *Marine Biology*, *113*, 319–328.

Kandori, H. (2015). Ion-pumping microbial rhodopsins. *Frontiers in Molecular Biosciences*, *2*, 52. https://doi.org/10.3389/fmolb.2015.00052

Kassim, N. S., Lee, L. K., Hii, K. S., Mohd Azmi, N. F., Baharudin, S. N., Liu, M., Gu, H., Lim, P. T., & Leaw, C. P. (2025). Molecular diversity of benthic harmful dinoflagellates on a tropical reef: Comparing natural and artificial substrate sampling methods using DNA metabarcoding and morphological analysis. *Harmful Algae*, *142*, 102795. https://doi.org/10.1016/j.hal.2024.102795

Kato, H. E., Zhang, F., Yizhar, O., Ramakrishnan, C., Nishizawa, T., Hirata, K., Ito, J., Aita, Y., Tsukazaki, T., Hayashi, S., Hegemann, P., Maturana, A. D., Ishitani, R., Deisseroth, K., & Nureki, O. (2012). Crystal structure of the channelrhodopsin light-gated cation channel. *Nature*, *482*(7385), 369–374. https://doi.org/10.1038/nature10870

Katoh, K., Misawa, K., Kuma, K., & Miyata, T. (2002). MAFFT: A novel method for rapid multiple sequence alignment based on fast Fourier transform. *Nucleic Acids Research*, *30*(14), 3059–3066. https://doi.org/10.1093/nar/gkf436

Katz, J., & Sheng, J. (2010). Applications of holography in fluid mechanics and particle dynamics. *Annual Review of Fluid Mechanics*, *42*, 531–555. https://doi.org/10.1146/annurev-fluid-121108-145508

Kennelly, S. J., & Underwood, A. J. (1984). Underwater microscopic sampling of a sublittoral kelp community. *Journal of Experimental Marine Biology and Ecology*, *76*(1), 67–78. https://doi.org/10.1016/0022-0981(84)90017-0

Kibler, S. R., Litaker, R. W., Holland, W. C., Vandersea, M. W., & Tester, P. A. (2012). Growth of eight *Gambierdiscus* (Dinophyceae) species: Effects of temperature, salinity and irradiance. *Harmful Algae*, *19*, 1–14. https://doi.org/10.1016/j.hal.2012.04.007

Kiih, M., & Jorgensen, B. B. (1994). The light field of microbenthic communities: Radiance distribution and microscale optics of sandy coastal sediments. *Limnology and Oceanography*, *39*(6), 1368–1398. https://doi.org/10.4319/lo.1994.39.6.1368

Kim, M. K. (2010). Principles and techniques of digital holographic microscopy. *SPIE Reviews*, *1*(1), 018005. https://doi.org/10.1117/6.0000006

Kim, P., Kaur, M., Jang, H.-I., & Kim, Y.-I. (2020). The Circadian Clock—A Molecular Tool for Survival in Cyanobacteria. *Life*, *10*(12), 365. https://doi.org/10.3390/life10120365

Kolbe, M., Besir, H., Essen, L.-O., & Oesterhelt, D. (2000). Structure of the Light-Driven Chloride Pump Halorhodopsin at 1.8 Å Resolution. *Science*, *288*(5470), 1390–1396. https://doi.org/10.1126/science.288.5470.1390

Kovalev, K., Volkov, D., Astashkin, R., Alekseev, A., Gushchin, I., Haro-Moreno, J. M., Chizhov, I., Siletsky, S., Mamedov, M., Rogachev, A., Balandin, T., Borshchevskiy, V., Popov, A., Bourenkov, G., Bamberg, E., Rodriguez-Valera, F., Büldt, G., & Gordeliy, V. (2020). High-resolution structural insights into the heliorhodopsin family. *Proceedings of*

the National Academy of Sciences, *117*(8), 4131–4141. https://doi.org/10.1073/pnas.1915888117

Kretzschmar, A. L., Verma, A., Kohli, G., & Murray, S. (2019). Development of a quantitative PCR assay for the detection and enumeration of a potentially ciguatoxin-producing dinoflagellate, *Gambierdiscus lapillus* (Gonyaulacales, Dinophyceae). *PloS One*, *14*(11), e0224664. https://doi.org/10.1371/journal.pone.0224664

Kuhn, H. W. (1955). The Hungarian method for the assignment problem. *Naval Research Logistics Quarterly*, *2*(1–2), 83–97. https://doi.org/10.1002/nav.3800020109

Kurihara, M., & Sudo, Y. (2015). Microbial rhodopsins: Wide distribution, rich diversity and great potential. *Biophysics and Physicobiology*, *12*, 121–129. https://doi.org/10.2142/biophysico.12.0_121

Lalli, C. M., & Parsons, T. R. (1997). CHAPTER 7—BENTHOS. In C. M. Lalli & T. R. Parsons (Eds.), *Biological Oceanography: An Introduction (Second Edition)* (pp. 177–195). Butterworth-Heinemann. https://doi.org/10.1016/B978-075063384-0/50063-3

Lambert, B. S., Fernandez, V. I., & Stocker, R. (2019). Motility drives bacterial encounter with particles responsible for carbon export throughout the ocean. *Limnology and Oceanography Letters*, *4*(5), 113–118. https://doi.org/10.1002/lol2.10113

Langhans, V. H. (1907). Die Ursachen der periodischen Variationen der Planktozoen. *Lotos - Zeitschrift Fuer Naturwissenschaften*, *55*, 13–15.

Larkin, S. L., & Adams, C. M. (2013). Economic Consequences of Harmful Algal Blooms: Literature Summary. *EDIS*, *2013*(11). https://doi.org/10.32473/edis-fe936-2013

Larkum, A. W. D., Koch, E.-M. W., & Kühl, M. (2003). Diffusive boundary layers and photosynthesis of the epilithic algal community of coral reefs. *Marine Biology*, *142*(6), 1073–1082. https://doi.org/10.1007/s00227-003-1022-y

Leblond, P. H., & Taylor, F. J. (1976). The propulsive mechanism of the dinoflagellate transverse flagellum reconsidered. *Bio Systems*, *8*(1), 33–39. https://doi.org/10.1016/0303-2647(76)90005-8

Lee, L. K., Lim, Z. F., Gu, H., Chan, L. L., Litaker, R. W., Tester, P. A., Leaw, C. P., & Lim, P. T. (2020). Effects of substratum and depth on benthic harmful dinoflagellate assemblages. *Scientific Reports*, *10*(1), 11251. https://doi.org/10.1038/s41598-020-68136-6

Lessard, E. J. (1991). The trophic role of heterotrophic dinoflagellates in diverse marine environments. *The Trophic Role of Heterotrophic Dinoflagellates in Diverse Marine Environments*, *5*(1), 49–58.

Levin, S. A. (1992). The Problem of Pattern and Scale in Ecology: The Robert H. MacArthur Award Lecture. *Ecology*, *73*(6), 1943–1967. https://doi.org/10.2307/1941447

Lewis, N. I., Xu, W., Jericho, S. K., Kreuzer, H. J., Jericho, M. H., & Cembella, A. D. (2006). Swimming speed of three species of *Alexandrium* (Dinophyceae) as determined by digital in-line holography. *Phycologia*, *45*(1), 61–70. https://doi.org/10.2216/04-59.1

Li, A., Stoecker, D. K., & Coats, D. W. (2000). Mixotrophy in *Gyrodinium galatheanum* (DINOPHYCEAE): Grazing responses to light intensity and inorganic nutrients*. *Journal of Phycology*, *36*(1), 33–45. https://doi.org/10.1046/j.1529-8817.2000.98076.x

Liefer, J. D., Richlen, M. L., Smith, T. B., DeBose, J. L., Xu, Y., Anderson, D. M., & Robertson, A. (2021). Asynchrony of *Gambierdiscus* spp. Abundance and Toxicity in the U.S.

Virgin Islands: Implications for Monitoring and Management of Ciguatera. *Toxins*, *13*(6), 413. https://doi.org/10.3390/toxins13060413

Lin, S. (2011). Genomic understanding of dinoflagellates. *Research in Microbiology*, *162*(6), 551–569. https://doi.org/10.1016/j.resmic.2011.04.006

Lin, S. (2024). A decade of dinoflagellate genomics illuminating an enigmatic eukaryote cell. *BMC Genomics*, *25*(1), 932. https://doi.org/10.1186/s12864-024-10847-5

Lin, S., Zhang, H., Zhuang, Y., Tran, B., & Gill, J. (2010). Spliced leader–based metatranscriptomic analyses lead to recognition of hidden genomic features in dinoflagellates. *Proceedings of the National Academy of Sciences*, *107*(46), 20033–20038. https://doi.org/10.1073/pnas.1007246107

Lindström, J., Grebner, W., Rigby, K., & Selander, E. (2017). Effects of predator lipids on dinoflagellate defence mechanisms—Increased bioluminescence capacity. *Scientific Reports 2017 7:1*, *7*(1), 1–9. https://doi.org/10.1038/s41598-017-13293-4

Liscum, E., Askinosie, S. K., Leuchtman, D. L., Morrow, J., Willenburg, K. T., & Coats, D. R. (2014). Phototropism: Growing towards an Understanding of Plant Movement[OPEN]. *The Plant Cell*, *26*(1), 38–55. https://doi.org/10.1105/tpc.113.119727

Lisicki, M., Velho Rodrigues, M. F., Goldstein, R. E., & Lauga, E. (2019). Swimming eukaryotic microorganisms exhibit a universal speed distribution. *eLife*, *8*, e44907. https://doi.org/10.7554/eLife.44907

Litaker, R. W., Vandersea, M. W., Faust, M. A., Kibler, S. R., Chinain, M., Holmes, M. J., Holland, W. C., & Tester, P. A. (2009). Taxonomy of *Gambierdiscus* including four new species, *Gambierdiscus caribaeus*, *Gambierdiscus carolinianus*, *Gambierdiscus*

carpenteri and *Gambierdiscus ruetzleri* (Gonyaulacales, Dinophyceae). *Phycologia*, *48*(5), 344–390. https://doi.org/10.2216/07-15.1

Litaker, R. W., Vandersea, M. W., Faust, M. A., Kibler, S. R., Nau, A. W., Holland, W. C., Chinain, M., Holmes, M. J., & Tester, P. A. (2010). Global distribution of ciguatera causing dinoflagellates in the genus *Gambierdiscus*. *Toxicon*, *56*(5), 711–730. https://doi.org/10.1016/j.toxicon.2010.05.017

Lobel, P. S., Anderson, D. M., & Durand-Clement, M. (1988). Assessment of Ciguatera Dinoflagellate Populations: Sample Variability and Algal Substrate Selection. *The Biological Bulletin*, *175*(1), 94–101. https://doi.org/10.2307/1541896

Loeffler, C. R., Tartaglione, L., Friedemann, M., Spielmeyer, A., Kappenstein, O., & Bodi, D. (2021). Ciguatera Mini Review: 21st Century Environmental Challenges and the Interdisciplinary Research Efforts Rising to Meet Them. *International Journal of Environmental Research and Public Health*, *18*(6), Article 6. https://doi.org/10.3390/ijerph18063027

Lohmann, H. (DE-588)6. (1908). *Untersuchungen zur Feststellung des vollständigen Gehaltes des Meeres an Plankton /von H. Lohmann*. Schmidt & Klaunig.

Long, J., John, Lammert, A., Strother, J., & McHenry, M. (2003). *Biologically-inspired control of perception-action systems: Helical klinotaxis in 2D robots*.

Luecke, H., Schobert, B., Cartailler, J.-P., Richter, H.-T., Rosengarth, A., Needleman, R., & Lanyi, J. K. (2000). Coupling photoisomerization of retinal to directional transport in bacteriorhodopsin1. *Journal of Molecular Biology*, *300*(5), 1237–1255. https://doi.org/10.1006/jmbi.2000.3884

Luecke, H., Schobert, B., Lanyi, J. K., Spudich, E. N., & Spudich, J. L. (2001). Crystal Structure of Sensory Rhodopsin II at 2.4 Angstroms: Insights into Color Tuning and Transducer Interaction. *Science*, *293*(5534), 1499–1503. https://doi.org/10.1126/science.1062977

Ma, M., Shi, X., & Lin, S. (2020). Heterologous expression and cell membrane localization of dinoflagellate opsins (rhodopsin proteins) in mammalian cells. *Marine Life Science & Technology*, *2*(3), 302–308. https://doi.org/10.1007/s42995-020-00043-1

Malakar, P., Gholami, S., Aarabi, M., Rivalta, I., Sheves, M., Garavelli, M., & Ruhman, S. (2024). Retinal photoisomerization versus counterion protonation in light and dark-adapted bacteriorhodopsin and its primary photoproduct. *Nature Communications*, *15*(1), 2136. https://doi.org/10.1038/s41467-024-46061-w

Marcinko, C. L. J., Painter, S. C., Martin, A. P., & Allen, J. T. (2013). A review of the measurement and modelling of dinoflagellate bioluminescence. *Progress in Oceanography*, *109*, 117–129. https://doi.org/10.1016/j.pocean.2012.10.008

Marti, T., Rösselet, S. J., Otto, H., Heyn, M. P., & Khorana, H. G. (1991). The retinylidene Schiff base counterion in bacteriorhodopsin. *The Journal of Biological Chemistry*, *266*(28), 18674–18683.

Martins, C. P. P., Wall, M., Schubert, P., Wilke, T., & Ziegler, M. (2024). Variability of the surface boundary layer of reef-building coral species. *Coral Reefs*, *43*(5), 1223–1233. https://doi.org/10.1007/s00338-024-02531-7

Maška, M., Ulman, V., Delgado-Rodriguez, P., Gómez-de-Mariscal, E., Nečasová, T., Guerrero Peña, F. A., Ren, T. I., Meyerowitz, E. M., Scherr, T., Löffler, K., Mikut, R., Guo, T., Wang, Y., Allebach, J. P., Bao, R., Al-Shakarji, N. M., Rahmon, G., Toubal, I. E., Palaniappan, K., … Ortiz-de-Solórzano, C. (2023). The Cell Tracking Challenge: 10

years of objective benchmarking. *Nature Methods*, *20*(7), 1010–1020. https://doi.org/10.1038/s41592-023-01879-y

Mathe, S. E., Kondaveeti, H. K., Vappangi, S., Vanambathina, S. D., & Kumaravelu, N. K. (2024). A comprehensive review on applications of Raspberry Pi. *Computer Science Review*, *52*, 100636. https://doi.org/10.1016/j.cosrev.2024.100636

Matsen, F. A., Kodner, R. B., & Armbrust, E. V. (2010). pplacer: Linear time maximum-likelihood and Bayesian phylogenetic placement of sequences onto a fixed reference tree. *BMC Bioinformatics*, *11*(1), 538. https://doi.org/10.1186/1471-2105-11-538

McKay, L., Kamykowski, D., Milligan, E., Schaeffer, B., & Sinclair, G. (2006). Comparison of swimming speed and photophysiological responses to different external conditions among three *Karenia brevis* strains. *Harmful Algae*, *5*(6), 623–636. https://doi.org/10.1016/J.HAL.2005.12.001

Meng, R., Zhou, C., Zhu, X., Huang, H., Xu, J., Luo, Q., & Yan, X. (2019). Critical light-related gene expression varies in two different strains of the dinoflagellate *Karlodinium veneficum* in response to the light spectrum and light intensity. *Journal of Photochemistry and Photobiology B: Biology*, *194*, 76–83. https://doi.org/10.1016/J.JPHOTOBIOL.2019.03.009

Menon, S. N., Varuni, P., Bunbury, F., Bhaya, D., & Menon, G. I. (2021). Phototaxis in Cyanobacteria: From Mutants to Models of Collective Behavior. *mBio*, *12*(6), e02398-21. https://doi.org/10.1128/mBio.02398-21

Menon, S. N., Varuni, P., & Menon, G. I. (2020). Information integration and collective motility in phototactic cyanobacteria. *PLOS Computational Biology*, *16*(4), e1007807. https://doi.org/10.1371/journal.pcbi.1007807

Meroni, L., Chiantore, M., Petrillo, M., & Asnaghi, V. (2018). Habitat effects on *Ostreopsis* cf. *Ovata* bloom dynamics. *Harmful Algae*, *80*, 64–71. https://doi.org/10.1016/j.hal.2018.09.006

Mirarab, S., Nguyen, N., & Warnow, T. (2012). SEPP: SATé-enabled phylogenetic placement. *Pacific Symposium on Biocomputing. Pacific Symposium on Biocomputing*, 247–258. https://doi.org/10.1142/9789814366496_0024

Miyasaka, I., Nanba, K., Furuya, K., Nimura, Y., & Azuma, A. (2004). Functional roles of the transverse and longitudinal flagella in the swimming motility of *Prorocentrum minimum* (Dinophyceae). *Journal of Experimental Biology*, *207*(17), 3055–3066. https://doi.org/10.1242/jeb.01141

Miyata, M., Robinson, R. C., Uyeda, T. Q. P., Fukumori, Y., Fukushima, S.-I., Haruta, S., Homma, M., Inaba, K., Ito, M., Kaito, C., Kato, K., Kenri, T., Kinosita, Y., Kojima, S., Minamino, T., Mori, H., Nakamura, S., Nakane, D., Nakayama, K., … Wakabayashi, K.-I. (2020). Tree of motility—A proposed history of motility systems in the tree of life. *Genes to Cells: Devoted to Molecular & Cellular Mechanisms*, *25*(1), 6–21. https://doi.org/10.1111/gtc.12737

Morelle, J., Bastos, A., Frankenbach, S., Frommlet, J. C., Campbell, D. A., Lavaud, J., & Serôdio, J. (2024). The Photoprotective Behavior of a Motile Benthic Diatom as Elucidated from the Interplay Between Cell Motility and Physiological Responses to a Light Microgradient Using a Novel Experimental Setup. *Microbial Ecology*, *87*(1), 40. https://doi.org/10.1007/s00248-024-02354-7

Moriera, A., & Tester, P. A. (2016). Methods for sampling benthic microalgae. In *Guide for Designing and Implementing a Plan to Monitor Toxin-Producing Microalgae* (2nd ed.,

pp. 19–28). Intergovernmental Oceanographic Commission (IOC) of UNESCO and International Atomic Energy Agency. https://unesdoc.unesco.org/in/documentViewer.xhtml?v=2.1.196&id=p::usmarcdef_0000214510_eng&file=/in/rest/annotationSVC/DownloadWatermarkedAttachment/attach_import_d44c9418-7aa9-4f4d-9280-7ca3e866bcce%3F_%3D214510eng.pdf&locale=en&multi=true&ark=/ark:/48223/pf0000214510_eng/PDF/214510eng.pdf#%5B%7B%22num%22%3A26%2C%22gen%22%3A0%7D%2C%7B%22name%22%3A%22XYZ%22%7D%2Cnull%2Cnull%2C0%5D

Morten, M., Øjvind, M., & Per Juel, H. (2013). Loss of phototaxis and degeneration of an eyespot in long-term algal cultures: Evidence from ultrastructure and behaviour in the dinoflagellate *Kryptoperidinium foliaceum*. *The Journal of Eukaryotic Microbiology*, *60*(4), 327–334. https://doi.org/10.1111/JEU.12036

Moszczyński, K., Mackiewicz, P., & Bodył, A. (2012). Evidence for Horizontal Gene Transfer from Bacteroidetes Bacteria to Dinoflagellate Minicircles. *Molecular Biology and Evolution*, *29*(3), 887–892. https://doi.org/10.1093/molbev/msr276

Mullen, A. D., Treibitz, T., Roberts, P. L. D., Kelly, E. L. A., Horwitz, R., Smith, J. E., & Jaffe, J. S. (2016). Underwater microscopy for in situ studies of benthic ecosystems. *Nature Communications*, *7*(1), Article 1. https://doi.org/10.1038/ncomms12093

Munir, S., Siddiqui, P. J. A., & Morton, S. L. (2011). The occurrence of the ciguatera fish poisoning producing dinoflagellate genus Gambierdiscus in Pakistan waters. *ALGAE*, *26*(4), 317–325. https://doi.org/10.4490/algae.2011.26.4.317

Murray, S. A., Kohli, G. S., Farrell, H., Spiers, Z. B., Place, A. R., Dorantes-Aranda, J. J., & Ruszczyk, J. (2015). A fish kill associated with a bloom of *Amphidinium carterae* in a

coastal lagoon in Sydney, Australia. *Harmful Algae*, *49*, 19–28. https://doi.org/10.1016/j.hal.2015.08.003

Murray, S., & Patterson, D. J. (2002). The benthic dinoflagellate genus *Amphidinium* in south-eastern Australian waters, including three new species. *European Journal of Phycology*, *37*(2), 279–298. https://doi.org/10.1017/S0967026202003591

Mustapa, N. I., Yong, H. L., Lee, L. K., Lim, Z. F., Lim, H. C., Teng, S. T., Luo, Z., Gu, H., Leaw, C. P., & Lim, P. T. (2019). Growth and epiphytic behavior of three *Gambierdiscus* species (Dinophyceae) associated with various macroalgal substrates. *Harmful Algae*, *89*, 101671. https://doi.org/10.1016/j.hal.2019.101671

Nagata, T., & Inoue, K. (2021). Rhodopsins at a glance. *Journal of Cell Science*, *134*(22), jcs258989. https://doi.org/10.1242/jcs.258989

Nagel, G., Ollig, D., Fuhrmann, M., Kateriya, S., Musti, A. M., Bamberg, E., & Hegemann, P. (2002). Channelrhodopsin-1: A Light-Gated Proton Channel in Green Algae. *Science*, *296*(5577), 2395–2398. https://doi.org/10.1126/science.1072068

Nagel, G., Szellas, T., Huhn, W., Kateriya, S., Adeishvili, N., Berthold, P., Ollig, D., Hegemann, P., & Bamberg, E. (2003). Channelrhodopsin-2, a directly light-gated cation-selective membrane channel. *Proceedings of the National Academy of Sciences*, *100*(24), 13940–13945. https://doi.org/10.1073/pnas.1936192100

Nakahara, H., Sakami, T., Chinain, M., & Ishida, Y. (1996). The role of macroalgae in epiphytism of the toxic dinoflagellate *Gambierdiscus toxicus* (Dinophyceae). *Phycological Research*, *44*(2), 113–117. https://doi.org/10.1111/j.1440-1835.1996.tb00385.x

Nand, A., Zhan, Y., Salazar, O. R., Aranda, M., Voolstra, C. R., & Dekker, J. (2021). Genetic and spatial organization of the unusual chromosomes of the dinoflagellate *Symbiodinium microadriaticum*. *Nature Genetics*, *53*(5), 618–629. https://doi.org/10.1038/s41588-021-00841-y

Nascimento, S. M., Melo ,Guilherme, Salgueiro ,Fabiano, Diniz ,Bruna dos Santos, & and Fraga, S. (2015). Morphology of *Gambierdiscus excentricus* (Dinophyceae) with emphasis on sulcal plates. *Phycologia*, *54*(6), 628–639. https://doi.org/10.2216/15-61.1

Nathan, R., Getz, W. M., Revilla, E., Holyoak, M., Kadmon, R., Saltz, D., & Smouse, P. E. (2008). A movement ecology paradigm for unifying organismal movement research. *Proceedings of the National Academy of Sciences*, *105*(49), 19052–19059. https://doi.org/10.1073/pnas.0800375105

Needleman, R., Chang, M., Ni, B., Váró, G., Fornés, J., White, S. H., & Lanyi, J. K. (1991). Properties of Asp212—Asn bacteriorhodopsin suggest that Asp212 and Asp85 both participate in a counterion and proton acceptor complex near the Schiff base. *The Journal of Biological Chemistry*, *266*(18), 11478–11484.

Neushul, M. (1972). Underwater microscopy with an encased incident-light dipping-cone microscope. *Journal of Microscopy*, *95*(3), 421–424. https://doi.org/10.1111/j.1365-2818.1972.tb01043.x

Oellermann, M., Jolles, J. W., Ortiz, D., Seabra, R., Wenzel, T., Wilson, H., & Tanner, R. L. (2022). Open Hardware in Science: The Benefits of Open Electronics. *Integrative and Comparative Biology*, *62*(4), 1061–1075. https://doi.org/10.1093/icb/icac043

Oesterhelt, D., & Stoeckenius, W. (1971). Rhodopsin-like Protein from the Purple Membrane of *Halobacterium halobium*. *Nature New Biology*, *233*(39), 149–152. https://doi.org/10.1038/newbio233149a0

Oesterhelt, D., & Stoeckenius, W. (1973). Functions of a New Photoreceptor Membrane. *Proceedings of the National Academy of Sciences*, *70*(10), 2853–2857. https://doi.org/10.1073/pnas.70.10.2853

Oh, J.-W., Pushparaj, S. S. C., Muthu, M., & Gopal, J. (2023). Review of Harmful Algal Blooms (HABs) Causing Marine Fish Kills: Toxicity and Mitigation. *Plants*, *12*(23), 3936. https://doi.org/10.3390/plants12233936

Okolab—Leica H301-LG-DLS. (n.d.). Retrieved September 8, 2025, from https://www.oko-lab.com/ivf/index.php?Itemid=570&id=217&option=com_content&view=article&utm_source=chatgpt.com

Olli, K. (1999). Diel vertical migration of phytoplankton and heterotrophic flagellates in the Gulf of Riga. *Journal of Marine Systems*, *23*(1), 145–163. https://doi.org/10.1016/S0924-7963(99)00055-X

Ott, B. M., Litaker, R. W., Holland, W. C., & Delwiche, C. F. (2022). Using RDNA sequences to define dinoflagellate species. *PloS One*, *17*(2), e0264143. https://doi.org/10.1371/journal.pone.0264143

Otto, H., Marti, T., Holz, M., Mogi, T., Lindau, M., Khorana, H. G., & Heyn, M. P. (1989). Aspartic acid-96 is the internal proton donor in the reprotonation of the Schiff base of bacteriorhodopsin. *Proceedings of the National Academy of Sciences*, *86*(23), 9228–9232. https://doi.org/10.1073/pnas.86.23.9228

Parallel Computing Toolbox Documentation. (n.d.). Retrieved September 7, 2025, from https://www.mathworks.com/help/parallel-computing/index.html

Parsons, M. L., Richlen, M. L., Smith, T. B., Solow, A. R., & Anderson, D. M. (2021). Evaluation of 24-h screen deployments as a standardized platform to monitor *Gambierdiscus* populations in the Florida Keys and U.S. Virgin Islands. *Harmful Algae*, *103*, 101998. https://doi.org/10.1016/j.hal.2021.101998

Parsons, M. L., Settlemier, C. J., & Ballauer, J. M. (2011). An examination of the epiphytic nature of *Gambierdiscus toxicus*, a dinoflagellate involved in ciguatera fish poisoning. *Harmful Algae*, *10*(6), 598–605. https://doi.org/10.1016/j.hal.2011.04.011

Passow, U. (2002). Transparent exopolymer particles (TEP) in aquatic environments. *Progress in Oceanography*, *55*(3), 287–333. https://doi.org/10.1016/S0079-6611(02)00138-6

Pettersen, E. F., Goddard, T. D., Huang, C. C., Meng, E. C., Couch, G. S., Croll, T. I., Morris, J. H., & Ferrin, T. E. (2021). UCSF ChimeraX: Structure visualization for researchers, educators, and developers. *Protein Science: A Publication of the Protein Society*, *30*(1), 70–82. https://doi.org/10.1002/pro.3943

PipeCam: Low-Cost Autonomous Underwater Camera. (n.d.). Retrieved October 30, 2023, from https://hackaday.io/project/21222-pipecam-low-cost-autonomous-underwater-camera

Pitz, K. J., Richlen, M. L., Fachon, E., Smith, T. B., Parsons, M. L., & Anderson, D. M. (2021). Development of fluorescence in situ hybridization (FISH) probes to detect and enumerate *Gambierdiscus* species. *Harmful Algae*, *101*, 101914. https://doi.org/10.1016/j.hal.2020.101914

Place, A. R., Ramos-Franco, J., Waters, A. L., Peng, J., & Hamann, M. T. (2024). Sterolysin from a 1950s culture of *Karlodinium veneficum* (aka *Gymnodinium veneficum* Ballantine)

forms lethal sterol dependent membrane pores. *Scientific Reports*, *14*(1), 17998. https://doi.org/10.1038/s41598-024-68669-0

Potter, S. C., Luciani, A., Eddy, S. R., Park, Y., Lopez, R., & Finn, R. D. (2018). HMMER web server: 2018 update. *Nucleic Acids Research*, *46*(W1), W200–W204. https://doi.org/10.1093/nar/gky448

Rains, L. K., & Parsons, M. L. (2015). *Gambierdiscus* species exhibit different epiphytic behaviors toward a variety of macroalgal hosts. *Harmful Algae*, *49*, 29–39. https://doi.org/10.1016/j.hal.2015.08.005

Ramos-Santiago, A. E., Band-Schmidt, C. J., Leyva-Valencia, I., Fernández-Herrera, L. J., Núñez-Vázquez, E. J., & Okolodkov, Y. B. (2024). *Gambierdiscus carpenteri* (Dinophyceae) from Bahía de La Paz, Gulf of California: Morphology, genetic affinities, and mouse toxicity. *Botanica Marina*, *67*(4), 309–324. https://doi.org/10.1515/bot-2024-0017

Ran, T., Ozorowski, G., Gao, Y., Sineshchekov, O. A., Wang, W., Spudich, J. L., & Luecke, H. (2013). Cross-protomer interaction with the photoactive site in oligomeric proteorhodopsin complexes. *Acta Crystallographica Section D: Biological Crystallography*, *69*(10), 1965–1980. https://doi.org/10.1107/S0907444913017575

Riaz, S., Sui, Z., Niaz, Z., Khan, S., Liu, Y., & Liu, H. (2018). Distinctive Nuclear Features of Dinoflagellates with A Particular Focus on Histone and Histone-Replacement Proteins. *Microorganisms*, *6*(4), 128. https://doi.org/10.3390/microorganisms6040128

Richlen, M. L., Horn, K., Uva, V., Fachon, E., Heidmann, S. L., Smith, T. B., Parsons, M. L., & Anderson, D. M. (2024). *Gambierdiscus* species diversity and community structure in St.

Thomas, USVI and the Florida Keys, USA. *Harmful Algae*, *131*, 102562. https://doi.org/10.1016/j.hal.2023.102562

Riding, J. B., Fensome, R. A., Soyer-Gobillard, M.-O., & Medlin, L. K. (2023). A Review of the Dinoflagellates and Their Evolution from Fossils to Modern. *Journal of Marine Science and Engineering*, *11*(1), 1. https://doi.org/10.3390/jmse11010001

Roberts, R. J., Chang, Y.-C., Hu, Z., Rachlin, J. N., Anton, B. P., Pokrzywa, R. M., Choi, H.-P., Faller, L. L., Guleria, J., Housman, G., Klitgord, N., Mazumdar, V., McGettrick, M. G., Osmani, L., Swaminathan, R., Tao, K. R., Letovsky, S., Vitkup, D., Segrè, D., … Kasif, S. (2011). COMBREX: A project to accelerate the functional annotation of prokaryotic genomes. *Nucleic Acids Research*, *39*(Database issue), D11–D14. https://doi.org/10.1093/nar/gkq1168

Roenneberg, T., Colfax, G. N., & Hastings, J. W. (1989). A Circadian Rhythm of Population Behavior in *Gonyaulax polyedra*. *Journal of Biological Rhythms*, *4*(2), 89–104. https://doi.org/10.1177/074873048900400208

Roenneberg, T., & Merrow, M. (2002). Life before the clock: Modeling circadian evolution. *Journal of Biological Rhythms*, *17*(6), 495–505. https://doi.org/10.1177/0748730402238231

Salido, J., Sánchez, C., Ruiz-Santaquiteria, J., Cristóbal, G., Blanco, S., & Bueno, G. (2020). A Low-Cost Automated Digital Microscopy Platform for Automatic Identification of Diatoms. *Applied Sciences*, *10*(17), 6033. https://doi.org/10.3390/app10176033

Schenone, S., Bartl, I., & Thrush, S. (2024). Sediment microtopography predicts localised benthic ecosystem functioning and the effect of species interactions. *Marine Ecology Progress Series*, *749*, 47–55. https://doi.org/10.3354/meps14735

Schindler, D. E., Scheuerell, M. D., Moore, J. W., Gende, S. M., Francis, T. B., & Palen, W. J. (2003). Pacific salmon and the ecology of coastal ecosystems. *Frontiers in Ecology and the Environment*, *1*(1), 31–37. https://doi.org/10.1890/1540-9295(2003)001%255B0031:PSATEO%255D2.0.CO;2

Schnoes, A. M., Ream, D. C., Thorman, A. W., Babbitt, P. C., & Friedberg, I. (2013). Biases in the Experimental Annotations of Protein Function and Their Effect on Our Understanding of Protein Function Space. *PLOS Computational Biology*, *9*(5), e1003063. https://doi.org/10.1371/journal.pcbi.1003063

Schuech, R., Nielsen, L. T., Humphries, S., Smith, D., & Kiørboe, T. (2025). Fluid dynamics of dinoflagellate feeding and swimming. *Limnology and Oceanography*, *70*(2), 349–359. https://doi.org/10.1002/lno.12764

Scorzetti, G., Brand, L. E., Hitchcock, G. L., Rein, K. S., Sinigalliano, C. D., & Fell, J. W. (2009). Multiple simultaneous detection of Harmful Algal Blooms (HABs) through a high throughput bead array technology, with potential use in phytoplankton community analysis. *Harmful Algae*, *8*(2), 196–211. https://doi.org/10.1016/j.hal.2008.05.003

Sela, M., Church, J. R., Schapiro, I., & Schneidman-Duhovny, D. (2024). RhoMax: Computational Prediction of Rhodopsin Absorption Maxima Using Geometric Deep Learning. *Journal of Chemical Information and Modeling*, *64*(12), 4630–4639. https://doi.org/10.1021/acs.jcim.4c00467

Shahani, K., Song, H., Mehdi, S. R., Sharma, A., Tunio, G., Qureshi, J., Kalhoro, N., & Khaskheli, N. (2021). Design and Testing of an Underwater Microscope with Variable Objective Lens for the Study of Benthic Communities. *Journal of Marine Science and Application*, *20*(1), 170–178. https://doi.org/10.1007/s11804-020-00185-9

Sheng, J., Malkiel, E., Katz, J., Adolf, J., Belas, R., & Place, A. R. (2007). Digital holographic microscopy reveals prey-induced changes in swimming behavior of predatory dinoflagellates. *Proceedings of the National Academy of Sciences of the United States of America*, *104*(44), 17512–17517. https://doi.org/10.1073/PNAS.0704658104/SUPPL_FILE/PNAS_SUPPL_3.PDF

Sheng, J., Malkiel, E., Katz, J., Adolf, J. E., & Place, A. R. (2010). A dinoflagellate exploits toxins to immobilize prey prior to ingestion. *Proceedings of the National Academy of Sciences of the United States of America*, *107*(5), 2082–2087. https://doi.org/10.1073/pnas.0912254107

Shi, X., Li, L., Guo, C., Lin, X., Li, M., & Lin, S. (2015). Rhodopsin gene expression regulated by the light dark cycle, light spectrum and light intensity in the dinoflagellate *Prorocentrum*. *Frontiers in Microbiology*, *6*, 555. https://doi.org/10.3389/fmicb.2015.00555

Shim, J., Cho, S.-G., Kim, S.-H., Chuon, K., Meas, S., Choi, A., & Jung, K.-H. (2022). Heliorhodopsin Helps Photolyase to Enhance the DNA Repair Capacity. *Microbiology Spectrum*, *10*(6), e02215-22. https://doi.org/10.1128/spectrum.02215-22

Sieradzki, E. T., Fuhrman, J. A., Rivero-Calle, S., & Gómez-Consarnau, L. (2018). Proteorhodopsins dominate the expression of phototrophic mechanisms in seasonal and dynamic marine picoplankton communities. *PeerJ*, *6*, e5798. https://doi.org/10.7717/peerj.5798

Sineshchekov, O. A., Jung, K.-H., & Spudich, J. L. (2002). Two rhodopsins mediate phototaxis to low- and high-intensity light in *Chlamydomonas reinhardtii*. *Proceedings of the*

National Academy of Sciences of the United States of America, *99*(13), 8689–8694. https://doi.org/10.1073/pnas.122243399

Slamovits, C. H., Okamoto, N., Burri, L., James, E. R., & Keeling, P. J. (2011). A bacterial proteorhodopsin proton pump in marine eukaryotes. *Nature Communications*, *2*(1), 183. https://doi.org/10.1038/ncomms1188

Smayda, T. J. (2010). Adaptations and selection of harmful and other dinoflagellate species in upwelling systems. 2. Motility and migratory behaviour. *Progress in Oceanography*, *85*(1), 71–91. https://doi.org/10.1016/j.pocean.2010.02.005

Soneji, P., Challita, E. J., & Bhamla, S. (2024). Trackoscope: A low-cost, open, autonomous tracking microscope for long-term observations of microscale organisms. *PLOS ONE*, *19*(7), e0306700. https://doi.org/10.1371/journal.pone.0306700

Sorek, M., & Levy, O. (2012). Influence of the Quantity and Quality of Light on Photosynthetic Periodicity in Coral Endosymbiotic Algae. *PLOS ONE*, *7*(8), e43264. https://doi.org/10.1371/journal.pone.0043264

Staley, J. T. (1971). Growth Rates of Algae Determined in Situ Using an Immersed Microscope. *Journal of Phycology*, *7*(1), 13–17. https://doi.org/10.1111/j.1529-8817.1971.tb01472.x

Stephanie A., B., E. Starr, H., Erik E., S., & Frances M., V. D. (2007). Characterization of a dinoflagellate cryptochrome blue-light receptor with a possible role in circadian control of the cell cycle. *Journal of Phycology*, *43*(3), 509–518. https://doi.org/10.1111/j.1529-8817.2007.00339.x

Stephens, T. G., Ragan, M. A., Bhattacharya, D., & Chan, C. X. (2018). Core genes in diverse dinoflagellate lineages include a wealth of conserved dark genes with unknown functions. *Scientific Reports*, *8*(1), 17175. https://doi.org/10.1038/s41598-018-35620-z

Strasburger, E. (1878). Wirkung des lichtes und der wärme auf schwärmsporen. *Jenaische Zeitschrift Für Naturwissenschaft*, *12*(551), 78.

Subramaniam, S., & Henderson, R. (2000). Molecular mechanism of vectorial proton translocation by bacteriorhodopsin. *Nature*, *406*(6796), 653–657. https://doi.org/10.1038/35020614

Suggett, D. J., Warner, M. E., & Leggat, W. (2017). Symbiotic Dinoflagellate Functional Diversity Mediates Coral Survival under Ecological Crisis. *Trends in Ecology & Evolution*, *32*(10), 735–745. https://doi.org/10.1016/j.tree.2017.07.013

Suzuki, K., Del Carmen Marín, M., Konno, M., Bagherzadeh, R., Murata, T., & Inoue, K. (2022). Structural characterization of proton-pumping rhodopsin lacking a cytoplasmic proton donor residue by X-ray crystallography. *The Journal of Biological Chemistry*, *298*(3), 101722. https://doi.org/10.1016/j.jbc.2022.101722

Sweeney, B. M. (1986). The Loss of the Circadian Rhythm in Photosynthesis in an Old Strain of *Gonyaulax polyedra* . *Plant Physiology*, *80*(4), 978–981. https://doi.org/10.1104/pp.80.4.978

Takeo, H., Hiroshi, K., Mamoru, K., Tetsuo, T., & Masakatsu, W. (1999). Phototactic responses of four marine dinoflagellates with different types of eyespot and chloroplast. *Phycological Research*, *47*(2), 101–107. https://doi.org/10.1046/J.1440-1835.1999.47220158.X

Taylor, F., & Gustavson, M. (1986). An underwater survey of the organism chiefly responsible for “ciguatera” fish poisoning in the eastern Caribbean region: The benthic dinoflagellate Gambierdiscus toxicus. *Proceedings of the 7th. International Diving Science Symposium. Padova, Italy. CMAS, University of Padua, Italy*, 95–111.

Tester, P. A., Kibler, S. R., Holland, W. C., Usup, G., Vandersea, M. W., Leaw, C. P., Teen, L. P., Larsen, J., Mohammad-Noor, N., Faust, M. A., & Litaker, R. W. (2014). Sampling harmful benthic dinoflagellates: Comparison of artificial and natural substrate methods. *Harmful Algae*, *39*, 8–25. https://doi.org/10.1016/j.hal.2014.06.009

Tester, P. A., Litaker, R. W., Soler-Onís, E., Fernández-Zabala, J., & Berdalet, E. (2022). Using artificial substrates to quantify *Gambierdiscus* and other toxic benthic dinoflagellates for monitoring purposes. *Harmful Algae*, *120*, 102351. https://doi.org/10.1016/j.hal.2022.102351

Tian, Y., Gao, S., von der Heyde, E. L., Hallmann, A., & Nagel, G. (2018). Two-component cyclase opsins of green algae are ATP-dependent and light-inhibited guanylyl cyclases. *BMC Biology*, *16*(1), 144. https://doi.org/10.1186/s12915-018-0613-5

Tinevez, J.-Y., Perry, N., Schindelin, J., Hoopes, G. M., Reynolds, G. D., Laplantine, E., Bednarek, S. Y., Shorte, S. L., & Eliceiri, K. W. (2017). TrackMate: An open and extensible platform for single-particle tracking. *Methods*, *115*, 80–90. https://doi.org/10.1016/j.ymeth.2016.09.016

Tornberg, E. C. (2019). *Physiological characterization of the mixotrophic dinoflagellate* Amphidinium carterae. Oregon State University.

TransDecoder/TransDecoder. (2025). [Perl]. TransDecoder. https://github.com/TransDecoder/TransDecoder (Original work published 2015)

Trouble in the Tropics. (n.d.). *Https://Www.Whoi.Edu/*. Retrieved March 27, 2025, from https://www.whoi.edu/oceanus/feature/trouble-in-the-tropics/

Tu, W., Saeed, H., & Huang, W. E. (2024). Rhodopsin-based light-harvesting system for sustainable synthetic biology. *Microbial Biotechnology*, *17*(7), e14521. https://doi.org/10.1111/1751-7915.14521

Tudó, À., Gaiani, G., Rey Varela, M., Tsumuraya, T., Andree, K. B., Fernández-Tejedor, M., Campàs, M., & Diogène, J. (2020). Further Advance of *Gambierdiscus* Species in the Canary Islands, with the First Report of *Gambierdiscus belizeanus*. *Toxins*, *12*(11), Article 11. https://doi.org/10.3390/toxins12110692

Vacarizas, J., Benico, G., Austero, N., & Azanza, R. (2018). Taxonomy and toxin production of *Gambierdiscus carpenteri* (Dinophyceae) in a tropical marine ecosystem: The first record from the Philippines. *Marine Pollution Bulletin*, *137*, 430–443. https://doi.org/10.1016/j.marpolbul.2018.10.034

van Dolah, F. M., Leighfield, T. A., Sandel, H. D., & Hsu, C. K. (1995). CELL DIVISION IN THE DINOFLAGELLATE *GAMBIERDISCUS TOXICUS* IS PHASED TO THE DIURNAL CYCLE AND ACCOMPANIED BY ACTIVATION OF THE CELL CYCLE REGULATORY PROTEIN, CDC2 KINASE. *Journal of Phycology*, *31*(3), 395–400. https://doi.org/10.1111/j.0022-3646.1995.00395.x

Vandersea, M. W., Kibler, S. R., Holland, W. C., Tester, P. A., Schultz, T. F., Faust, M. A., Holmes, M. J., Chinain, M., & Wayne Litaker, R. (2012). DEVELOPMENT OF SEMI-QUANTITATIVE PCR ASSAYS FOR THE DETECTION AND ENUMERATION OF *GAMBIERDISCUS* SPECIES (GONYAULACALES, DINOPHYCEAE)[1]. *Journal of Phycology*, *48*(4), 902–915. https://doi.org/10.1111/j.1529-8817.2012.01146.x

Varadi, M., Bertoni, D., Magana, P., Paramval, U., Pidruchna, I., Radhakrishnan, M., Tsenkov, M., Nair, S., Mirdita, M., Yeo, J., Kovalevskiy, O., Tunyasuvunakool, K., Laydon, A.,

Žídek, A., Tomlinson, H., Hariharan, D., Abrahamson, J., Green, T., Jumper, J., … Velankar, S. (2024). AlphaFold Protein Structure Database in 2024: Providing structure coverage for over 214 million protein sequences. *Nucleic Acids Research*, *52*(D1), D368–D375. https://doi.org/10.1093/nar/gkad1011

Vassalli, M., Penna, A., Sbrana, F., Casabianca, S., Gjeci, N., Capellacci, S., Asnaghi, V., Ottaviani, E., Giussani, V., Pugliese, L., Jauzein, C., Lemée, R., Hachani, M. A., Turki, S., Açaf, L., Saab, M. A.-A., Fricke, A., Mangialajo, L., Bertolotto, R., … Chiantore, M. (2018). Intercalibration of counting methods for *Ostreopsis* spp. Blooms in the Mediterranean Sea. *Ecological Indicators*, *85*, 1092–1100. https://doi.org/10.1016/j.ecolind.2017.07.063

Vicker, M. G., Becker, J., Gebauer, G., Schill, W., & Rensing, L. (1988). Circadian Rhythms of Cell Cycle Processes in the Marine Dinoflagellate *Gonyaulax Polyedra*. *Chronobiology International*. https://doi.org/10.3109/07420528809078548

Villareal, T. A., & Morton, S. L. (2002). Use of Cell-Specific PAM-Fluorometry to Characterize Host Shading in the Epiphytic Dinoflagellate *Gambierdiscus toxicus*. *Marine Ecology*, *23*(2), 127–140. https://doi.org/10.1046/j.1439-0485.2002.02777.x

W, C. S. (1981). Temporal patterns of cell division of unicellualar algae. *Can.Bull.Fish.Aquat.Sci.*, *210*, 150–181.

Wang, D.-Z., Li, C., Xie, Z.-X., Dong, H.-P., Lin, L., & Hong, H.-S. (2011). Homology-Driven Proteomics of Dinoflagellates with Unsequenced Genomes Using MALDI-TOF/TOF and Automated De Novo Sequencing. *Evidence-Based Complementary and Alternative Medicine : eCAM*, *2011*, 471020. https://doi.org/10.1155/2011/471020

Wang, D.-Z., Zhang, H., Zhang, Y., & Zhang, S.-F. (2014). Marine dinoflagellate proteomics: Current status and future perspectives. *Journal of Proteomics*, *105*, 121–132. https://doi.org/10.1016/j.jprot.2014.01.026

Watari, M., Ikuta, T., Yamada, D., Shihoya, W., Yoshida, K., Tsunoda, S. P., Nureki, O., & Kandori, H. (2019). Spectroscopic study of the transmembrane domain of a rhodopsin–phosphodiesterase fusion protein from a unicellular eukaryote. *Journal of Biological Chemistry*, *294*(10), 3432–3443. https://doi.org/10.1074/jbc.RA118.006277

Wellkamp, M., García-Camacho, F., Durán-Riveroll, L. M., Tebben, J., Tillmann, U., & Krock, B. (2020). LC-MS/MS Method Development for the Discovery and Identification of Amphidinols Produced by *Amphidinium*. *Marine Drugs*, *18*(10), 497. https://doi.org/10.3390/md18100497

Westermann, M., Hoischen, C., Wöhlbrand, L., Rabus, R., & Rhiel, E. (2023). Light and prey influence the abundances of two rhodopsins in the dinoflagellate v. *Protoplasma*, *260*(2), 529–544. https://doi.org/10.1007/s00709-022-01795-6

Whitman, W. B., Coleman, D. C., & Wiebe, W. J. (1998). Prokaryotes: The unseen majority. *Proceedings of the National Academy of Sciences*, *95*(12), 6578–6583. https://doi.org/10.1073/pnas.95.12.6578

Williams, E. P., Bachvaroff, T. R., & Place, A. R. (2021). A Global Approach to Estimating the Abundance and Duplication of Polyketide Synthase Domains in Dinoflagellates. *Evolutionary Bioinformatics*, *17*, 11769343211031871. https://doi.org/10.1177/11769343211031871

Wisecaver, J. H., Brosnahan, M. L., & Hackett, J. D. (2013). Horizontal Gene Transfer is a Significant Driver of Gene Innovation in Dinoflagellates. *Genome Biology and Evolution*, *5*(12), 2368–2381. https://doi.org/10.1093/gbe/evt179

Wisnoski, N. I., & Lennon, J. T. (2023). Scaling up and down: Movement ecology for microorganisms. *Trends in Microbiology*, *31*(3), 242–253. https://doi.org/10.1016/j.tim.2022.09.016

Wu, R., Ding, F., Wang, R., Shen, R., Zhang, X., Luo, S., Su, C., Wu, Z., Xie, Q., Berger, B., Ma, J., & Peng, J. (2022). *High-resolution de novo structure prediction from primary sequence* (p. 2022.07.21.500999). bioRxiv. https://doi.org/10.1101/2022.07.21.500999

Xu, Y., He, X., Lee, W. H., Chan, L. L., Lu, D., Wang, P., Tao, X., Li, H., & Yu, K. (2021). Ciguatoxin-Producing Dinoflagellate *Gambierdiscus* in the Beibu Gulf: First Report of Toxic *Gambierdiscus* in Chinese Waters. *Toxins*, *13*(9), Article 9. https://doi.org/10.3390/toxins13090643

Xu, Y., Richlen, M. L., Liefer, J. D., Robertson, A., Kulis, D., Smith, T. B., Parsons, M. L., & Anderson, D. M. (2016). Influence of Environmental Variables on *Gambierdiscus* spp. (Dinophyceae) Growth and Distribution. *PLOS ONE*, *11*(4), e0153197. https://doi.org/10.1371/journal.pone.0153197

Yang, X., Chen, Y., Wang, F., Chen, S., Cao, Z., Feng, Y., Wang, L., & Feng, W. (2025). Bioinspired artificial phototaxis and phototropism enabled by photoresponsive smart materials. *Materials Today*, *87*, 348–377. https://doi.org/10.1016/j.mattod.2025.05.004

Yasumoto, T. (1978). Ecological Survey on a Dinoflagellate Possibly Responsible for the Induction of Ciguatera. *Bulletin of the Japanese Society of Scientific Ffisheries*.

Yasumoto, T., Nakajima, I., Bagnis, R., & Adachi, R. (1977). Finding of a Dinoflagellate as a Likely Culprit of Ciguatera. *Nippon Suisan Gakkaishi*, *43*(8), 1021–1026. https://doi.org/10.2331/suisan.43.1021

Yon, T., Réveillon, D., Sibat, M., Holland, C., Litaker, R. W., Nascimento, S. M., Rossignoli, A. E., Riobó, P., Hess, P., & Bertrand, S. (2024). Targeted and non-targeted mass spectrometry to explore the chemical diversity of the genus *Gambierdiscus* in the Atlantic Ocean. *Phytochemistry*, *222*, 114095. https://doi.org/10.1016/j.phytochem.2024.114095

Yong, H. L., Mustapa, N. I., Lee, L. K., Lim, Z. F., Tan, T. H., Usup, G., Gu, H., Litaker, R. W., Tester, P. A., Lim, P. T., & Leaw, C. P. (2018). Habitat complexity affects benthic harmful dinoflagellate assemblages in the fringing reef of Rawa Island, Malaysia. *Harmful Algae*, *78*, 56–68. https://doi.org/10.1016/j.hal.2018.07.009

Yoon, H. S., Hackett, J. D., & Bhattacharya, D. (2002). A single origin of the peridinin- and fucoxanthin-containing plastids in dinoflagellates through tertiary endosymbiosis. *Proceedings of the National Academy of Sciences*, *99*(18), 11724–11729. https://doi.org/10.1073/pnas.172234799

Yuan, K.-K., Li, H.-Y., & Yang, W.-D. (2024). Marine Algal Toxins and Public Health: Insights from Shellfish and Fish, the Main Biological Vectors. *Marine Drugs*, *22*(11), 510. https://doi.org/10.3390/md22110510

Zapata, M., Fraga, S., Rodríguez, F., & Garrido, J. L. (2012). Pigment-based chloroplast types in dinoflagellates. *Marine Ecology Progress Series*, *465*, 33–52. https://doi.org/10.3354/meps09879

Zhang, H., Nulick, K. J., Burris, Z., Pierce, M., Ma, M., & Lin, S. (2024). Dinoflagellate Proton-Pump Rhodopsin Genes in Long Island Sound: Diversity and Spatiotemporal

Distribution. *Microorganisms*, *12*(3), 628. https://doi.org/10.3390/microorganisms12030628

Zheng, B., Lucas, A. J., Franks, P. J. S., Schlosser, T. L., Anderson, C. R., Send, U., Davis, K., Barton, A. D., & Sosik, H. M. (2023). Dinoflagellate vertical migration fuels an intense red tide. *Proceedings of the National Academy of Sciences*, *120*(36), e2304590120. https://doi.org/10.1073/pnas.2304590120

Zimmer, C., Zhang, B., Dufour, A., Thebaud, A., Berlemont, S., Meas-Yedid, V., & Marin, J.-C. O. (2006). On the digital trail of mobile cells. *IEEE Signal Processing Magazine*, *23*(3), 54–62. IEEE Signal Processing Magazine. https://doi.org/10.1109/MSP.2006.1628878

Zingone, A., & Oksfeldt Enevoldsen, H. (2000). The diversity of harmful algal blooms: A challenge for science and management. *Ocean & Coastal Management*, *43*(8), 725–748. https://doi.org/10.1016/S0964-5691(00)00056-9